Hyperglycemia-induced thioredoxin reductase degradation accelerates ferroptotic cell death propagation in diabetic renal tubules

Maremonti, Francesca

Awarding institution:
King's College London

Aus der Medizinischen Klinik 3 der Medizinischen Fakultät Carl Gustav Carus der Technischen Universität Dresden
Direktor: Prof. Dr. med. Dr. Stefan Bornstein

Hyperglycemia-induced thioredoxin reductase degradation accelerates ferroptotic cell death propagation in diabetic renal tubules

Dissertationsschrift

zur Erlangung des akademischen Grades

Doctor of Philosophy (Ph.D.)

vorgelegt

der Medizinischen Fakultät

Carl Gustav Carus der Technischen

Universität Dresden

von

M.Sc., Francesca Maremonti

aus Trieste, Italien

Dresden   2024 (der Einreichung im Dekanat)

2. Blatt (2. Seite)

1. Gutachter:

2. Gutachter:

Tag der mündlichen Prüfung: (Verteidigungstermin)

gez.:
Vorsitzender der Promotionskommission

"I guess I've been working so hard, I forgot what it's like to be hardly working".

Michael Scott

Acknowledgments

I extend my deepest gratitude to my primary advisor, Prof. Andreas Linkermann, whose unwavering support, guidance, and intellectual insight have been indispensable throughout my doctoral journey. Your mentorship has not only shaped the direction of this research but has also profoundly influenced my academic and personal growth.

I am grateful to the members of my Thesis Advisory Committee, Prof. Ünal Coskun, Dr. Natalia Rodriguez Muela, and Prof. Christer Hogstrand, for their invaluable feedback and constructive criticism over these four years. Your contributions significantly enhanced the quality of this thesis, and each of you brought unique perspectives that enriched the overall merit of my work. Thank you for trusting the project from its beginning.

Special thanks go to Arantxa and the entire DIGS-BB doctoral program for providing an intellectually stimulating and supportive environment. The academic resources, facilities, and collaborative atmosphere have been fundamental for the completion of my project.

I would like to express my appreciation to the IRTG program for providing me with the opportunity to expand my knowledge from mere molecular biology to the broader perspective represented by the diabetes field. Additionally, I am grateful for the chance to visit and be a part of the academic environment at King's College London.

My heartfelt thanks extend to my current and former lab colleagues who have become friends over these years. Romy, Anne, Shubhangi, and Marlena, thank you for the guidance, expertise, and delightful lunches and coffee breaks we shared. A special thank you goes to Alexia, who consistently stood by my side in both experimental and everyday life situations, truly making my journey better. Another special thank you to my former colleague, Cloudy, for her energy and wise advice. To the rest of the lab, from Karolin to Mirela, thank you for the academic discussions, collaborative efforts, and friendly encouragement that made this academic journey both enjoyable and rewarding.

I want to express my deep gratitude to my beautiful group of friends, Rachele, Vittoria, Giulia, and Ludovica. We met during the selection for the doctoral program,

and since then, you have been the best friends one could ask for. Even Ludovica, who joined our group later, left a significant mark on my experience here in Dresden. I cannot find enough words to express how much our friendship has meant to me during these years.

I wouldn't be the person I am today without my family, Papà, Mamma, and Emma. Thank you for your unconditional love, encouragement, and understanding. Your unwavering belief in my abilities has been a constant source of motivation, and I am profoundly grateful for your endless support.

Last but not least, I want to express my gratitude to all those who may not be mentioned explicitly but have played a role, big or small, in shaping my academic and personal life during this Ph.D. journey. This thesis is a culmination of the collective efforts, support, and encouragement from the people mentioned above, and I am truly thankful for the privilege of having such a remarkable network of individuals in my life.

Table of Contents

Abstract

Diabetes mellitus and its complications stands as arguably the most formidable pandemic of the 21st century. While rodent models of diabetes mellitus have been extensively explored, none have managed to faithfully replicate the full spectrum of pathological hallmarks and secondary complications witnessed in diabetic patients. Among the commonly affected organs is the kidney, manifesting in the form of diabetic kidney disease (DKD). Recently, our clinical understanding of incretins as critical regulators of disease progression in diabetic patients including DKD has undergone significant expansion.

In particular, the incretin hormone gastric inhibitory polypeptide (GIP) axis has taken central stage. A ground-breaking development in this realm was the creation of a GIP receptor dominant negative (GIPR^{dn}) mouse, exhibiting all the characteristic features observed in DKD patients. This study sheds light on the heightened susceptibility of these mice to lethal acute kidney injury (AKI) induced by ischemia-reperfusion injury (IRI). Notably, isolated renal GIPR^{dn}-tubules displayed accelerated cell death propagation and increased tubular necrosis.

Expanding on previous cell culture experiments involving hyperglycemia, it became apparent that tubules of GIPR^{dn} mice express elevated levels of the intracellular thioredoxin interacting protein (TXNIP), previously reported to be responsible for the degradation of glucose transporter 1 (GLUT1). This phenomenon is crucial in maintaining intracellular glucose homeostasis. The study further indicates an association between TXNIP and the downregulation of thioredoxin reductase 1 (TXNRD1), a selenoenzyme playing a pivotal role in protecting renal tubules from ferroptosis in a glutathione-independent manner.

Intriguingly, the inhibition of TXNRD1 with the small molecule ferroptocide (FTC) in GIPR^{dn} tubules resulted in severe tubular necrosis, a condition effectively reversed by the ferroptosis inhibitor ferrostatin 1 (Fer-1). This nuanced exploration establishes a connection between DKD and a heightened sensitivity to kidney tubular ferroptosis, thereby presenting a potential avenue for intervention with ferrostatins. Importantly, the administration of a single dose of Fer-1 significantly prolonged the survival of GIPR^{dn} mice following IRI.

In conclusion, this study illuminates the intricate dynamics of DKD, highlighting a pronounced sensitization to kidney tubular ferroptosis. The findings suggest that ferrostatins, particularly exemplified by Fer-1, hold promise as potential therapeutic agents in mitigating the severity of this condition, offering hope for improved outcomes in individuals struggling with diabetes-related kidney complications.

Zusammenfassung

Diabetes mellitus und seine zahlreichen Komplikationen stellen möglicherweise die schwerwiegendste Pandemie des 21. Jahrhunderts dar. Obwohl Nagetiermodelle des Diabetes mellitus umfassend erforscht wurden, ist es bisher keinem gelungen, das gesamte Spektrum der pathologischen Merkmale und sekundären Komplikationen realitätsgetreu abzubilden, die bei diabetischen Patienten klinisch auftreten. Zu den häufig betroffenen Organen gehört die Niere, die sich in Form der diabetischen Nierenerkrankung (DKD) manifestiert. In letzter Zeit hat unser klinisches Verständnis von Inkretinen als entscheidende Regulatoren im Verlauf von Diabetes, einschließlich DKD, erhebliche Fortschritte gemacht.

Insbesondere hat die Inkretin-Hormon-Gastroinhibitorisches Peptid (GIP)-Achse eine zentrale Rolle eingenommen. Eine bahnbrechende Entwicklung in diesem Bereich ist die Schaffung einer GIP-Rezeptor-dominant-negativen (GIPR^{dn})-Maus, die alle charakteristischen Merkmale von DKD-Patienten aufweist. Die vorliegende Studie wirft Licht auf die erhöhte Anfälligkeit dieser Mäuse für tödliche akute Nierenschädigungen, die durch Ischämie-Reperfusionsschäden (IRI) ausgelöst werden. Insbesondere zeigten isolierte renale GIPR^{dn}-Tubuli beschleunigte Ausbreitung von Zelltod und erhöhte tubuläre Nekrose.

Aufbauend auf früheren Zellkulturversuchen mit Hyperglykämie wurde offensichtlich, dass die Tubuli von GIPR^{dn}-Mäusen erhöhte Mengen des intrazellulären Proteins thioredoxin interacting protein (TXNIP) exprimieren, das für den Abbau von Glukosetransporter 1 (GLUT1) verantwortlich ist. Dieses Phänomen ist entscheidend für die Aufrechterhaltung der intrazellulären Glukosehomöostase. Die Arbeit offenbart weiterhin eine Verbindung zwischen TXNIP und der Herunterregulierung der Thioredoxin-Reduktase 1 (TXNRD1), einem Selenenzym, das eine entscheidende Rolle bei der Abwehr von Ferroptose in Nierentubuli auf Glutathion-unabhängige Weise spielt.

Interessanterweise führte die Blockade von TXNRD1 mit dem kleinen Molekül Ferroptocide (FTC) in GIPR^{dn}-Tubuli zu schwerer tubulärer Nekrose, die durch den Ferroptose-Inhibitor Fer-1 effektiv umgekehrt werden konnten. Diese nuancierte Untersuchung etabliert eine Verbindung zwischen DKD und einer erhöhten Empfindlichkeit für Ferroptose in Nierentubuli und bietet somit einen potenziellen Ansatz für die Intervention mit Ferrostatinen. Wichtig ist, dass die Verabreichung einer einzigen Dosis Fer-1 die Überlebenszeit von GIPR^{dn}-Mäusen nach IRI signifikant verlängerte.

Zusammenfassend beleuchtet diese Studie die komplexen Dynamiken von DKD und hebt eine ausgeprägte Sensibilisierung für Ferroptose in Nierentubuli hervor. Die Ergebnisse legen nahe, dass Ferrostatine, hier insbesondere exemplarisch durch Fer-1 gezeigt, vielversprechende therapeutische Mittel zur Linderung der Schwere dieser Erkrankung

darstellen und Hoffnung auf verbesserte Ergebnisse für Patienten bieten, die mit diabetesbedingten Nierenkomplikationen kämpfen.

List of abbreviations

ACSL4	acyl-CoA synthetase long chain family member 4
AGPS	alkylglycerone phosphate synthase
AIFM2	apoptosis-inducing factor 2
AKI	acute kidney injury
ATN	acute tubular necrosis
BTBR	Black and Tan BRachyury
CBS	Cystathionine-β-synthase
CKD	chronic kidney disease
CoQ10	coenzyme Q10
CSE	cystathionine γ-lyase
DAMPs	damage associated molecular patterns
DKD	diabetes kidney disease
DM	diabetes mellitus
DN	diabetic nephropathy
DPP-4	dipeptidyl peptidase 4
eNOS	endothelial nitric oxide synthase
ER	endoplasmic reticulum
ESCRT-III	endosomal sorting complexes required for transport III
ESRD	end-stage renal disease
ETHE1	ethylmalonic encephalopathy 1 protein
FA	fatty acid
FACS	fluorescence-activated cell sorting
FAR1	Fatty acyl-CoA reductase 1
Fer-1	ferrostatin-1
FINs	ferroptosis inducers
FPG	Fasting plasma glucose
FSP1	ferroptosis-supressing protein 1
FTC	ferroptocide
GCL	glutamate-cysteine ligase
GIP	glucose-dependent insulinotropic polypeptide
GIPR	glucose-dependent insulinotropic polypeptide receptor
GIPR^{dn}	glucose-dependent insulinotropic polypeptide receptor dominant-negative
GLP-1	Glucagon like peptide 1

GLP-1R	GLP-1 receptor
GLP1-RA	GLP-1 receptor agonist
GLUT1	glucose transporter 1
GLUT4	glucose transporter 4
GPCR	G-protein coupled receptor
GPX4	glutathione peroxidase 4
GSDMD	gasdermin D
GSH	glutathione
GSS	glutathione synthetase
GSSG	glutathione disulfide
HbA1C	hemoglobin A1C
H_2O_2	hydrogen peroxide
IDF	International Diabetes Federation
IGT	impaired glucose tolerance
IR	insulin resistance
IRI	ischemia reperfusion injury
LC-MS	Liquid chromatography–mass spectrometry
LDH	lactate dehydrogenase
LOX	protein-lysine 6-oxidase
LPCAT3	lysophosphatidylcholine acyltransferase 3
MLKL	mixed lineage kinase domain-like protein
MODY	maturity-onset diabetes of the young
MOMP	mitochondrial outer membrane permeabilization
NADPH	Nicotinamide-adenine dinucleotide phosphate
Nec-1	necrostatin-1
NLRP3	NLR Family Pyrin Domain Containing 3
NO	nitric oxide
NON	Non diabetic non obese
NOS3	nitric oxide synthase 3
PL-OOH	phospholipid hydroperoxide
POR	cytochrome P450 Oxidoreductase
PP	pancreatic polypeptide
PUFAs	polyunsaturated fatty acids
RCD	regulated cell death
RIPK1	receptor-interacting protein kinase 1

RIPK3	receptor-interacting protein kinase 3
RN	regulated necrosis
ROS	reactive oxygen species
RTA	radical trapping antioxidant
SGLT2	sodium glucose transport protien 2
SGLT2i	sodium glucose transport protien 2 inhibitor
SQR	Sulfide-quinone reductase
SRN	synchronized regulated necrosis
STZ	streptozotocin
T1DM	type 1 diabetes mellitus
T2DM	Type 2 diabetes mellitus
TRX1	thioredoxin 1
TXNIP	thioredoxin interacting protien
TXNRD1	thioredoxin reductase 1
VDUP1	Vitamin D3 Up-Regulated Protein 1

List of tables

List of Figures

Introduction

1. Introduction

1.1. Diabetes mellitus

1.1.1. Definition and description

Diabetes mellitus (DM) comprehend a group of prevalent metabolic disorders characterized by hyperglycemia. The development of various types of DM results from a complex interplay between genetic factors and environmental influences. Depending on the specific etiology of DM, factors contributing to elevated blood glucose levels include diminished insulin secretion, reduced glucose utilization and heightened glucose production ("Harrison's Principles of Internal Medicine, 21e | AccessMedicine | McGraw Hill Medical," 2022).

Signs of diabetes mellitus, such as hyperglycemia, polyuria, polydipsia, weight loss and hyperphagia are indicative. Chronic hyperglycemia may be associated with growth impairment and increased vulnerability to specific infections. Diabetes can also lead to acute and potentially life-threatening conditions, including hyperglycemia with ketoacidosis or the nonketotic hyperosmolar syndrome (American Diabetes Association, 2010).

The persistent glycemic dysregulation associated with diabetes mellitus is the cause of a series of chronic complications involving multiple organ systems, leading to the high morbidity and mortality associated with the disease (The Expert Committee on the Diagnosis and Classification of Diabetes Mellitus, 2003).

1.1.2. Epidemiology

Over the past two decades, the global prevalence of DM has increased significantly, escalating from an estimated 30 million cases in 1985 to 463 million in 2019. Projected trends anticipate the number to reach 1.3 billion individuals with diabetes by 2050 (The Lancet, 2023). While both type 1 and type 2 DM are on the rise worldwide, the prevalence of type 2 DM is increasing at a more accelerated pace, likely attributed to dietary shifts, escalating obesity rates, diminished physical activity with industrialization, and an aging population. In 2019, the worldwide prevalence of diabetes in individuals aged 20–79 years stood at 9.3%, ranging from 4.7% to 12.2%. Moreover, the IDF (International Diabetes Federation) indicated that diabetes was responsible for nearly 4.2 million deaths worldwide, accounting for 11.3% of global all-cause mortality in adults aged 20–79 years (International Diabetes Federation, 2019) . The economic implications of DM are substantial, with an estimated $760 billion spent on diabetes-related healthcare expenditures worldwide, ranging from 8% to 19% of total expenditures across regions (R. Williams *et al.*, 2020).

The incidence of type 1 diabetes globally has been steadily rising at a rate of 3% per year, with notable geographical variations. The cause for this uptrend is not fully understood, but there's a discernible trend of type 1 DM being diagnosed at younger ages (Gregory *et al.*, 2022). Among the three primary forms of diabetes, Type 2 diabetes mellitus (T2DM) is more prevalent than either Type 1 diabetes mellitus (T1DM) or gestational diabetes. It constitutes 90% of the approximately 537 million diabetes cases globally, with this number projected to escalate to 783 million by 2045 (Sun *et al.,* 2022). The rising global incidence of T2DM is associated with a rise in obesity trends (Klein *et al.*, 2022).

1.1.3. Classification of diabetes mellitus

DM is categorized based on the underlying pathogenic processes leading to hyperglycemia. The primary classification includes two broad categories known as type 1 and type 2 DM. While classification is crucial for treatment decisions, certain individuals defy clear categorization as either type 1 or type 2 at the time of diagnosis. The conventional notions of type 2 diabetes manifesting exclusively in adults and type 1 diabetes exclusively in children are no longer precise, as both conditions can occur in both age groups. Moreover, there is a growing acknowledgment of additional diabetes forms in which the molecular pathogenesis is better understood and may be linked to a single gene defect. These alternative and "atypical" forms may exhibit characteristics shared with type 1 and/or type 2 DM. Diabetes may be categorized into the following general classifications (ElSayed *et al.*, 2023):

- **Type 1 Diabetes Mellitus**: resulting from autoimmune destruction of β-cells and typically leading to absolute insulin deficiency, this category includes latent autoimmune DM of adulthood.
- **Type 2 Diabetes Mellitus**: arises from a non-autoimmune progressive reduction in β-cell insulin secretion, often in the context of insulin resistance and metabolic syndrome.
- **Specific Types of Diabetes (monogenic or MODY)**: originates from various causes, including monogenic diabetes syndromes (e.g., neonatal diabetes and maturity-onset diabetes of the young - MODY), diseases affecting the exocrine pancreas (e.g., cystic fibrosis and pancreatitis), and diabetes induced by drugs or chemicals (e.g., glucocorticoid use, HIV/AIDS treatment, or post-organ transplantation).
- **Gestational Diabetes Mellitus**: diagnosed in the second or third trimester of pregnancy, this form of diabetes was not clearly evident before gestation and is distinct from overt diabetes.
- **Atypical diabetes**: Some forms of diabetes exhibit features of both type 1 and type 2, distinguishing them from monogenic forms like MODY without single gene defects.

Atypical diabetes includes instances where a type 2 diabetes phenotype emerges before puberty or in very lean individuals. Ketosis-prone diabetes is another example, characterized by ketoacidosis without the need for long-term exogenous insulin therapy. Mechanisms governing these atypical forms are currently under active investigation.

1.1.4. Diagnosis of diabetes mellitus

Glucose tolerance is categorized into three main groups: normal glucose homeostasis, impaired glucose homeostasis, or DM. The glucose tolerance can be evaluated based on plasma glucose, either the fasting plasma glucose (FPG) value or the 2-h plasma glucose value during a 75-g oral glucose tolerance test or hemoglobin A1C (HbA1c) criteria. The same tests can be employed to both screen for and diagnose diabetes, as well as identify individuals with prediabetes (Chadha *et al.*, 2020). Diabetes may manifest in various clinical scenarios, ranging from seemingly low-risk individuals undergoing glucose testing to those screened based on diabetes risk assessment, and even in asymptomatic patients. Normal glucose tolerance is defined by FPG < 5.6 mmol/L (100 mg/dL), plasma glucose < 7.9 mmol/L (140 mg/dL) after an oral glucose challenge, and HbA1c < 5.7%. Abnormal glucose homeostasis is diagnosed by an impaired fasting glucose (IFG), defined as FPG of 5.6–6.9 mmol/L (100–125 mg/dL), impaired glucose tolerance (IGT) with a plasma glucose level of 7.8–11 mmol/L (140–199 mg/dL) post oral glucose challenge, and a HbA1c of 5.7–6.4%, indicating dysglycemia. While these criteria identify different individuals based on diverse biological mechanisms, alterations in them indicate an elevated risk of developing T2DM and cardiovascular disease. This underscores the need for risk reduction counseling. It is crucial to note that FPG, oral glucose challenge, and HbA1c values are continuous variables, with comorbidity risk increasing continuously. Criteria for overt diabetes diagnosis include FPG ≥ 7.0 mmol/L (126 mg/dL), glucose ≥ 11.1 mmol/L (200 mg/dL) 2 hours after an oral glucose challenge, or HbA1c ≥ 6.5%. A random plasma glucose ≥ 11.1 mmol/L (200 mg/dL) with classic DM symptoms suffices for diagnosis (Ahmad *et al.*, 2022; ElSayed *et al.*, 2023).

1.1.5. Type 2 Diabetes Mellitus

T2DM is increasingly recognized as a complex spectrum of disorders sharing the common characteristic of hyperglycemia (Ahmad *et al.*, 2022). In general, the development of the disease is associated with the dysregulation of carbohydrate, lipid, and protein metabolism, arising from compromised insulin secretion, insulin resistance, or a combination

of both (Chatterjee *et al.*, 2017). The primary cause is the gradual decline in insulin secretion by pancreatic β-cells, typically occurring against a backdrop of pre-existing insulin resistance in skeletal muscles, liver, adipose tissue and hyperinsulinemia (Ahmad *et al.*, 2022; DeFronzo *et al.*, 2015).

After a meal, when blood glucose levels and other metabolite levels rise, pancreatic β-cells release insulin to coordinate the overall regulation of glucose in the body. This well-regulated homeostatic process involves various mechanisms across multiple organs, including the reduction of glucose release from the liver (hepatic glucose output), heightened uptake of glucose by muscle and fat (where it is stored as glycogen), suppression of free fatty acid release from adipocytes (lipolysis), and increased accumulation of lipids in the liver and adipocytes *(James et al., 2021)*. People diagnosed with T2DM exhibit compromised insulin-induced glucose absorption by muscle and adipocytes, as well as impaired insulin inhibition of hepatic glucose output, leading to their classification as "insulin resistant" (**Figure 1**) (Roden and Shulman, 2019). In the early stages of the condition, glucose tolerance remains relatively normal despite the presence of insulin resistance. This is due to compensatory mechanisms where pancreatic β-cells increase insulin output. As insulin resistance and compensatory hyperinsulinemia advance, some individuals experience a failure in sustaining the hyperinsulinemic state in pancreatic islets, leading to impaired glucose tolerance (IGT), characterized by elevated postprandial glucose levels. A decline in insulin secretion and/or an increase in glucagon secretion contribute to heightened hepatic glucose production, resulting in fasting hyperglycemia. Ultimately, the culmination of these mechanisms results in frank β-cell failure, leading to the manifestation of T2DM (Petersen & Shulman, 2018).
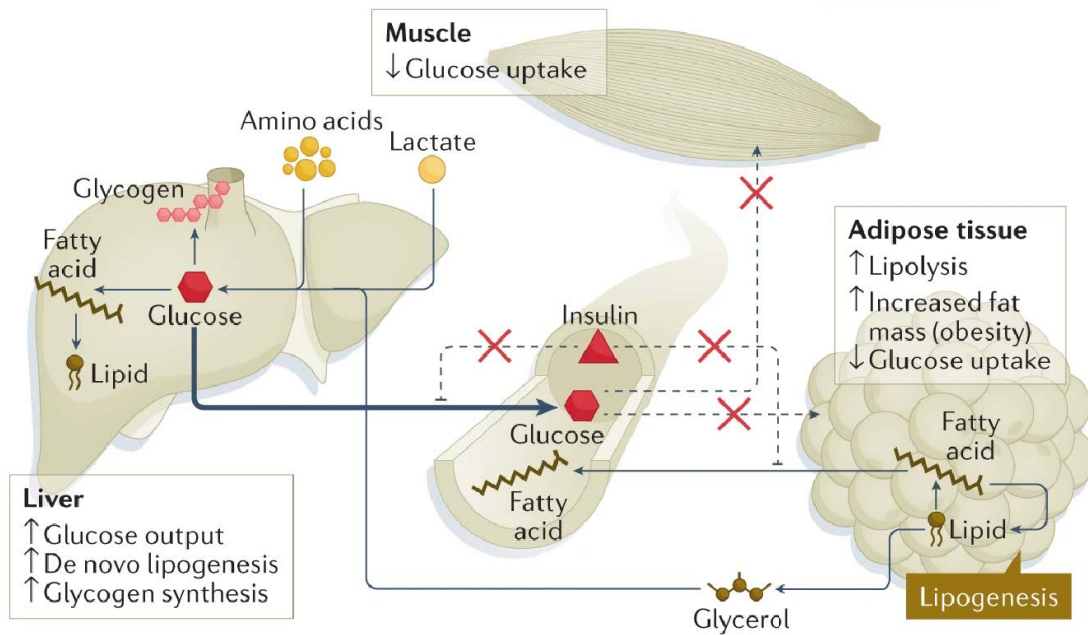
Figure 1. Tissue-specific regulation in insulin resistance.

In individuals with insulin resistance (IR), insulin's effectiveness in controlling hepatic glucose release and promoting glucose absorption by muscle and adipose cells is compromised (dashed lines). This is often accompanied by increased hepatic glucose output, primarily driven by heightened gluconeogenesis. Elevated levels of circulating free fatty acids in IR may result from a decline in insulin's ability to inhibit lipolysis (dashed lines) or the presence of excessive fat mass. Furthermore, insulin-regulated processes, including lipogenesis, remain elevated in IR, potentially contributing to the worsening of insulin resistance (image adapted from James *et al.*, 2021).

Various pathophysiologic mechanisms contribute to the development of T2DM, and their significance varies among individuals. Since 2009, alongside with the conventional trio muscle, liver and β-cells interactions, the pathophysiology of T2DM was linked to defects in 11 interconnected pathways, with hyperglycemia serving as the unifying factor linking them (DeFronzo, 2009; Schwartz *et al.*, 2016) (**Figure 2**).
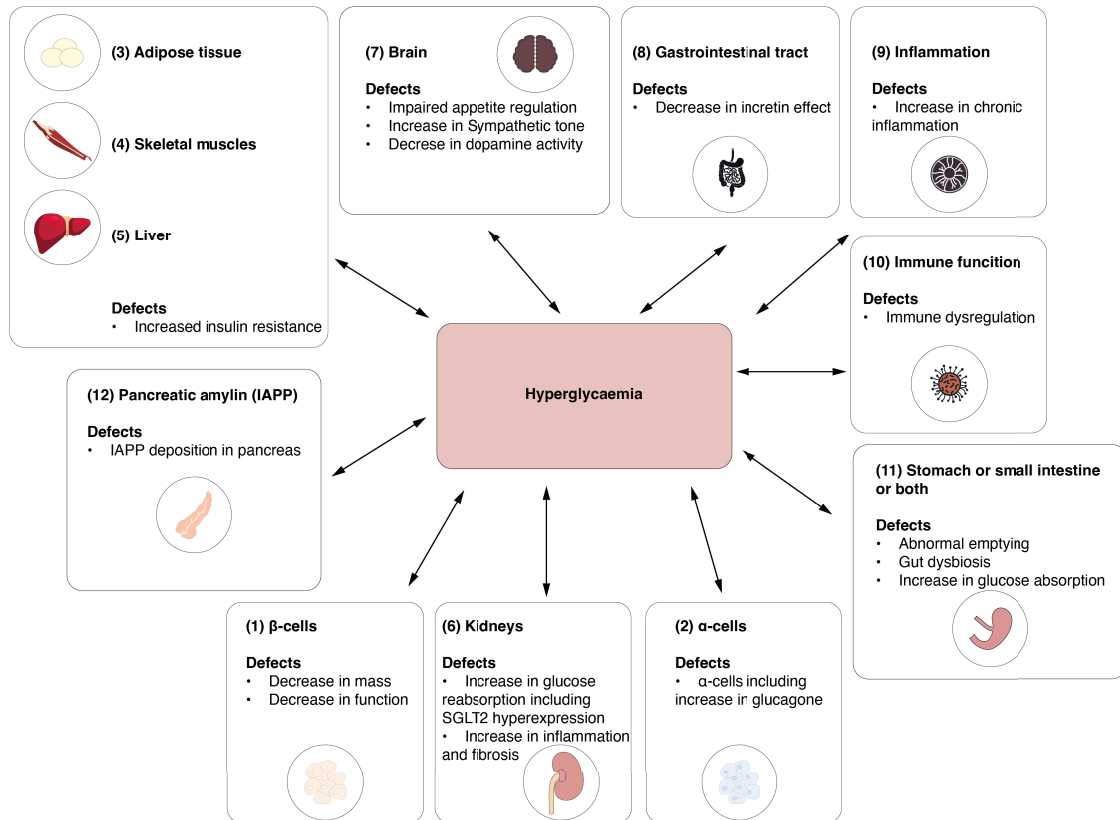
Figure 2. Pathophysiological factors contributing to β-cell failure in T2DM.
Pathophysiological factors contributing to hyperglycemia. The model incorporates 12 different interlocking pathways. IAPP=islet amyloid polypeptide. (image adapted from Ahmad *et al.*, 2022).

1.1.6. Long-term complications of T2DM

The persistent glycemic dysregulation associated with DM is the cause of a series of chronic complications involving multiple organ systems, leading to the high morbidity and mortality associated with the disease (Kasper & Harrison, 2005). Since T2DM often has an extended asymptomatic period of elevated blood sugar levels before diagnosis, patients with this form of diabetes commonly experience complications related to both glucose and insulin resistance at the time of diagnosis. Fortunately, many diabetes-related complications can be prevented or alleviated through proactive management of glycemic, lipid, and blood pressure levels, along with early detection efforts (Ahmad *et al.*, 2022).

Such chronic complications can be divided into vascular and nonvascular, with the former further subdivided into macrovascular (coronary artery disease, peripheral arterial disease, cerebrovascular disease) and microvascular complications (retinopathy, neuropathy, nephropathy). Nonvascular complications encompass infections, skin changes, hearing loss, and an elevated risk of dementia and impaired cognitive function (DeFronzo *et al.*, 2015).

1.1.6.1. Diabetic Nephropathy

Among microvascular complications, the kidney is one of the most sensitive organs. Approximately half of all patients with T2DM and one-third with T1DM, will develop chronic kidney disease (CKD), which in turn leads to end-stage renal disease (ESRD) and requiring renal replacement therapy (Y. Chen *et al.*, 2020a). Although it is suggested that chronic hyperglycemia leads to hemodynamic alterations in the renal microcirculation and structural changes in the glomerulus resulting in diabetic nephropathy (Fineberg *et al.*, 2013a), most of the factors involved still remain to be elucidated. It is clear, however, that progression of diabetic nephropathy involves injury of the renal tubules and glomerulosclerosis.

Traditionally, diabetic nephropathy (DN), also known as diabetic kidney disease (DKD), has been characterized as a progressive condition starting with the increased presence of albumin a protein normally found in the blood. In the early stages of DKD, there may be a gradual leakage of small amounts of albumin into the urine, a condition known as microalbuminuria (30-300 mg per day). As the disease progresses, larger quantities of albumin are excreted into the urine, leading to a stage known as macroalbuminuria or overt nephropathy (> 300 mg per day) (Mogensen *et al.*, 1983) (**Table 1**). By the time clinical manifestations of diabetic nephropathy emerge, including the onset of persistent microalbuminuria, structural damage to the kidneys is often significantly advanced. Various alterations involving the kidneys, such as nodular and diffuse glomerulosclerosis, can both contribute to the development of chronic renal failure (Andy KH Lim, 2014). The progression of diabetic nephropathy is characterized by increasing microalbuminuria, declining glomerular filtration rate (GFR), and the onset or exacerbation of hypertension, along with other diabetes-related conditions (Gross *et al.*, 2005).

Table 1. The stages of diabetic nephropathy (table adapted from Gross *et al.*, 2005).

Stage	Glomerular filtration	Albuminuria	Blood pressure
STAGE 1: Renal hyperfunction	Elevated	Absent	Normal
STAGE 2: Clinical latency	High normal	Absent	
STRAGE 3: Microalbuminuria (incipient nephropathy)	Within the normal range	20-200 µg/min (30-300 mg/day)	
STAGE 4: Macroalbuminuria or persisting proteinuria	Decreasing	> 200 µg/min (> 300 mg/day)	Increased

| **STAGE 5: Renal failure (ESRD)** | Diminished | Massive | Increased |

DN undergoes distinct stages of progression. The nephron experiences functional alterations at the glomerular level, such as glomerular hyperfiltration and hyperperfusion, occurring prior to any clinically measurable changes (Thomas *et al.*, 2015). Following, there is a subsequent occurrence of morphological changes in the glomeruli, detailed as follows:

- **Class I**: Glomerular basement membrane thickening of > 430 nm in men and > 395 nm in women
- **Class II**: Mild (IIa) or severe (IIb) mesangial expansion, with glomeruli exhibiting mild or severe mesangial expansion but lacking nodular sclerosis (Kimmelstiel-Wilson lesions) or global glomerulosclerosis in over 50% of glomeruli.
- **Class III**: Nodular sclerosis (Kimmelstiel-Wilson lesions, first described in 1936), characterized by at least one glomerulus with nodular mesangial matrix increase (Kimmelstiel & Wilson, 1936) without changes described in Class IV.
- **Class IV**: Advanced diabetic glomerulosclerosis, with more than 50% global glomerulosclerosis with or without nodules (Thomas *et al.*, 2015).

Glomerular changes present in DN are summarized in a schematic representation in **Figure 3**.
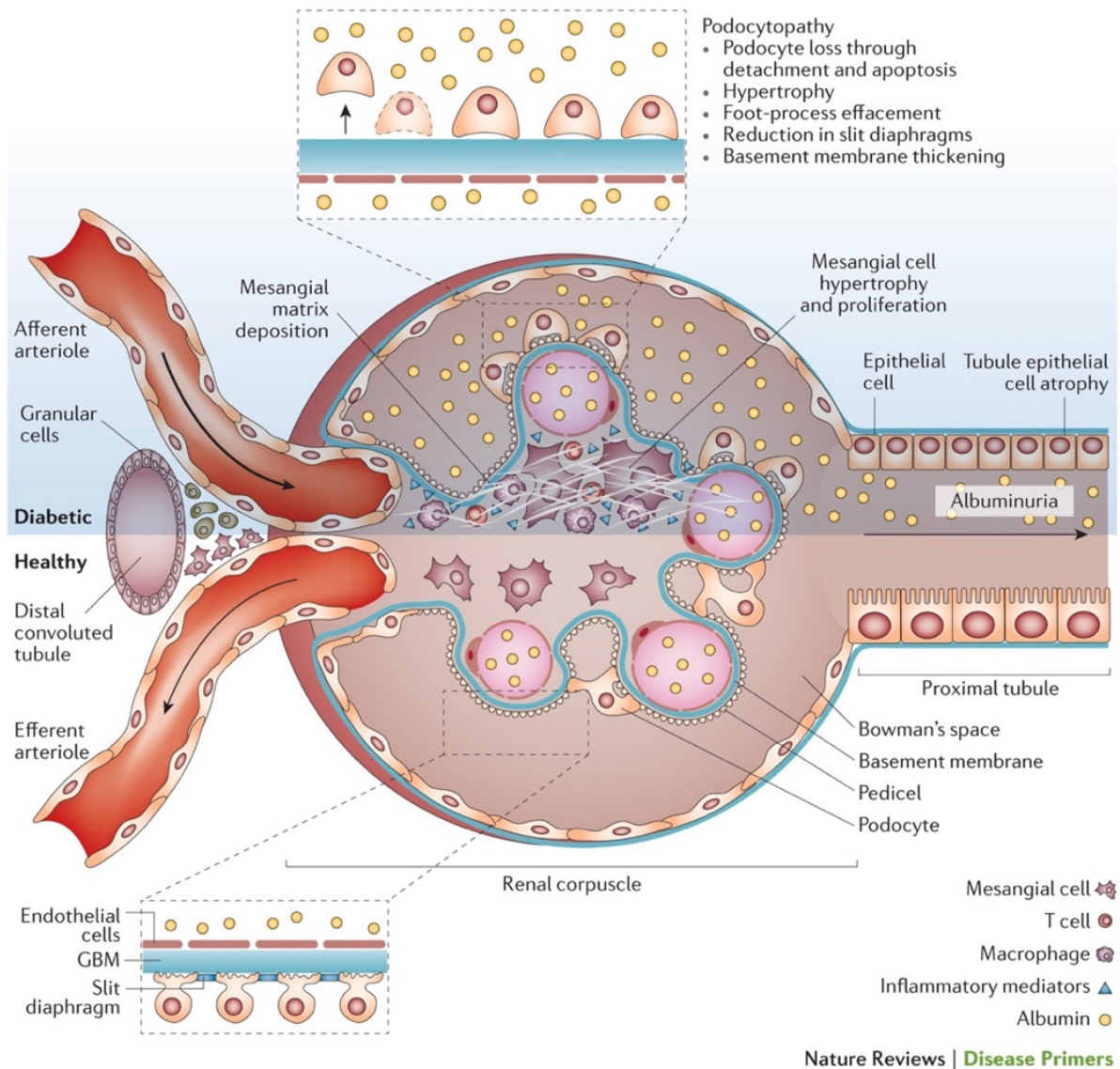
Figure 3. Glomerular alteration in DN.

Morphological and functional alterations to renal glomeruli are one of the hallmarks of DKD. GBM, glomerular basement membrane (image adapted from Thomas *et al.*, 2015).

Even though diabetic nephropathy has mainly been associated with damage at the level of the glomeruli (glomerulosclerosis), tubular changes and damages are also part of the disease. Indeed, the proximal convoluted segment of tubules in the diabetic kidney often exhibits a finely vacuolated appearance, with lipid content discernible in frozen sections, which is indicative of tubular damage (Vallon, 2011). In more advanced stages of the condition, there is evident tubular loss, and atrophic tubules display thickened basement membranes. Glycogen deposits in the epithelial cells of the *pars recta* of the proximal tubule, once considered a characteristic feature of diabetes (Armanni-Ebstein lesions), are now only sporadically observed (Zhou et al., 2013). Additionally, there is an onset of migration of macrophages and other inflammatory cells into the tubulointerstitium (Ziyadeh & Wolf, 2008).

The best studied mechanism extensively involved in tubular damage was identified as ferroptosis (see **Section 1.3**). Although, its well-established role in various pathological conditions, its specific involvement in the pathophysiological progression of diabetic nephropathy has, until recently, remained largely unexplored. However, the current scientific landscape has witnessed a notable surge in literature devoted to unraveling the intricate role of ferroptosis within the context of DKD. Notably, recent studies (Huang *et al.*, 2022; Jin & Chen, 2022; S. Kim *et al.*, 2021; D. Liu *et al.*, 2022; Q. Lu *et al.*, 2023), have contributed significantly to shedding light on the emerging connections between ferroptosis and the complex pathogenesis of DKD. These investigations provide valuable insights that may pave the way for a deeper understanding of the molecular mechanisms involved and potentially open new avenues for targeted therapeutic interventions in managing diabetic nephropathy.

1.1.6.2. Therapies for diabetic nephropathy

Robust management of diabetes, involving the concurrent regulation of glucose, lipids, and blood pressure, coupled with dietary and lifestyle modifications, holds the potential to slow down the progression of established DKD (Andrésdóttir *et al.*, 2014; Gæde *et al.*, 2003; Z. Zhang *et al.*, 2008). In the last years, two class of antidiabetic drugs have also demonstrated promising results in terms of renal protection. The first one comprehends the sodium-glucose cotransporter 2 (SGLT2) inhibitors (DeFronzo *et al.*, 2021). Typically, SGLT2 is responsible for roughly 90% of glucose reabsorption in the renal proximal tubule (Wright *et al.*, 2011). These inhibitors offer benefits such as weight loss, reduced serum uric acid, lowered blood pressure, and mitigated glomerular hyperfiltration, likely associated with natriuresis accompanying glycosuria (Gallo *et al.*, 2015). These outcomes result from increased urinary excretion of glucose and sodium, osmotic diuresis, and an improved tubule-glomerular feedback mechanism (Y. Chen *et al.*, 2020a; Van Bommel *et al.*, 2017). Among the SGLT2 inhibitors, empagliflozin has been proved to have both renal and cardiovascular beneficial effects in patients suffering from T2DM (Wanner *et al.*, 2016; Zinman *et al.*, 2015), effectively slowing kidney disease progression and reducing clinically significant renal events compared to placebo (Wanner *et al.,* 2016). Empagliflozin also demonstrates effectiveness in individuals with heart failure or CKD who do not have type 2 diabetes mellitus (Anker *et al.*, 2021; The EMPA-KIDNEY Collaborative Group, 2023), highlighting the fact that its specific mechanism has, up to now, not been fully comprehended. Recent *in vitro* and *in vivo* findings point towards a role of empagliflozin in the inhibition of one of the major regulated cell death mechanism involved in kidney injury such as ferroptosis (**see Section 1.3.3.**) (Q. Lu *et al.*, 2023). Still its impact on diabetic-related ferroptosis and the underlying mechanisms remain to be elucidated.

A second class of glucose-lowering medication that has recently proved its renal beneficial effects is the one of GLP-1 receptor agonists (RAs). Glucagon-like peptide-1 (GLP-1) belongs to the incretin hormones released from the intestine after food intake and enhances the secretion of insulin (Holst *et al.*, 1987; Mojsov *et al.*, 1987). In type 2 diabetic patients, the incretin effect is diminished or no longer present, however the insulinotropic effects of GLP-1 are preserved, therefore a pharmacological stimulation of GLP-1 receptors results in reduced plasma glucose and improved glycemic control (Nauck *et al.*, 1993, 1998). The GLP-1 RA liraglutide administration in type 2 diabetic patients, not only reduces nonfatal myocardial infarction, nonfatal stroke or death from cardiovascular causes, but also reduces the incidence of new persistent macroalbuminuria and progression of DKD compared to placebo (Mann *et al.*, 2017). Similarly, in another randomized study comprising 3,297 patients with type 2 diabetes, those receiving semaglutide, another GLP-1 analog, demonstrated lower rates of new or worsening nephropathy compared to the placebo group (Marso *et al.*, 2016).

1.1.7. Animal models for diabetic kidney disease

DN poses a significant complication in diabetes mellitus, leading to end-stage renal failure and necessitating treatments like dialysis or transplantation (Y. Chen *et al.*, 2020a). Despite recent therapeutic advancements in therapeutically targeting DKD, recent therapeutic advancements in therapeutically targeting DKD, treatment of DKD and AKI is still mostly symptomatic. Therefore, there's an urgent need to identify the mechanistic basis in DN to prevent kidney failure in diabetic patients, highlighting the necessity for reliable animal models. However, existing murine models, while providing some advantages, have crucial limitations. Indeed, classical mouse models of diabetes (such as db/db, ob/ob, STZ mice) often exhibit features seen in the early stages of human DKD, like mild renal lesions, but manifestations like decreased glomerular filtration rate (GFR), progressive renal insufficiency, glomerulosclerosis, tubular atrophy, or interstitial fibrosis are less frequently observed (Azushima *et al.*, 2018). DN's complex origin involves multiple genes and environmental factors, making it challenging to manipulate all contributors. Efforts have focused on improving existing models or creating new ones, using approaches like backcrossing and genetic modifications. While these models offer an improved disease severity range, still none fully comprise all features observed in human DN (Giralt-López *et al.*, 2020).

Some of these animal models are presented below in order to give a brief overview of the most commonly used models.

1.1.7.1. Diabetic eNOS knockout mouse

Nitric oxide (NO) serves as a vasodilator derived from endothelial cells, playing a crucial role in modulating vascular permeability. In diabetes, there is a disturbance in the activity of vascular endothelial NO synthase (eNOS), and functionally significant polymorphisms in the NOS3 gene contribute to reduce NO production. This decrease in NO production is linked to the progression of advanced nephropathy in individuals with both type 1 and type 2 diabetes (Ksiazek *et al.*, 2003; Zanchi *et al.*, 2000).

Targeting NOS3, the gene responsible for eNOS, induces nephropathic alterations in mouse models of both type 1 diabetes (streptozotocin-induced) and type 2 diabetes (db/db mouse), closely mirroring many aspects of human disease (Nakagawa *et al.*, 2007; Zhao *et al.*, 2006). The systemic depletion of eNOS in a diabetic context allows for the simultaneous examination of vascular and renal pathology within the same animal. In terms of DN characteristics, these mice develop significant albuminuria, reduced glomerular filtration rate, mesangial expansion, thickening of the glomerular basement membrane, arteriolar hyalinosis, mesangiolysis, nodular glomerulosclerosis and tubulointerstitial injury. These features render the eNOS$^{-/-}$ db/db model highly promising for studying the mechanism underlying the progression of DN. Additionally, eNOS knockout mice on a db/db background offer a valuable platform to assess the effectiveness of drug therapies targeting multi-organ pathologies (Mohan *et al.*, 2008). However, there have been no follow-up publications on this model after the first publication (Zhao *et al.*, 2006), that might be attributed to challenges in breeding mice with this combined mutations (Brosius *et al.*, 2009).

To model type 1 diabetes with impaired eNOS activity, diabetic conditions were induced by administering streptozotocin (STZ) injections in eNOS-deficient mice on a C57BL/6 background. These diabetic eNOS mice exhibit notable increases in mesangial expansion, mesangiolysis, and focal sclerosis (Nakagawa *et al.*, 2007). However, the high STZ doses used in this initial study led to high mortality. When lower doses of STZ were used in a follow-up study (Kanetsuna *et al.*, 2007), only a mild DN phenotype was observed, characterized by the absence of significant renal insufficiency and only mild mesangial expansion. Moreover, following investigations demonstrated that the phenotypic features of diabetic glomerulopathy, such as mesangiolysis and mesangial nodule formation, are a consequence of hypertension caused by the depletion of eNOS rather than diabetes (Kosugi *et al.*, 2009).

1.1.7.2. Bradykinin B2 Receptor (B2R) deficient Ins2$^{Akita/+}$ mouse

This mouse model results from the crossing of Akita mice (with a single point mutation in the insulin 2 gene – Ins2C96Y -) and a mouse strain with a targeted deletion of the

bradykinin 2 receptor (B2R) gene. These mice display a substantial four-fold increase in albuminuria and significant mesangial expansion, closely resembling the glomerular alterations characteristic of human diabetic glomerulosclerosis. However, there are no observable changes in the glomerular endothelial cells or podocytes. Additionally, these mice exhibit mitochondrial DNA damage in the kidneys and other tissues, suggesting a generalized aging process (Kakoki *et al.*, 2004). In contrast, Akita mice with functional B1 and/or B2 receptors are not considered a robust model for nephropathy (Brosius *et al.*, 2009).

1.1.7.3. Decorin-deficient streptozotocin diabetic mouse

A deficiency in decorin is linked to accelerated kidney damage, as this protein plays a role in inflammatory and fibrosis processes by binding to growth factors such as transforming growth factor β (TGF-β), platelet-derived growth factor (PDGF), and epidermal growth factor (EGF) (Schönherr *et al.*, 2004, 2005). In decorin deficient C57BL/6J mice induced with low-dose STZ for type 1 diabetes, advanced diabetic nephropathy (DN) manifests due to the continuous stimulation of TGF-β-mediated processes, including fibrosis and inflammation. These animals exhibit elevated urine albumin excretion and a decline in renal function. Additionally, they experience an increase in mesangial matrix expansion and kidney inflammation, characterized by macrophage infiltration and up-regulation of Nox4. However, nodular sclerosis or tubulointerstitial lesions are not observed (K. J. Williams *et al.*, 2007).

1.1.7.4. NONcNZO mouse

The NONcNZO mouse model is a congenic strain derived from a cross between the Nonobese Nondiabetic (NON) mouse and the New Zealand Obese (NZO) mouse, presenting a model of polygenic type 2 diabetes. Unlike mice with null mutations in a single gene that lead to morbid obesity, this mouse model experiences milder obesity due to the interaction of numerous genes with relatively small effects (Leiter and Reifsnyder 2004). Around 8 months of age, NONcNZO mice develop notable and progressively increasing albuminuria. While their glomerular histopathology is remarkably abnormal, it displays features that, in addition to glomerulosclerosis, are atypical for diabetic nephropathy (Leiter & Reifsnyder, 2004; Reifsnyder & Leiter, 2002). One of the major limitations include the high probability of these mice to develop autoimmune disease and consequently circulating antibodies to native and single-strained DNA (Haskell *et al.*, 2002)

1.1.7.5. OVE26 mouse

The OVE26 (Overbeek Overexpression model with transgene insertion at position 26) mouse, represents an overexpression transgenic model on a Friend leukemia virus B (FVB) mouse background of early onset of type 1 diabetes. These mice develop diabetes within the initial weeks of life due to β-cell toxicity caused by the overexpression of the calmodulin gene controlled by the insulin promoter. At 9 months of age, these mice exhibit progressively increasing albuminuria alongside hypalbuminemia, elevated blood pressure, and a declining glomerular filtration rate (GFR). The mice undergo progressive enlargement of glomeruli, with diffuse and nodular expansion of the mesangial matrix, tubulointerstitial fibrosis, and thickening of the glomerular basement membrane (Zheng *et al.*, 2004).

A significant limitation of this mouse model involves the necessity for the mutation to be expressed in the FVB background to obtain the desired phenotypic features. Indeed, introducing the same transgene on a C57BL/6 background results in only subdued albuminuria, reduced mesangial expansion, and fibrosis. This specific strain dependence complicates the introduction of additional genetic mutations from different mouse strains into this model (Brosius *et al.*, 2009). Furthermore, these mice experience a reduction in podocyte number and density, primarily occurring late in the disease course (as evaluated at days 60, 150, and 450), following rather than preceding other diabetic nephropathy manifestations (Teiken *et al.*, 2008). Finally, challenges related to mouse viability have also been reported (Reiniger *et al.*, 2010).

1.1.7.6. Black and tan, brachyuric (BTBR) ob/ob mouse

Another strong model for DN is the crossbreed of black and tan Brachyuric (BTBR) mouse strain, characterized by insulin resistance with the *ob/ob*, leptin mutation (Hudkins *et al.*, 2010). This model shows severe type 2 diabetes, insulin resistance, and progressive renal damage. These mice exhibit proteinuria by four weeks of age, followed by hypertrophy and accumulation of mesangial matrix at eight weeks, glomerular lesions at 20 weeks, and an increase in glomerular basement membrane (GBM) thickness at 22 weeks. Additional observations include focal arteriolar hyalinosis, diffuse mesangial sclerosis, mesangiolysis, mild focal interstitial fibrosis, and loss of podocytes (Clee *et al.*, 2005). This mouse model presents notable limitations, including the infertility of the animals. This infertility complicates breeding in sufficient numbers for interventional studies, making it both labor-intensive and expensive. Additionally, the fact that the BTBR strain is not commonly studied adds to the

challenges, making the introduction of genetic mutations in these mice a complex process that requires extensive backcrossing strategies (Kong *et al.*, 2013).

Although extensive efforts have been made to improve existing models of DN or create new ones, it is crucial to recognize that most of these models come with their own set of limitations, that are difficult to overcome. Recognizing these limitations across different mouse models has prompted the need for a new and more effective strategy. The growing understanding of the entero-insular axis and the role of the incretin hormones in the development of diabetes mellitus has paved the way for the creation of a novel mouse model known as GIPR^{dn}.

1.1.8. Incretin hormones and GIPR^{dn} diabetic mouse model

The GIPR^{dn} transgenic mouse model express a dominant-negative overexpression of the GIP (glucose-dependent insulinotropic polypeptide) receptor (GIPR^{dn}), at the level of the pancreatic β-cells, leading to the onset of severe diabetes mellitus (Herbach *et al.*, 2005). GIP, together with GLP-1, is an incretin hormone belonging to the enteroinsular axis. This axis encompasses hormonal, neural and substrate stimulation, representing all signals originating from the gastrointestinal tract that reach the endocrine pancreas where they stimulate, reduce or modify the secretion of insulin, glucagon, somatostatin and pancreatic polypeptide (PP) (Brown, 1988). Oral glucose triggers greater insulin secretory responses than intravenous glucose, even though both induce similar levels of glycaemia in healthy individuals. This phenomenon is denoted incretin effect (Nauck & Meier, 2016).

Both GIP and GLP-1 are secreted from specialized entero-endocrine cells in the small intestine mucosa. GLP-1 is secreted by L-cells residing throughout the intestine and increase in abundance towards the ileum and colon (Eissele *et al.*, 1992), while GIP is produced by the K-cells, which reside mainly in the duodenum and upper jejunum (Buchan *et al.*, 1978). The two hormones have their specific G-protein (GTP binding protein)-coupled receptors (GPCR) expressed in high numbers at the level of the pancreatic β-cells. Both receptors are linked to a G protein. The α subunit S ($G_{\alpha S}$) of the G protein, initiates the activation of adenylate cyclase and the formation of cAMP. Subsequent signaling, including the activation of protein kinase A and the EPAC2 pathway, is responsible for insulin granule exocytosis (Holst, 2019). Alongside their insulinotropic effect, both GIP and GLP-1 also activate the transcription of genes necessary for insulin production. Additionally, they may induce trophic actions on young β-cells, promoting their proliferation. Moreover, GLP-1 exerts glucoregulatory actions via slowing

of gastric emptying and glucose-dependent inhibition of glucagon secretion (Holst, 2019; Nauck & Meier, 2018).

Upon release, GIP and GLP-1 are rapidly (5-7 min in humans), degraded by dipeptidylpeptidase-4 (DPP)-4, a ubiquitous enzyme. DPP-4 cleaves the N-terminal dipeptide from these incretin hormones, rendering them inactive (Kieffer *et al.*, 1995; Mentlein *et al.*, 1993). This process is a crucial regulatory step in controlling the duration and magnitude of the incretin effect.

In patients with T2DM, the incretin effect is severely reduced or absent. Indeed, in these patients the secretion of GIP is near normal, but its effect on insulin secretion, particularly in the late phase, is severely impaired. GLP-1 secretion, is impaired too, but the hormone retains its insulinotropic and glucagon-suppressive actions, although its potency is decreased compared to healthy individuals (Knop *et al.*, 2012; Muscelli *et al.*, 2008). For these reasons, incretin-based therapies, including GLP-1 RA (Mann *et al.*, 2017; Marso *et al.*, 2016) (see **Section 1.1.6.2**) and DPP-4 inhibitors (Vardarli *et al.*, 2011, 2014), have become one of the leading principles in drug treatment for T2DM.

1.1.8.1.   Generation of GIPR^{dn} diabetic mouse model

The overexpression of a dominant negative version of the human GIP receptor (GIPR^{dn}), under the control of a rat proinsulin 2 gene promoter on a CD1 mouse background, induces an early onset of DM, in parallel with premature onset of DKD in mice (Herbach *et al.*, 2005, 2009). The targeted mutation of the human GIP receptor aimed at maintaining GIP binding affinity while disabling its capacity for signal transduction, resulting in the creation of a dominant negative GIP receptor, which is referred to as GIPR^{dn}. To achieve this, the crucial third intracellular G-protein coupling loop of the GIP receptor, vital for signal transduction, was specifically altered in the cDNA of the human GIP receptor (see **Figure 4**). This modification involved introducing a point mutation at nucleotide position 1019 (Ala340Glu on amino acid level) and a deletion of 24 base pairs coding for 8 amino acids (nucleotide positions 955-978, which is amino acid positions 319-326). These changes were implemented using oligonucleotides containing the specific mutations.
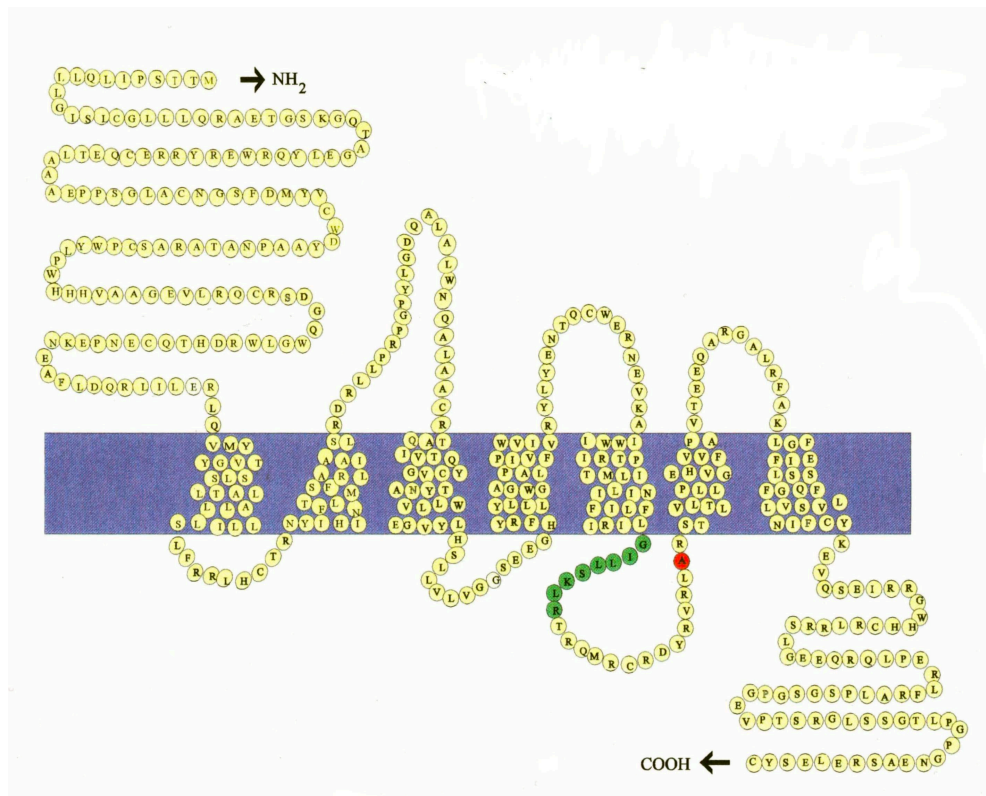
Figure 4. The amino acid sequence of the human GIP receptor and the locations subjected to targeted mutations.

Specifically, the cDNA of the human GIP receptor underwent mutations in the area encoding the third intracellular loop, involving the introduction of a point mutation resulting in an amino acid change at amino acid position 340 (Ala to Glu, marked in red) and a deletion of 8 amino acids at positions 319-326 (highlighted in green) (Volz *et al.*, 1995).

The modified cDNA of the human GIP receptor was inserted into the XbaI/HindIII site within the RIP1 vector, which includes the rat proinsulin gene promoter II. This vector has proven effective in achieving β-cell specific expression of cDNA constructs in transgenic mice (Hanahan, 1985). Fragments of the vector were obtained through SalI/SspI digestion, and the resulting fragments were separated using an ethidium bromide-free gel. Following additional purification and dialysis, the RIP1-GIPR[dn] cDNA construct was injected into the male pronucleus of mouse zygotes from CD1 females at a final concentration of 400 copies/pl. Subsequently, these zygotes were transferred into cycle-synchronized females.

These GIPR[dn] transgenic mice exhibit early disturbances in pancreatic islet development, characterized by significantly reduced β-cell mass, altered islet composition, and diminished islet neogenesis (Herbach *et al.*, 2005). Moreover, they manifest decreased insulin secretion, leading to early-onset diabetes mellitus without concurrent obesity or insulin resistance (Herbach *et al.*, 2008). Glucosuria is observed in GIPR[dn] transgenic mice between 14 and 21 days of age, and by 30 days, they exhibit markedly elevated blood glucose levels

and absolute insulin deficiency (Herbach *et al.*, 2005). The development, dimensions, and histological patterns of kidney lesions observed in GIPR[dn] transgenic mice bear similarities to diabetes-associated kidney injury in humans, to an extent not observed in any of the previous mouse models, establishing them as a promising animal model for studying the onset and progression of diabetic nephropathy for the first time (Herbach *et al.*, 2009).

1.2. Regulated cell death

Regulated cell death (RCD) processes, play a fundamental role in the pathogenesis of DN, contributing significantly to nephron loss and ultimately culminating in ESRD. Understanding and targeting these processes may offer potential new approaches for therapeutic intervention in mitigating the devastating impact of DN on kidney function.

Cell death is a fundamental process in multicellular organisms, crucial for development, tissue homeostasis, and immune responses. Historically, apoptosis has been considered the primary mechanism of programmed cell death. However, recent years have witnessed a paradigm shift with the discovery and recognition of various forms of regulated necrosis (RN) as essential contributors to cell demise (Galluzzi *et al.*, 2018). RN refers to a group of programmed cell death pathways that, unlike apoptosis, exhibit features of necrosis, such as plasma membrane rupture and inflammation. The disruption of the plasma membrane can be caused either through traumatic events or RCD. This phenomenon is crucial for maintaining homeostasis and, in certain instances, enables adaptation to stress stimuli (Tonnus, Belavgeni, *et al.*, 2021a). Under physiological or pathophysiological conditions *in vivo*, necrosis can lead to tissue dysfunction and the release of molecules known as damage-associated molecular patterns (DAMPs) (Sarhan *et al.*, 2018; Tonnus *et al.*, 2019). The subsequent release of DAMPs has the capacity to modulate the immune system, triggering an immune response known as necroinflammation, a process that is gaining increasing relevance (Maremonti *et al.*, 2022).

Key forms of regulated necrosis include among others necroptosis, pyroptosis, and ferroptosis, each characterized by distinct molecular and biochemical mechanisms (**Figure 5**). Briefly, necroptosis is a form of regulated necrosis driven by receptor-interacting protein kinase 1 (RIPK1) and RIPK3. The formation of the necrosome, a signalling platform, triggers phosphorylation of mixed lineage kinase domain-like protein (MLKL), leading to plasma membrane permeabilization (Linkermann & Green, 2014; Oberst *et al.*, 2011). Pyroptosis is an inflammatory form of regulated necrosis triggered by inflammasomes. Activation of caspase-1 or caspase-11 leads to gasdermin D (GSDMD)-mediated plasma membrane rupture and release of pro-inflammatory cytokines (Shi *et al.*, 2017). While necroptosis and

pyroptosis can be referred to as caspase-controlled systems (Tonnus, Gembardt, *et al.,* 2018), ferroptosis is a completely different form of RCD. Indeed, this form of cell death is characterized by an iron-dependent accumulation of lipid peroxides, leading to oxidative damage and cell membrane disruption. Unlike apoptosis or necroptosis, ferroptosis involves the dysregulation of the cellular redox balance and lipid metabolism (Dixon *et al.*, 2012a; Stockwell, Friedmann Angeli, *et al.,* 2017). **Figure 5** provides schematic illustrations of the various regulated cell death pathways. More information on Ferroptosis can be found in **Section 1.3.**.
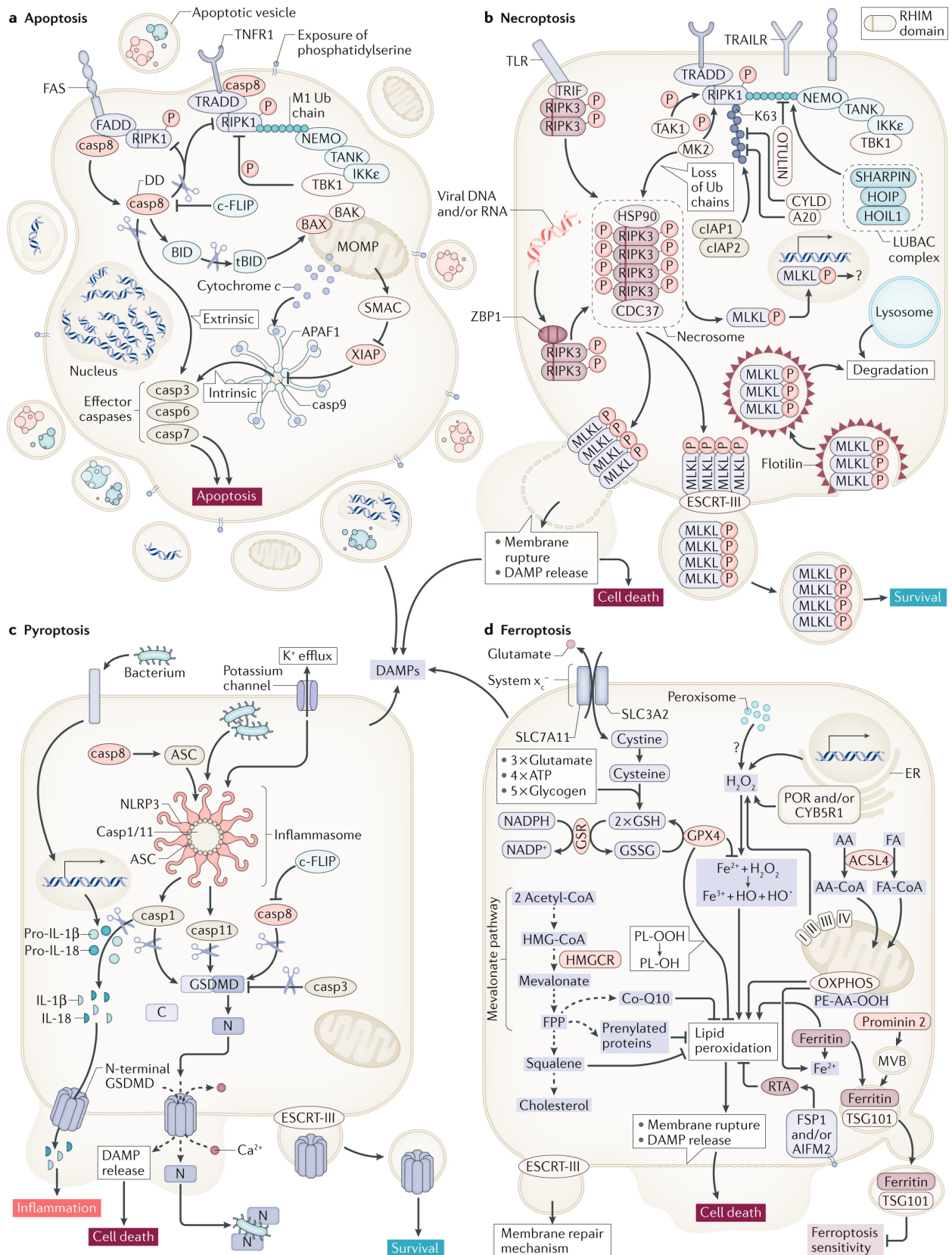
Figure 5. The regulated cell death pathways.

A. Apoptosis, a non-inflammatory process mediated by caspases, involves intrinsic and extrinsic pathways that can be triggered by death receptors like the tumour necrosis factor receptor family 1 (TNFR1). Caspase cleavages, initiated by caspase 8 (casp8), activate effector caspases (casp3,

6, and 7). In the intrinsic pathway, mitochondrial outer membrane permeabilization (MOMP) occurs. B. Necroptosis, a kinase-mediated pathway, relies on RIPK1 and RIPK3, forming the necrosome. RIPK3 phosphorylates MLKL, leading to plasma membrane rupture. This can be countered by the ESCRT-III complex. C. Pyroptosis, distinct from apoptosis, involves inflammasomes activating caspases 1, 4, and 11. This cleaves pro-IL-1β, pro-IL-18, and GSDMD, forming pores in the plasma membrane and thus releasing pro-inflammatory cytokines. D. Ferroptosis, an iron-dependent form of regulated cell death, is characterized by plasma membrane lipid peroxidation causing its rupture. Lipid peroxidation is prevented by glutathione peroxidase 4 (GPX4) in a GSH-dependent manner. Other molecules, such as the oxidoreductase ferroptosis-supressing protein 1 (FSP1), also known as apoptosis inducing factor mitochondria associated 2 (AIFM2) prevent the lipid peroxidation upon myristoylation-dependent recruitment to the plasma membrane in a GSH-independent manner. Abbreviations: casp, caspase; DAMP, damage-associated molecular pattern; DD, death domain; DED, death effector domain; ER, endoplasmic reticulum; FA, fatty acid; GSDMD, gasdermin D; MLKL, mixed lineage kinase domain-like protein; PL-OH, phospholipid alcohol; PL-OOH, phospholipid hydroperoxide; RIPK1, receptor-interacting protein kinase 1; RIPK3, receptor-interacting protein kinase 3; RTA, radical trapping antioxidant (Image source: W Tonnus *et al.*, 2021).

1.3.   Ferroptosis

Introduced in 2012 by Dixon and colleagues, ferroptosis stands out as a distinct cell death mechanism separate from conventional apoptosis and regulated necrosis pathways (Dixon *et al.*, 2012). The discovery of this non-apoptotic form of regulated cell death dates back to the early 2000s. In 2003, Stockwell and colleagues conducted a high-throughput screening of over 20,000 small molecules for their ability to kill tumor cells, revealing the compound erastin. This compound induced a non-apoptotic cell death dependent on oxidative stress and cellular iron levels (Dolma *et al.*, 2003; Yagoda *et al.*, 2007). Subsequently, in 2008, a second small molecule capable of inducing the same form of cell death (RSL3) was discovered through a similar approach (Yang & Stockwell, 2008). Concurrently, the involvement of GPX4 and system X_c^- in both the induction and prevention of this novel non-apoptotic cell death was identified (Banjac *et al.*, 2008; Seiler *et al.*, 2008). In 2012, the term ferroptosis was finally coined, referring to a unique form of cellular demise that relies on iron-dependent lipid peroxidation, leading to plasma membrane rupture (Dixon *et al.*, 2012; Stockwell *et al.*, 2017).

1.3.1   Mechanism of ferroptosis

In vitro studies have shown that ferroptosis initiation is independent of death receptors or DNA sensors (Riegman *et al.*, 2019). Reactive oxygen species (ROS) can result from iron-catalyzed reactions, also called Fenton reactions, potentially leading to lipid peroxidation.

Under normal healthy conditions, cellular anti-redox systems typically prevent this process (Tonnus *et al.*, 2019). Failure of these systems leads to plasma membrane oxidation and rupture through poorly understood mechanisms (Dixon *et al.*, 2012b; Dixon & Stockwell, 2014). For these reasons, ferroptosis is a form of cell death that necessitates constant surveillance by endogenous repair and protection systems. In essence, ferroptosis can be viewed as a form of regulated cell death that requires continuous monitoring and maintenance rather than an event that needs explicit activation. Yet, the specific signal instigating ferroptosis *in vivo* remains uncertain (Katikaneni *et al.*, 2020), marking one of the most pivotal research areas in the field of ferroptosis. The mechanisms underlying ferroptosis are schematically depicted in **Figure 6.**

The initiation of lipid peroxidation in ferroptosis involves removal of a bisallylic hydrogen atom, situated between two carbon–carbon double bonds, from polyunsaturated fatty acid (PUFA) moieties in phospholipids (PUFA-PLs) within lipid bilayers. This process leads to the creation of a carbon-centered phospholipid radical (PL•), which subsequently reacts with molecular oxygen, consequently giving rise to a phospholipid peroxyl radical (PLOO•) (Conrad & Pratt, 2019; X. Jiang *et al.*, 2021). The susceptibility to peroxidation depends on the strength of carbon-hydrogen bonds (Yin *et al.*, 2011).

PUFAs, known for their vulnerability due to weak C–H bonds between adjacent C=C double bonds, are particularly sensitive to free radicals like reactive oxygen species (ROS). This sensitivity initiates a chain reaction, resulting in the formation of complex oxidized products such as peroxyl radicals, especially in PUFAs with more double bonds. This chain reaction can persist by interacting with another molecule or even with the initiating molecule itself (X. Jiang *et al.*, 2021). The ongoing process eventually generates various secondary products, including breakdown products of lipid peroxides and oxidized and modified proteins. Ultimately, the chain reaction may compromise membrane integrity, potentially leading to the rupture of organelle and/or cell membranes. (Conrad & Pratt, 2019; Yin *et al.*, 2011). The first ferroptosis drivers to be identified were Acyl-CoA Synthetase Long Chain Family Member 4 (ACSL4), and lysophosphatidylcholine acyltransferase 3 (LPCAT3), both involved in facilitating the incorporation of PUFAs into lipid membranes (Dixon *et al.*, 2015; Kagan *et al.*, 2017). ACSL4 ligates preferably long-chain PUFAs with coenzyme A, which can then be used to generate esterified lysophospholipids by LPCAT3 (or other protein family members), thus increasing the pool of long-chain PUFAs in lipids and membranes (Conrad & Pratt, 2019; X. Jiang *et al.,* 2021). Consequently, loss of these genes leads to a resistance against ferroptosis (Dixon *et al.*, 2015; Doll *et al.*, 2017).

On a molecular level, the GPX4-GSH-cysteine axis constitutes a critical cellular defense mechanism against oxidative stress and is essential in regulating ferroptosis (Seibt *et al.*, 2019). At the core of this axis are three key components: glutathione peroxidase 4 (GPX4), glutathione (GSH), and cysteine. Upstream of the axis there is the system X_c^- (Bannai & Kitamura, 1980), a highly specific co-transporter for cystine, the oxidized form of cysteine, and cystathionine at an exchange ratio of 1:1M with glutamate (Seibt *et al.*, 2019). Elevated glutamate levels inhibit system Xc- and trigger ferroptosis (Dixon *et al.*, 2012b). Upon uptake by system X_c^-, cystine undergoes reduction to cysteine through the action of GSH and/or thioredoxin reductase 1 (TXRND1). Subsequently, cysteine is utilized for GSH biosynthesis (Conrad & Pratt, 2019). Pivotal studies on system X_c^- demonstrated how its inhibition via small molecules, such as erastin, directly triggers ferroptotic cell death (Dolma *et al.*, 2003a; Yagoda., 2007), while the genetic overexpression of its light chain protects cells from ferroptosis (Banjac *et al.*, 2008).

Cysteine is a rate-limiting precursor for GSH synthesis. Therefore, the cell has alternative sources for providing cysteine such as the transsulfuration pathway. In this pathway, enzymes like cystathionine beta-synthase (CBS) and cystathionine gamma-lyase (CSE) play pivotal roles in converting homocysteine into cysteine, starting from methionine. CBS catalyzes the formation of cystathionine from homocysteine and serine, while CSE facilitates the subsequent conversion of cystathionine to cysteine (Stockwell, 2022). The transsulfuration pathway is emerging to be a determinant in conferring resistance to ferroptosis. Depletion of CBS, CSE, or cysteinyl-tRNA synthase (CARS, another integral player in the pathway) heightens sensitivity to ferroptosis, while their genetic overexpression protects cells against erastin-induced ferroptosis (Hayano *et al.*, 2016; N. Liu *et al.*, 2020; L. Wang *et al.*, 2018).

The selenoprotein GPX4 is the major enzyme catalyzing the detoxification of PLOOHs within mammalian cell membranes (Ingold *et al.*, 2018; Stockwell, Angeli, *et al.*, 2017). Its function involves reducing lipid hydroperoxides to their corresponding alcohols, thus preventing the uncontrolled propagation of oxidative damage (X. Jiang *et al.*, 2021). For this process to occur efficiently, GPX4 relies on the availability of GSH (Sarhan *et al.*, 2018). Glutathione, a tripeptide composed of glutamate, cysteine, and glycine, serves as both a critical antioxidant and a cofactor for GPX4. GSH directly interacts with GPX4 by donating electrons to facilitate the reduction of lipid hydroperoxides. During this reaction, GSH undergoes oxidation to form glutathione disulfide (GSSG). The recycling of GSH from GSSG is ensured by the enzyme glutathione reductase, which maintains a continuous supply of reduced glutathione (X. Jiang *et al.*, 2021; Seibt *et al.*, 2019; Stockwell, Angeli, *et al.*, 2017).

The metabolism-driven depletion of GSH results in an increase in intracellular NADPH levels. Particularly in specific cell types such as renal tubular cells, gap junctions and tight junctions facilitate the free diffusion of NADPH through the cytoplasm of interconnected cells. Depletion of GSH or NADPH has adverse effects on GPX4 function and disrupts its role in reducing continuously generated peroxidized lipids (Belavgeni *et al.*, 2020; Maremonti *et al.*, 2022). As a consequence, GPX4 acts as a counterbalance to Fenton reactions, maintaining homeostasis alongside low intracellular levels of H_2O_2. Both enzymatic inhibition (Shimada *et al.*, 2016a; Yang & Stockwell, 2008), and genetic degradation of GPX4 (Friedmann Angeli *et al.*, 2014a; Seiler *et al.*, 2008) trigger ferroptosis. Moreover, GPX4 deficiency is embryonically lethal in mice (Ingold *et al.*, 2018).

Additional GPX4-independent mechanisms for ferroptosis surveillance include FSP1 and the Thioredoxin (TRX) system. FSP1 has demonstrated its ability to protect cells from ferroptosis induced by GPX4 inhibition or genetic deletion (Bersuker *et al.*, 2019; Doll *et al.*, 2019). FSP1 is known to be myristoylated and associates with various cellular membranes, the Golgi apparatus, and perinuclear structures (Elguindy & Nakamaru-Ogiso, 2015). The protective action of FSP1 against lipid peroxidation and ferroptosis is attributed to its NADH:ubiquinone (coenzyme Q10) oxidoreductase activity. Through this activity, FSP1 reduces ubiquinone or its partially oxidized form, semihydroquinone, generating ubiquinol. Ubiquinol can directly reduce lipid radicals, thereby terminating lipid autoxidation. Alternatively, FSP1 may indirectly contribute to this process by regenerating oxidized α-tocopheryl radical (vitamin E), a potent natural antioxidant (Bersuker *et al.*, 2019; Doll *et al.*, 2019). Interestingly, in contrast to GPX4 deficient mice (Ingold *et al.*, 2018), FSP1 knockout mice are not embryonically lethal (Bersuker *et al.*, 2019).

Running parallel to the cysteine-GSH-GPX4 axis and FSP1 oxidoreductase, the TRX system comprising NADPH, TXNRD1, and TRX1, serves a crucial role as a cellular antioxidant system (J. Lu & Holmgren, 2014). TRX1, a ubiquitous 12 kDa oxidoreductase, is pivotal in regulating the protein dithiol-disulfide balance through its disulfide reductase activity. TRX1 utilizes electrons from NADPH, which are transferred by thioredoxin reductase, to reduce disulfide bonds in target proteins and thus operates as a mediator in protein reduction via a thiol-disulfide exchange mechanism. Simultaneously, the TRX system contributes electrons to thiol-dependent peroxidases, including peroxiredoxins, enabling a swift reaction to eliminate reactive oxygen and nitrogen species. This reduction of disulfide bonds is indispensable for preserving cellular redox homeostasis and preventing oxidative damage (Arnér & Holmgren, 2000; J. Lu & Holmgren, 2014). Inhibiting the enzymatic activity of TRX1 via the small molecule ferroptocide results in a ferroptosis-like cell death in various cancer cells that can be prevented

via pretreatment with known ferroptosis inhibitors (Llabani *et al.,* 2019). However, there is no direct evidence linking ferroptocide to lipid peroxidation. Moreover, the inhibition of TXNRD1 has been considered as a therapeutic strategy to selectively eliminate cancer cells with an elevated reliance on managing oxidative stress (Stafford *et al.,* 2018). This approach of specifically inhibiting TXNRD1 is suggested to enhance the susceptibility of cancer cells to additional disruptions that amplify oxidative stress (Harris *et al.,* 2015). A major negative regulator of the thioredoxin system is mediated by thioredoxin interacting protein (TXNIP). TXNIP also known as Vitamin D3 upregulated protein 1 (VDUP1) or Thioredoxin Binding Protein (TBP-2) (Nishiyama *et al.,* 1999). TXNIP is a relatively small protein, typically composed of approximately 391 amino acids in humans. It consists of several functional domains that contribute to its intricate roles within cellular processes. The primary structural feature of TXNIP is the thioredoxin (Trx)-binding domain, which enables its interaction with thioredoxin. The binding of TXNIP to thioredoxin is crucial for its regulatory function, as it inhibits the antioxidant activity of thioredoxin, leading to an increase in cellular oxidative stress (Hwang *et al.,* 2014). In addition to its TXN-regulatory role, TXNIP has emerged as a key player in cellular energy metabolism and glucose homeostasis. Notably, hyperglycemia has been demonstrated to induce AMPK-dependent TXNIP degradation to drive GLUT1 and GLUT4 incorporation into the plasma membrane, protecting the cytosol from glucose overload (Waldhart *et al.,* 2017; N. Wu *et al.,* 2013). Interestingly, TXNIP has been linked to the activation of the nucleotide-binding oligomerization domain (NOD)-like receptor protein-3 (NLRP3) inflammasome and the stimulation of another form of cell death, pyroptosis (He *et al.,* 2015; Oslowski *et al.,* 2012). Moreover, TXNIP has been associated with both CKD and DN in both human patients (Park *et al.,* 2022) and mice (Shah *et al.,* 2015).

Other oxidoreductases such as cytochrome P450 oxidoreductase (POR) have been proposed to have a role in initiating lipid peroxidation. Upon receiving electrons from POR with NADPH as an electron donor, downstream electron acceptors like cytochrome P450 and CYB5A undergo reduction. This reduction may subsequently trigger lipid peroxidation either directly or indirectly by removing hydrogen from PUFAs or by reducing ferric iron (Fe^{3+}) to its ferrous form (Fe^{2+}). The reciprocal conversion between ferric and ferrous iron is crucial for the Fenton reaction and lipid peroxidation (Y. Zou, Li, *et al.,* 2020).

There is growing evidence indicating the participation of additional signaling pathways in both the surveillance and sensitization of ferroptosis such as Nuclear factor erythroid 2-related factor 2, hypoxia pathway and AMP-activated protein kinase signaling (X. Jiang *et al.,* 2021; Stockwell, 2022). Even though exploring all individual molecules and pathways in detail

is beyond the scope of this thesis, in the following sections two emerging pathways are briefly discussed.
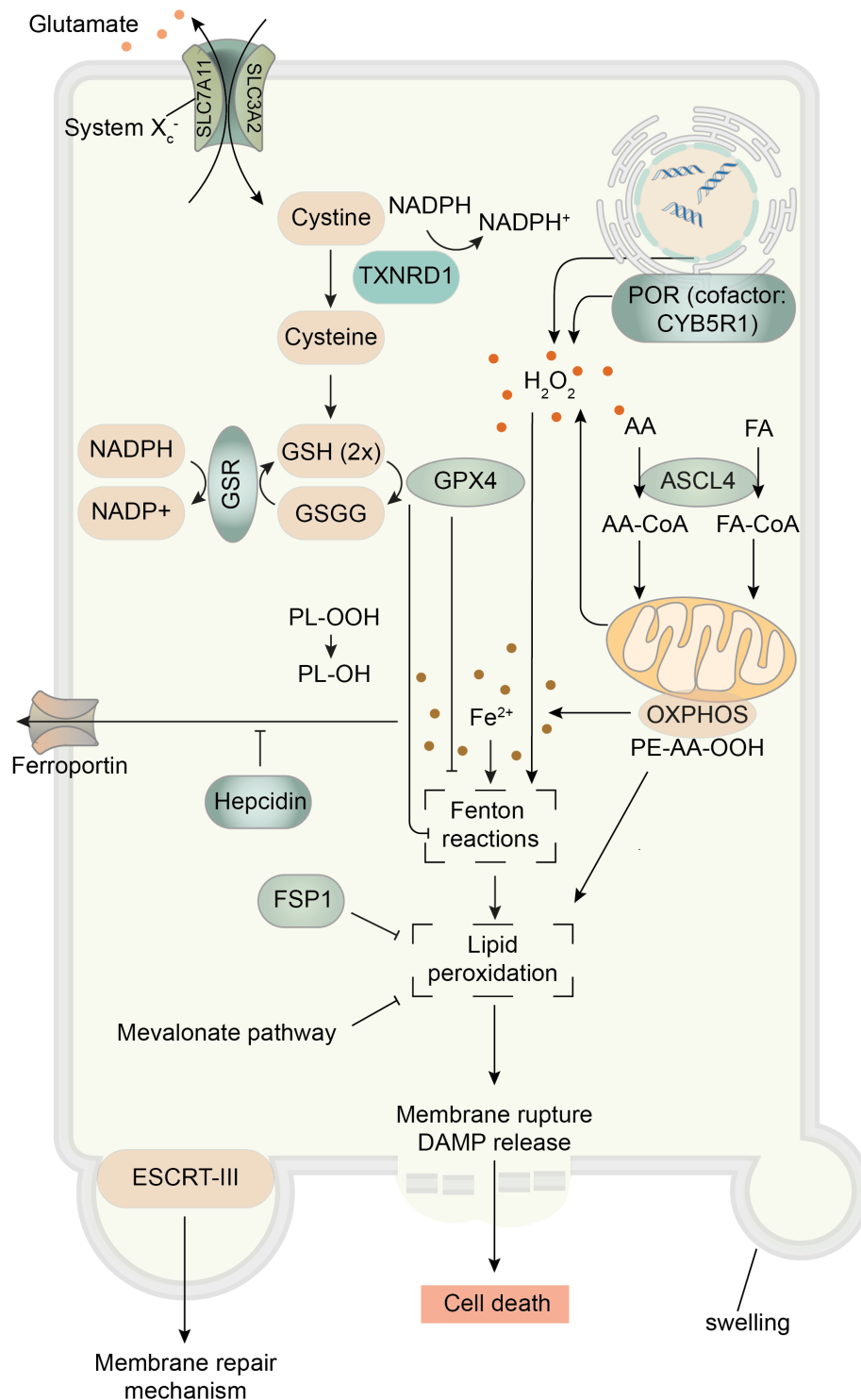
Figure 6. **Mechanisms of ferroptosis.**

Within cellular homeostasis, the concentrations of H_2O_2 and iron-catalysed Fenton reactions are controlled by diverse cellular anti-redox systems. The most extensively researched system relies on GSH, which is produced intracellularly and relies on the supply of Cystine through system X_c^-, a cysteine/glutamate antiporter situated in the plasma membrane, or the products of the trans-

sulfuration pathway. When GSH concentrations are sufficient, GPX4 prevents lipid peroxidation and averts plasma membrane rupture through unidentified mechanisms. In contrast, the oxidoreductase FSP1 (also known as AIFM2) prevents lipid peroxidation through myristoylation-dependent recruitment to the plasma membrane in a GSH-independent manner. Ferroptosis takes place as a noncell-autonomous mechanism in a process referred to as synchronized regulated necrosis (SRN). Abbreviations: AA (arachidonic acid), DAMP (damage-associated molecular pattern), FA (fatty acid), FSP1 (ferroptosis suppressor protein 1) GSH (glutathione), GSR (glutathione-disulphide reductase), GSSG (glutathione disulphide), OXPHOS (oxidative phosphorylation), PE-AA-OOH (oxidized arachidonic acid-phosphatidylethanolamines), PL-OH (phospholipid alcohol), PL-OOH (phospholipid hydroperoxide), RTA (radical trapping antioxidant), TXNRD1 (thioredoxin reductase 1) (Image adapted from Maremonti *et al.*, 2022).

1.3.1.1   Sensitization to ferroptosis by ether phospholipids

Aside from PUFAs, a second class of membrane lipids has recently been implicated in the ferroptotic process—polyunsaturated fatty acid-containing ether phospholipids (PUFA-ePLs). These lipids are characterized by the presence of PUFAs, which are prone to peroxidation, attached to the sn-2 position of the glycerol backbone through an ether bond. PUFA-ePLs are particularly enriched in the inner leaflet of the plasma membrane (Lorent *et al.*, 2020). The synthesis of ether phospholipids begins in peroxisomes and continues in the endoplasmic reticulum (ER) (Dean & Lodhi, 2018). At the peroxisomal level, alkyldihydroxyacetone phosphate synthase (AGPS) catalyzes the formation of alkylglycerone phosphate (AGP), a precursor for ether lipids, by adding an alkyl group to the glycerol backbone, thus creating the characteristic ether linkage. Fatty acyl-CoA reductase 1 (FAR1) plays a crucial role by converting fatty acyl-CoA molecules into fatty alcohols; it can be considered the rate-limiting enzyme for ether phospholipid synthesis by supplying the necessary fatty alcohol (Cheng & Russell, 2004). Both AGPS and FAR1 enzymes are crucial players essential for initiating ferroptosis. Their significance lies in their influence on the levels of PUFA-ePLs in the cell membrane. This connection is pivotal for understanding biochemical plasticity, highlighting the adaptability and dynamic nature of cellular processes associated with ferroptosis induction (Cui *et al.*, 2021; Y. Zou, Henry, *et al.,* 2020). However, how ePLs may govern ferroptosis is still not clear and necessitates future research.

1.3.1.2   Hydropersulfides and ferroptosis

CBS and CSE are enzymes integral to the transsulfuration pathway and convert homocysteine into cysteine, a crucial precursor for GSH synthesis. GSH in turn acts as a cofactor for GPX4, which is, as described above, the major enzyme defending against lipid hydroperoxides and ferroptosis (Jiang *et al.*, 2021; Stockwell, 2022). Simultaneously, CBS

and CSE play a key role in generating hydropersulfides, which are sulfur-containing molecules implicated in ferroptosis regulation (Barayeu *et al.*, 2023; Z. Wu *et al.*, 2022).

Persulfides are characterized by a sulfane sulfur adjacent to an ionizable proton and have gained attention for their antioxidant properties. These molecules act as radical-trapping antioxidants, thereby inhibiting phospholipid peroxidation and suppressing ferroptosis. Persulfides, especially those residing in membranes, play a pivotal role in breaking lipid peroxidation chain reactions, showcasing their efficacy in cellular defense against oxidative stress (Z. Wu *et al.*, 2022). Studies suggest that endogenously generated persulfides that were formed enzymatically or non-enzymatically from hydrogen sulfide impact ferroptosis sensitivity (Barayeu *et al.*, 2023; Lange & Olzmann, 2022; Z. Wu *et al.*, 2022). Genetic manipulations affecting hydrogen sulfide levels influence ferroptosis resistance or susceptibility, emphasizing the intricate regulation of persulfides in cellular responses (Barayeu *et al.*, 2023). The findings establish a unified model where persulfides, particularly GSSH, emerge as critical contributors to ferroptosis suppression. The significance of these factors in ferroptosis and their interactions with other resistance mechanisms remain open questions.

1.3.2 Ferroptosis inducers (FINs) and inhibitors

After the recognition of RSL3 and erastin as ferroptosis inducers (Dixon *et al.*, 2012a; Dolma *et al.*, 2003; Yang *et al.*, 2014; Yang & Stockwell, 2008), numerous small molecules have been developed to either enhance or inhibit ferroptosis. These molecules are explored for their potential in alleviating diverse diseases associated with ferroptosis, including their application as anticancer therapies (Conrad *et al.*, 2016; Yang & Stockwell, 2016) and for conditions like AKI (Friedmann Angeli *et al.*, 2014a; Linkermann *et al.*, 2014).

Ferroptosis inducers (FINs) are categorized into four major classes based on their mode of action. This includes molecules that deplete the intracellular GSH pool, directly inhibit GPX4 through inactivation or depletion, and FINs that induce an indirect loss of GPX4 activity while oxidizing iron (Hassannia *et al.*, 2019). Type I FINs act by inhibiting the X_c^- system. One example of this category is erastin, which was discovered in a high-throughput screening targeting oncogenic RAS mutant cell lines (Dolma *et al.*, 2003). RSL3, which inhibits the active center of GPX4, thereby conferring increased lethality in the presence of oncogenic RAS (Yang & Stockwell, 2008), and FIN56, which directly degrades the selenoenzyme GPX4 (Shimada *et al.*, 2016b), are classified as Type II and Type III FINs, respectively. Compounds belonging to the Type IV FIN class, like FINO2, induce an indirect loss of GPX4 enzymatic activity while directly oxidizing iron (Gaschler *et al.*, 2018). However, the exact mechanism of

how FINO2 induces ferroptosis remains unclear. Furthermore, the field of ferroptosis research has witnessed the development of small molecules specifically designed to target and inhibit this process (Degterev & Linkermann, 2016; Martin-Sanchez, Ruiz-Andres, Poveda, Carrasco, Cannata-Ortiz, Sanchez-Niño, Ruiz Ortega, *et al.*, 2017; Skouta *et al.*, 2014). The first synthetic ferroptosis inhibitor reported in literature was ferrostatin-1 (Fer-1), identified through a screen for inhibitors of erastin-induced ferroptosis in human fibrosarcoma (HT1080) cells (Dixon *et al.*, 2012b). Although initially recognized for preventing lipid hydroperoxide accumulation, recent revelations have clarified its role as a radical trapping antioxidant (Zilka *et al.*, 2021). Similarly, Liproxstatin-1 (Lip)-1 was selected from a small molecule screening in TAM-inducible gpx4$^{-/-}$ mouse embryonic fibroblasts (MEFs) (Friedmann Angeli *et al.*, 2014a). Notably, this study unveiled Necrostatin-1 (Nec-1), originally designed as a necroptosis inhibitor, to be effective in inhibiting ferroptosis as well. Another category of ferroptosis inhibitors includes iron chelators, which hinder lipid peroxidation either by binding iron in the catalytic center of lipoxygenase (LOX) or by chelating cytosolic labile iron pool (LIP), thereby inhibiting radical generation (Scarpellini *et al.*, 2023). Deferoxamine (DFO), a widely used iron chelator, has demonstrated beneficial effects in a model of ferroptosis-induced AKI (Zhu *et al.*, 2023). In conclusion, the evolving landscape of ferroptosis inhibitors showcases diverse molecules targeting different aspects of ferroptosis, offering promising avenues for therapeutic interventions.

1.3.3   Ferroptosis in the kidney

Since its discovery, ferroptosis has been proposed to be involved in many physiological and pathophysiological contexts. Accumulating evidence point toward a role for ferroptotic cell death in tumor growth suppression (L. Jiang *et al.*, 2015; S.-J. Wang *et al.*, 2016), neurodegeneration (L. Chen *et al.*, 2015; Hambright *et al.*, 2017), *Mycobacterium tuberculosis*-induced tissue necrosis (Amaral *et al.*, 2019, 2023) and autoimmune diseases (Hu *et al.*, 2019). Moreover, multiple studies have established a major role for ferroptosis in cell death associated with ischemic injuries in multiple organs such as heart (Gao *et al.*, 2015) and brain (Lau & Tymianski, 2010), caused at least partially by the oxidative stress induced by ischemia. Besides these two organs, the kidney is the most ferroptosis-sensitive organ identified. Indeed, proximal tubular cells were identified to be dependent on GPX4 to survive (Friedmann Angeli *et al.*, 2014b). Since 2014, the kidney tubular system has emerged as a pivotal model for investigating ferroptosis, marked by a remarkable surge in research publications. As of January 2024, a total of 694 manuscripts related to "ferroptosis" and "kidney" have been catalogued on PubMed, underscoring the growing significance of this field. Among them our

most recent review encapsulates the evolving landscape of ferroptosis research (Maremonti *et al.,* 2022). The first mention of ferroptosis inhibition in isolated kidney proximal tubules traces back to ten years ago (Skouta *et al.,* 2014). Following this, other breakthroughs include experiments involving isolated renal tubules perfused with a ferroptosis inducer demonstrating a synchronized propagation of cell death which resemble the clinical manifestation observed in humans (Linkermann *et al.,* 2014), and the discovery of GPX4 knockout mice succumbing to acute kidney injury (Friedmann Angeli *et al.,* 2014a). Notably, a dysfunctional mutant of GPX4 displayed heightened susceptibility to renal ischemia-reperfusion (Tonnus, Meyer, *et al.,* 2021). In the same publication, FSP1-deficient mice exhibited hypersensitivity to AKI, establishing a link between FSP1 function and renal health. Another pivotal discovery demonstrated that FSP1's role in regenerating vitamin K protects the kidney from ferroptosis (Mishima *et al.,* 2022). Adding a pharmacological dimension, Dexamethasone was found to sensitize renal tubular cells to ferroptosis (Von Mässenhausen et al., 2022). Despite this progress, the intricate mechanisms governing ferroptotic cell death propagation remain elusive. The current speculation as to how this death propagates is that the carriers of intracellular redox capacity (primarily NADPH) diffuse through intercellular junctions. Across a line of living and dying cells a NADPH gradient forms, increasing the risk of the neighboring cells to undergo ferroptosis (**Figure 7**) (Belavgeni *et al.,* 2020; Maremonti *et al.,* 2022; Tonnus, Meyer, *et al.,* 2021).
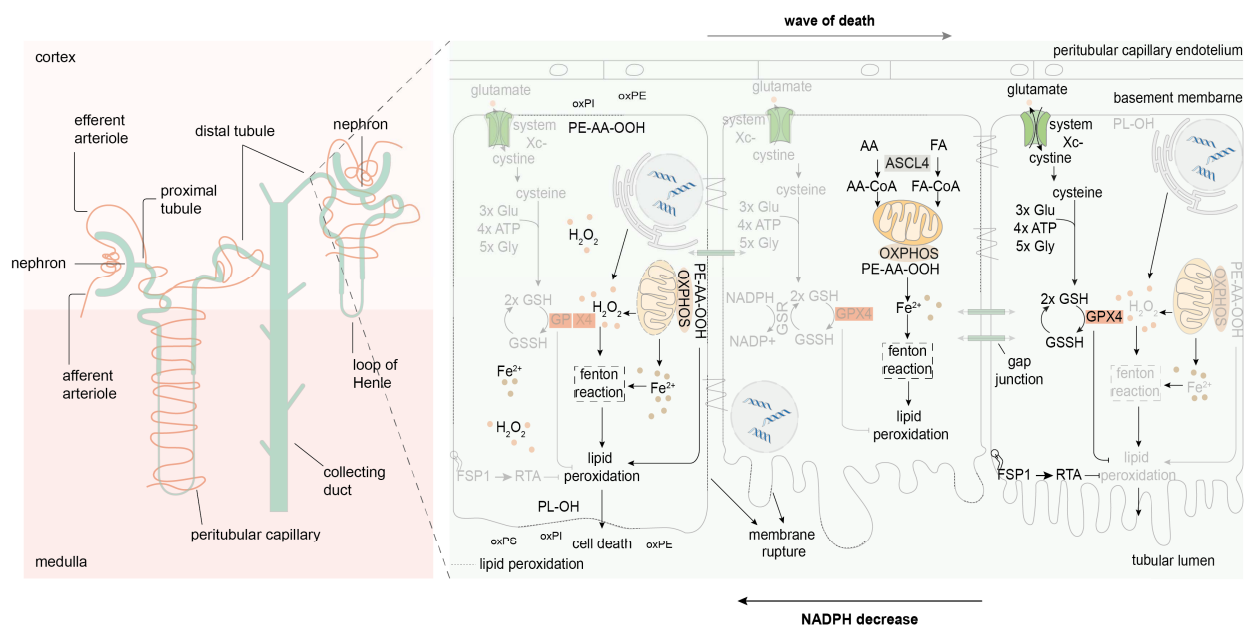
Figure 7. Synchronized regulated necrosis occurring in renal tubules.

Graphical representation of ferroptosis in kidney tubules. The figure highlights a propagation of cell death in a "wave-like" fashion. It is assumed that there exists a gradient of redox capacity, specifically in the concentration of NADP(H), along the spectrum of living and dying cells. As a result, a neighbouring cell faces an increased risk of undergoing regulated cell death. The abbreviations include AA (arachidonic acid), FA (fatty acid), GSH (glutathione), GSR (glutathione-

disulphide reductase), GSSG (glutathione disulphide), PL-OH (phospholipid alcohol), PL-OOH (phospholipid hydroperoxide), and RTA (radical trapping antioxidant) (Image source: Maremonti *et al.*, 2022).

1.4 Aims

Despite substantial progress in comprehending regulated cell death mechanisms, translating this scientific knowledge into a clinical context remains a formidable challenge. Nowhere is this more apparent than in the realm of diabetes and its long-term complications. A comprehensive understanding of cell death intricacies and the strategies cells employ to cope with persistent glycemic dysregulation is fundamental in addressing the complex dynamics induced by the disease. The kidney, in particular, emerges as a vital organ affected by this situation, with the majority of diabetes-related mortality stemming from the development of DKD and subsequent ESRD.

Kidneys, especially in AKI induced by ischemia-reperfusion injury (IRI), can be considered primary sites of ferroptosis. However, despite this significance, the field of kidney diseases remains insufficiently explored in the context of regulated cell death. Understanding the role of different regulated cell death pathways in the kidney, especially in the context of diabetes, is therefore crucial. Consequently, the primary aim of this Ph.D. thesis is to delve into the intricate connections between diabetes mellitus, focusing on DKD and the emerging paradigm of ferroptosis.

Utilizing a novel mouse model of Type 2 diabetes, termed GIPR^{dn}, which faithfully replicates features observed in DKD patients, the study seeks to characterize the onset and progression of DKD. This involves conducting a comprehensive analysis of accelerated cell death propagation and heightened tubular necrosis observed in isolated renal GIPR^{dn} tubules, thereby shedding light on the potential role of ferroptotic cell death in this specific diabetes mellitus complication. The study further aims to unveil the connection between glucose dysregulation, partially governed by the protein TXNIP and the loss of ferroptosis surveillance at the level of kidney tubules. This is associated with one of the most important antioxidant systems in mammalian cells, namely TXNRD1. On this line of investigation, another objective is to explore the therapeutic potential of ferrostatins, particularly exemplified by Fer-1, to ameliorate diabetic kidney complications, offering a glimpse into the translational implications of targeting ferroptosis in the clinical context of DKD.

In conclusion, this Ph.D. thesis aspires to provide a comprehensive understanding of the intricate dynamics between diabetes and ferroptosis using the GIPR^{dn} mouse model. The multifaceted approach encompasses unravelling molecular mechanisms, exploring cellular interactions, and investigating potential therapeutic interventions. The findings will contribute not only to the academic understanding of DKD but also hold promise for future translational applications, paving the way for novel therapeutic strategies in addressing the formidable challenges posed by diabetes kidney complications in the 21st century.

Materials and methods

2. Materials and Methods

2.1. Reagents

Table 2. Substances used in experimental procedures.

Chemicals	Source	Identifier
DMSO	Sigma Aldrich	Cat#D2650
ITS+1 Liquid Media Supplement	Sigma Aldrich	Cat#I2521
D(+)-Glucose Monohydrate	Millipore	Cat#K54772142 316
Erastin (type I FIN)	Sigma Aldrich	Cat# E7781
RSL3 (type II FIN)	Selleckchem	Cat#S8155
FIN56 (type III FIN)	Sigma Aldrich	Cat#SML1740
FINO2 (type IV FIN)	Keith Wörperl, Brent Stockwell	N/A
Ferroptocide (FTC)	Paul Hergenrother	N/A
Ferrostatin-1 (Fer-1)	Merck Millipore	Cat#341494
Empagliflozin	Selleckchem	Cat#S8022
SYTOX™ Green Nucleic Acid Stain	Life Technologies	Cat#S7020
BioTracker™ 609 Red Ca^{2+} AM dye	Merck Millipore	Cat#SCT021
7-AAD	BD Biosciences	Cat#559925
Annexin-V-FITC	BD Biosciences	Cat#556420
Annexin-V binding buffer	BD Biosciences	Cat#556454
Kits		
Bradford assay	Fisher Scientific	Cat#G1780
ECL™ Prime Western Blotting System	Fisher Scientific	Cat#GERPN2232
LDH release assay	Promega	Cat#G1780
Thioredoxin Reductase Activity Assay	Abcam	Cat#ab83463
Mouse Albumin ELISA Kit	Bethyl	Cat#E99-134
Creatinine Liquid Reagents Assay Kit	DIAZYME	Cat#DZ072B-KY1

2.2. Experimental models: cell lines and mouse strains

Table 3. Cell lines and mouse strains used during experimental procedures.

Cell line	Origin	Source
Human: HT1080	Fibrosarcoma	ATCC (CCL-121)
Mouse: NIH-3T3	Embryonic fibroblasts	ATCC (ERL-1685)
Human: CD10-135	Kidney tubular epithelial cells	Kindly provided by Prof. Rafael Kramann, Aachen
Mice	**Type of mice**	**Source**
CD1	Wild type (WT)	Charles River, Germany
GIPR^{dn}	Type I diabetes mice	Kindly provided by Prof. Christian Hugo, Dresden

2.2.1. Cell culture conditions

HT1080 and NIH-3T3 cells were cultured in DMEM (modified) medium (Gibco, 4966029) enriched with 10% FBS (Gibco, 10270106) and 100 U/ml penicillin, and 100 µg/ml streptomycin (Pen/Strep, Thermo Fisher, 15140122). CD10-135 cells were cultures in Dulbecco's Modified Eagle Medium F-12 Nutrient Mixture with Glutamax (DMEM/F12 Glutamax, Thermo Fisher, 10565018) supplemented with 10% (v/v) FBS (Thermo Fisher, 41966029), 100 U/ml penicillin, and 100 µg/ml streptomycin (Pen/Strep, Thermo Fisher, 15140122). To sustain the culture, the cells were split at an appropriate ratio once they reached 75% confluency.

2.2.2. Mice

The mice included in this study were all male heterozygous transgenic mice from 7 to 50 weeks of age, expressing a dominant-negative glucose dependent insulinotropic polypeptide receptor (GIPR^{dn}), along with age-matched non-transgenic littermate controls (CD1 wild type mice) (Volz *et al.*, 1995).

All mice in this study were maintained on a 12-hour light and 12-hour darkness cycle. The room temperature was maintained within a range of 20 to 24 °C, while the air humidity was controlled between 45 and 65%, as confirmed through daily monitoring. Unless stated otherwise, 3 mice per cage were co-housed in individually ventilated cages

(IVCs) in the animal facility at the Medizinisch-Theoretisches Zentrum (MTZ) at the Medical Faculty of the Technische Universität Dresden (TU Dresden). The mice had unrestricted access to sterilized standard pellet food and water. Furthermore, all cages and nestlets underwent sterilization via autoclaving prior to their usage.

Upon reaching 3 weeks postpartum, the mice were weaned, separated by gender, and marked through ear piercing. Tail tip biopsies were taken for genotyping. Throughout the study, blood samples were collected from each mouse at defined time points and their body weights were recorded periodically.

All mouse experiments conducted in this study adhered to the regulations outlined in German animal protection laws. The experiments were approved by the ethics committees and local authorities in Dresden (Germany).

The GIPR^{dn} mice were kindly provided by Prof. Christian Hugo.

2.2.2.1. Genotyping

To identify the transgenic mice, DNA extracted from tail tips was subjected to polymerase chain reaction (PCR) following standard protocols, as described in previous studies (Herbach *et al.*, 2005, 2008, 2009).

2.2.2.1.1. DNA isolation

Table 4. Reagents used for DNA extraction procedure.

Chemicals	Source	Identifier
Tail buffer	VIAGEN	Cat#102-T
Proteinase K	Promega	Cat#V3021

At 3 weeks of age, mice were weaned and tail tip biopsies were collected and stored at - 20 °C until further analysis. For DNA extraction, a tail tip of approximately 0.4 cm was placed in a tube containing 75 µl Tail Buffer supplemented with 2.25 µl Proteinase K and incubated overnight in a heating block at 55 °C, followed by a further heating step at 85 °C for 1 hour. The samples were then centrifugated at 10,000 rpm for 3 min in order to separate the DNA from the undigested components, the supernatant placed in new tubes (Eppendorf, Germany) and stored at + 4 °C.

2.2.2.1.2. Polymerase Chain Reaction (PCR)

Table 5. Primers used for the genotyping

Primer	Sequence	Source
sense	5'-ACA GNNTCT NAG GGG CAG ACG NCG GG-3' (Tra1)	Eurofin Genomic
antisense	5'-CCA GCA GNT NTACAT ATC GAA GG-3' (Tra3)	Eurofin Genomic

The selected primers were designed to target both the human cDNA of the mutated GIP receptor and the endogenous murine GIP receptor. These primers were strategically chosen from regions where the DNA sequence of the GIP receptor is highly conserved among human, rat, mouse, and hamster. The differentiation between the mutated human GIP receptor and the endogenous murine receptor was achieved by examining the resulting PCR products, which differed in their respective base pair lengths. The PCR product of the murine GIP receptor yielded approximately 500 base pairs while the PCR product of the mutated human GIP receptor consisted of approximately 140 base pairs. Before use, both primers were diluted at a ratio of 1:10 in Nuclease-Free water.

Table 6. Reagents used for the PCR Mastermix.

Reagent	Source	Identifier
dNTP mix	Meridian Bioscience	Cat#DM-121204,A
Nuclease-Free water	Promega	Cat#P119C
Primer sense (Tra1)	Eurofin Genomic	Cat#H531
Primer antisense (Tra3)	Eurofin Genomic	Cat#H532
5× Green GoTaq™ Flexi Buffer	Promega	Cat#M791A
GoTaq® Polymerase	Promega	Cat#M784B

To prepare the PCR samples, 2 µl of the DNA suspension was combined with 26,8 µl of the Master Mix in PCR analysis tubes (Sarstedt, Germany). Both the DNA and Master Mix components were kept on ice throughout the procedure.

For storage, the PCR samples were either kept at 4 °C (short-term) or at - 20 °C (long-term) until further use. A transgenic mouse's DNA served as the positive control, DNA from a wild-type mouse served as the negative control, and the Mastermix-only (no template), was used as a quality control. The PCR was performed using a Mastercycler

nexus Gx2 (Eppendorf, Germany), following the programmed steps as described in **Table 7.**

Table 7. PCR protocol followed for the genotyping.

Step	Temperature	Time
Denaturation	94°C	4 min
Denaturation	94°C	1 sec
Annealing	60°C	1 sec
Extension	72°C	2 sec
Final extension	72°C	10 min
Hold on	4°C	∞
		× 35 cycles

2.2.2.1.3. Gel electrophoresis

Table 8. Reagents used for gel electrophoresis

Reagent	Concentration	Source	Identifier
10 × TBE stock solution			
Tris	0.9 M	Carl Roth	Cat#4855.1
Ortho-Boric acid	0.9 M	VWR	Cat#20185.297
NaEDTA pH 8.0	0.5 M	Klink Apotheke des Universitätsklinikum Carl Gustav Carus	N/A

To separate DNA fragments based on their size, electrophoresis was performed using a 2 % TBE agarose gel (8 g agarose from SERVA, Germany, dissolved in 400 ml 1x TBE buffer). The gel was prepared with the addition of 15 µl Gel-Red® Nucleic Acid Stain (Biotium, USA) and casted in kuroGel Mini Plus 10 Electrophoresis Horizontal (VWR, Belgium). The gel chamber was filled with 1× TBE running buffer.

To estimate the size of the amplified fragments, 5 µl of gel Loading Dye Purple (New England BioLabs, USA) were placed at the beginning of each sample well row. The remaining wells were filled with 29 µl of the DNA samples.

The electrophoresis was conducted for approximately 45 minutes at 110 V and an output of approximately 200 mA using a kuroGel Mini Plus 10 Electrophoresis Horizontal (VWR, Belgium). Subsequently, the amplified products were visualized using UV light at a wavelength of 306 nm with an INTAS GelStick IMAGER (INTAS, Germany). A digital picture was taken to document the results.

2.2.2.2. Body weight

Animals' body weight was measured regularly every two weeks after weaning. The final documentation of body weights was conducted shortly before euthanasia. A precision scale (Kern KB 5000-1, Kern & Sohn GmbH, Germany) was used to measure the body weight of the animals to the nearest 0.1 g.

2.2.2.3. Blood glucose

Blood glucose levels were assessed at the defined time points shortly before euthanasia. The mice tail was cut and 0.5 µl of blood were directly placed on GlucoSmart® test strips of GlucoseSmart®Swing[2] mg/dl blood glucose meter.

2.2.2.4. Blood collection and serum parameters

Blood samples were collected from the retroorbital plexus using heparinized capillaries (Servoprax, Germany). The blood samples were immediately placed into Li-Heparin LH/1.3 microtubes (Sarstedt, Germany). Subsequently, the samples were sent to the Institut für Klinische Chemie und Laboratoriumsmedizin (IKL, Universitätsklinikum Dresden) for serum extraction and analysis. All samples were screened for serum creatinine and serum urea levels. The screening process was conducted using the Cobas c311 Analyzer (Roche, Germany), according to manufacturer instructions.

2.2.3. Isolation of primary murine renal tubules

Table 9. Substances used for preparation of kidney tubules.

Chemicals	Concentration	Source	Identifier
Preparation of 98b solution (pH 7.4)			
NaCl (liquid)	140 mM	Sigma	Cat#S6546
KH_2PO_4	0.4 mM	Sigma	Cat#SLCD1991
$K_2HPO_4 \times 3\ H_2O$	1.6 mM	Sigma	Cat#WXBC9871V
$MgSO_4 \times 7\ H_2O$	1 mM	Sigma	Cat#BCBZ8532
$CH_3COONa \times 3\ H_2O$	10 mM	Merck/KD	Cat#005-111219
α-ketoglutarate	1 mM	Sigma	Cat#BCBX4692
Ca-gluconate	1.3 mM	Sigma	Cat#G4625
Preparation of incubation solution from 98b solution			

Trypsin Inhibitor	48 µg/ml	Sigma	Cat#T9128-1G
DNAse I	25 µg/ml	Thermofisher	Cat#24966
Preparation of sorting solution from incubation solution			
albumin	0.5 mg/ml	Serva	Cat#11930.04
Preparation of collagenase solution from incubation solution			
Collagenase Type II	2 mg/ml	Worthington	Cat#LS004176

Primary murine renal tubules were isolated following a previously published protocol (Tonnus, Meyer, *et al.,* 2021).

Briefly, murine kidneys were surgically removed, rinsed with 1× PBS, decapsulated, and sectioned into four to five slices. Each kidney slice was placed in a 2 ml Eppendorf tube containing 1 ml collagenase solution. The tubes were incubated in a thermoblock at 37 °C, 850 rpm for 5 minutes to digest the kidney slices. The resulting first supernatant was discarded, due to the presence of damaged tubules occurring from the cutting of the kidneys. The digestion process with pre-warmed incubation solution was repeated. Collection of tubules is performed after 5 min. Unless otherwise mentioned, for this dissertation the supernatant occurring from a third incubation of the kidney slices with pre-warmed incubation solution was used. The collected tubules were transferred to a 2 ml Eppendorf tube containing 1 ml of ice-cold sorting solution. The tubes were kept on ice for 5 minutes to allow the tubules to precipitate, and then the supernatant was removed. The tubules were rinsed twice for 5 minutes with ice-cold incubation solution. Once the tubules settled, ice-cold sorting solution was added (volume adjusted based on the required number of samples) and distributed into a twenty-four-well plate (Costar, REF3526), containing DMEM/F12 Nutrient Mixture without glycine and phenol red (DMEM/F12, a custom-made medium provided by Cell Culture Technologies LLC). The medium was supplemented with 0.01 mg/ml recombinant human insulin, 5.5 µg/ml human transferrin, 0.005 µg/ml sodium selenite and 470 µg/ml linoleic acid (ITS + 1, Sigma Aldrich), 50 nM hydrocortisone, 100 U/ml penicillin, and 100 µg/ml streptomycin (Pen/Strep, Thermo Fisher). Images of the isolated tubules were captured using a 10×/0.22 PH1 objective on a Leica DMi1 microscope.

2.2.4. Generation of a 3D-printed double chamber

In order to perform live imaging experiments (see **Section 2.3.7.**) of isolated kidney tubules, 3D-printed silicon double chambers were created by the Microstructure Facility, a Core Facility of the CMCB Technology Platform at TU Dresden.

The chambers are composed of a border that includes a retainer designed to enclose the glass wall, effectively separating the two chambers. The border of the chamber was printed on top of a silinized microscope slide and cured at 100 °C for 30 minutes. The border was printed using a silicone elastomere (SE 1700; Dow Corning) using a 3DDiscovery bioprinter from RegenHU, employing a conical nozzle with an inner diameter of 250 µm. To achieve a printed line thickness of approximately 500 µm and a height of 8mm, adjustments were made to the printing speed and extrusion pressure. Print layouts were developed using the BIOCAD software provided by RegenHU.

To create a thinner line within the chambers, SE1700 was printed in the center at a higher printing speed, resulting in a thickness of approximately 200 µm, which is thinner than the border. The bonding of the glass wall to the retainer was achieved by manually applying SE1700 using a syringe with a conical needle. As for the glass wall itself, a cover slip measuring 20 x 20 mm with a thickness of 0.12 mm was cut down to a size of 8 x 20 mm. It was meticulously cleaned with ethanol and subjected to a 10-second treatment of air plasma using the Piezobrush PZ2-i, which is a cold-plasma generator equipped with a Nearfield nozzle from Relyon Plasma. The glass wall was then inserted into the retainer, pushed down until it made direct contact with the thin line of SE1700, and cured again at 100 °C for 30 minutes.

Afterwards, the structure was removed from the microscope slide, and both its bottom side and the inside of a six-well plate were treated with air plasma for approximately 10 seconds using the Piezobrush PZ2-i. The structure was attached to the six-well plate and kept at 60 °C for 2 hours to facilitate bonding. In cases where certain areas of the border did not adhere well to the surface, those spots were sealed manually with SE1700. Subsequently, the structure was placed back at 60 °C for an additional 4 hours.

2.3. Experimental procedures

2.3.1. Plating and treatment of cells

To detach the cell lines from the flasks, Trypsin-EDTA (Gibco, 25200056) was utilized. Cells were washed with DMEM (modified) medium supplemented with 10 % FBS and 1 % penicillin-streptomycin, followed by centrifugation at room temperature for 4 minutes at 3,000 rpm. The resulting cell pellet was resuspended in an appropriate amount of DMEM, and cells were subsequently seeded in six-well plates (Sarstedt, 83.3920) at a density of 1×10^5 cells in 2 ml of medium. The next day the medium was aspirated, and the cells were washed with 1 ml 1× PBS. Substances for treatments were dissolved in vehicle medium (as mentioned in **Section 2.1.**), diluted in fresh medium and then added at the specified concentrations, described below, in a total volume of 1 ml. Ferroptosis was induced by employing four different ferroptosis inducers (FINs): Type 1 FIN, erastin (Sigma Aldrich); Type 2 FIN, RSL3 (Selleckchem); Type 3 FIN, FIN56 (Sigma Aldrich); and Type 4 FIN, FINO2 (provided by Keith Wörpel & Brent Stockwell) (see **Table 2.**). Necrosis was also induced following the described method (Llabani *et al.*, 2019) using the thioredoxin reductase inhibitor ferroptocide (kindly provided by Paul J. Hergenrother). As ferroptosis inhibitor ferrostatin-1 (Fer-1) (Merck Millipore) was utilized. The SGLT2 inhibitor Empagliflozin (Selleckchem) was also utilized in combination with ferroptosis inducers and inhibitor.

Unless stated otherwise, the concentrations of the inducers used were 5 µM erastin, 1,13 µM RSL3, 10 µM FIN56, 10 µM FINO2, 10 µM ferroptocide, 1 µM Fer-1 and 1 or 10 µM Empagliflozin. At designated time points, cells were collected and prepared for flow cytometry, immunoblotting and/or LDH release assays (see sections below).

2.3.2. Fluorescence activated cell sorting (FACS)

For the preparation of samples for flow cytometry analysis, cells were detached from the six-well plate (Sarstedt, 83.3920) using Trypsin-EDTA (Gibco, Cat#25200056). The Trypsin-EDTA activity was stopped by adding the corresponding growth medium to the cells, followed by centrifugation at 3000 rpm for 4 minutes. The resulting cell pellets were washed twice with 1× PBS and filtered through polystyrene round-bottom tubes with cell-strainer caps (Corning, Cat#352235). Next, the cells were stained with 5 µl of annexin-V-FITC (BD Biosciences) and 5 µl of 7-AAD (BD Biosciences) added to 100 µl

of annexin-V binding buffer (BD Biosciences). Following a 15-minute incubation with the staining solution, the cells were analysed using the BD Biosciences LSRII flow cytometer with the FACS Diva 6.1.1 software (BD Biosciences). Data analysis was performed using FlowJo v10 software (Tree Star).

The flow cytometry experiments were conducted with the support of the Flow Cytometry Facility, which is a Core Facility of the CMCB Technology Platform at TU Dresden.

2.3.3. Western Blotting (WB)

Table 10. Reagents used for western blot samples preparation.

Chemicals	Concentration	Source	Identifier
NP40 buffer			
Tris-HCl, pH 7.5	50 mM	Carl Roth	Cat#4855.1
NaCl	150 mM	Sigma	Cat#SLCF4372
NP-40	1%	Sigma-Aldrich	Cat#11332473001
EDTA	5 mM	Invitrogen	Cat#15575-038
Lysis Buffer			
NP-40 buffer	to volume		
PMSF (modified Frackelton buffer) (100 × stock)	1 mM	Sigma-Aldrich	Cat#P7626-5g
Phosphostop (10× stock)	1×	Roche	Cat#04906845001
cOmplete Mini (proteinase inhibitor cocktail tablets) (7× stock)	1×	Sigma-Aldrich	Cat#11836153001
10× Running Buffer			
Tris Base	250 mM	Biorad	Cat# 1610734
glycine	1,92 M	Sigma	Cat#SLCH8988
SDS	1%	Carl Roth	Cat#2326.2
10× TBS			
Tris Base, pH 7.5	200 mM	Biorad	Cat#1610734
NaCl	1,5 M	Sigma	Cat#SLCF4372
1× TBS-T			

10× TBS			
Tween	0,1%	VWR	Cat#8.17072.1000
H$_2$O dest.	To volume		

The cell pellets were lysed in ice-cold NP-40 buffer with the addition of PMSF (1mM), Phosphostop (diluted 1× from a 10× stock), and cOmplete Mini (diluted 1× from a 7× stock), for 30 minutes on ice. Subsequently, the samples were centrifuged at 14,000 g for 30 minutes at 4 °C to remove insoluble material, and the resulting supernatant was transferred to a clean tube. The protein concentration was determined using a commercial Bradford assay kit following the manufacturer's instructions (ThermoFisher). For further sample preparation, the samples were denatured with ROTI Load (Carl Roth, K929) at 95 °C for 5 minutes. The samples were either kept at 4°C (short-term) or at -80°C (long-term) until further use.

Equal amounts of protein (typically 15-25 µg per lane) were loaded on a 4-15% gradient SDS/PAGE gel (Mini-PROTEAN TGX Gel, Biorad, 64432112) in 1× Running Buffer and run for approximately 30 min at 150-200 V (Mini Trans-Blot® Cell and Criterion™ Blotter, Biorad, Germany). To estimate the size of the proteins, 5 µl of Precision Plus Protein ™ Dual Color (Bio-Rad, Germany) were placed at the beginning of each sample well row.

Following the transfer of proteins onto a PVDF membrane (Biorad, Germany) (Trans-Blot Turbo Transfer System, Biorad, Germany), which was activated using methanol, the verification of protein transfer onto the membrane was carried out by performing Ponceau S staining (Sigma-Aldrich, Cat#P7170). Subsequently, the membranes were blocked using either 5% w/v BSA (Carl Roth, Cat#8076.4) or 5% powdered milk (AppliChem ITW Reagents, Cat#271-045-3) in TBS 0.1% Tween.

Table 11. Antibodies used for experimental procedures.

Antibodies	Dilution	Source	Identifier
Rabbit monoclonal **anti-ACSL4** (anti FACL4); human, mouse	1:5000	Abcam	Cat#ab155282
Rabbit polyclonal **anti-AGPS**; human, mouse	1:500	Abcam	Cat#ab236621
Mouse monoclonal **anti-CBS** (GT519); human, mouse	1:1000	Thermofisher	Cat#MA5-17273

Mouse monoclonal **anti-CSE** (anti gamma cystationase); human, mouse	1:2000	Proteintech	Cat#60234-1-Ig
Rabbit polyclonal **anti-GPX4** (EPNCIR144); human, mouse	1:5000	Abcam	Cat#ab125066
Rabbit polyclonal **anti-FAR1** (anti ether lipid synthesis enzyme); human, mouse	1:1000	Novus Biologicals	Cat#A107209
Rabbit **anti-ETHE1** (anti ETHE1 persulfide dioxygenase); mouse, human	1:1000	GeneTex	Cat#GTX115707
Mouse **anti-SQRDL** (anti sulfide quinone oxidoreductase); mouse, human	1:500	Abcam	Cat#ab71978
Rabbit **anti- PRX Pathway** (TRX, TXNRD1, PRX1) WB Cocktail	1:1000	Abcam	Cat# ab184868
Rabbit **anti-TXNIP** (anti thioredoxin interacting protein); human, mouse, rat, monkey	1:1000	Cell Signaling	Cat#14715
Rabbit monoclonal **anti-xCT/SLC7A11** (D2M7A); human	1:1000	Cell Signaling	Cat#12691
Mouse monoclonal **anti-β-actin** (8H10D19); human, mouse	1:1000	Cell Signaling	Cat#3700S
Rabbit monoclonal **anti-GAPDH** (14C10); human, mouse	1:1000	Cell Signaling	Cat#2118S

The primary antibodies used for all the western blots performed are listed in **Table 11**. The primary antibody incubation was performed overnight at 4 °C, while secondary antibodies, including anti-mouse HRP-linked antibody (Cell Signaling, Cat#70756S) and anti-rabbit HRP-linked antibody (Cell Signaling, Cat#7074S), were applied at a 1:5000 dilution in BSA or milk and incubated for 1 hour at room temperature. The blots were visualized using enhanced chemiluminescence (ECL) from Amersham Biosciences.

2.3.4. Induction of cell death on isolated murine tubules

To evaluate the effectiveness of the isolation procedure, all experiments incorporated a negative control to examine the release of LDH (lactate dehydrogenase) at the beginning of the incubation period (0 hours).

In general, isolated murine renal tubules were placed in twenty-four-well plates containing the respective agents diluted in DMEM/F12 Nutrient Mixture without phenol red (DMEM/F12, custom-made medium provided by Cell Culture Technologies LLC), mentioned above. After the indicated time points, the medium of each well was collected and prepared for the LDH release assay (see **Section 2.3.5**). The treated murine renal tubules were visualized using a Leica DMi1 microscope equipped with a 10×/0.23 PH1 objective, and images were captured.

2.3.5. LDH release assay

The LDH release of freshly isolated kidney tubules or primary tubular cells was assessed according to the instructions provided by the manufacturer (Promega, Cat# G1780) at specified time points. In summary, an aliquot of the supernatant was first collected, then, Lysis Solution was added to the well for 45 minutes to induce maximum LDH release. Subsequently, the entire supernatant was collected. The samples were then mixed with CytoTox 96® Reagent and incubated for 15 minutes at room temperature, protected from light. Following that, Stop Solution was added, and the absorbance was measured at 490 nm. The percentage (%) of LDH release was determined using the following formula:

$$\% \text{ of LDH} = 100 * (\text{supernatant LDH/maximal LDH}).$$

The resulting percentage allowed us to differentiate the initial cell death propagation-associated LDH release from baseline damage caused by the isolation procedure of the murine kidney tubules.

$$\text{Cell death propagation (additional \% LDH release after 0.5 hours)} = \%\text{LDH release}_{(yt)} - \%\text{LDH release}_{(0.5t)}$$

2.3.6. Evaluation of speed of cell death propagation (exponential plateau – growth equation)

The percentage of LDH release assay (Y values) was used to calculate the speed of cell death propagation spontaneously happening in kidney tubules. For the calculation the following formula was applied:

Y=YM -(YM-Y0)*exp(-k*x)

Where:

- Y0: is the starting population (same unit ad Y)
- YM: is the maximum population (same unit as Y)
- K: is the rate constant (inverse of X time units – slope of the curve)

2.3.7. Time lapse imaging and processing of the time lapse data

Videos of primary murine tubules stained with 50 nM SYTOX green nucleic acid (Life Technologies), were captured. The imaging was conducted using either a 2.5×/0.12 Fluar or 5×/0.16 M27 EC Plan Neofluar objective. In some cases, high-quality plastic-bottom slides (Ibidi 15 μ-slide 8-well, Cat#80826) were used for live imaging experiments with murine tubules. The isolated tubular cells were placed in a single well of a 3D-printed structure (see section 2.2.4.) and stained with 50 nM SYTOX green. An Axio Observer.Z1/7 microscope equipped with a large incubation chamber (maintaining 37 °C), 5 % CO_2, and humidity control was employed for all time-lapse imaging experiments. Both transmitted light and fluorescent images (using the GFP BP filter cube) were captured using an Orca flash camera. For acquisition and processing of the images the ZEN 10 software (Zeiss, Germany), was employed.

The subsequent analysis of the time-lapse data was performed using the open-source image processing software Fiji. The fluorescent channel corresponding to SYTOX green was processed using the Surface Plot plugin within the software. This processing technique generates a time-lapse video representing the intensity along the y' axis and the sample's dimensions along the x' and z' axes. Representative images derived from this video are presented at the results section.

The live imaging procedure was supported by the Light Microscopy Facility, a Core Facility of the CMCB Technology Platform at TU Dresden.

2.3.8. Fluorescence Lifetime Imaging Microscopy (FLIM)

The fluorescence lifetime imaging microscopy (FLIM) technique was utilized to investigate the changes in endogenous pool of NAD(P)H and FAD over time, in freshly isolated kidney tubules.

The experiments were performed with a Leica SP8 Falcon Multi Photon (MP) microscope, an inverse Laser Scanning Confocal microscope equipped with a White Light laser and a dual beam Insight X3 IR laser. The microscope featured 5 internal spectral detectors, a transmission channel, and a 4TUNE unit, enabling versatile spectral detection capabilities. For imaging, a HC PL APO 63×/1.20 WATER objective was used.

Briefly, the murine kidney tubules were isolated (see **Section 2.2.3.**) and immediately plated in high-quality plastic-bottom slides (Ibidi 15 µ-slide 8-well, Cat#80826) without staining. NAD(P)H and FAD autofluorescence were investigated at a 740 nm MP laser wavelength (pulse speed 8MHz), and respective lifetimes (see spectra in **Table 12**), were recorded with a detector HyD (435 nm-485 nm) in counting mode. The lifetime outputs were visualized with a LAS X software 3.5.7.23225 (Leica, Germany).

Table 12. NAD(P)H and FAD spectra and lifetimes.

Molecule	Spectra		Lifetime (τ)	
	Absorption	Emission	Short (τ_1)	Long (τ_2)
NAD(P)H	740 nm	450 nm	0.4-0.5 ns	1-4 ns
FAD	900 nm	500 nm	0.3 ns	~ 2 ns

2.3.8.1. Time domain data analysis

To derive fluorescence decay parameters, an iterative convolution process was utilized. This involved convoluting a suitable decay model with the instrument response function (IRF), which represents the detection system's response to the excitation pulse. The IRF can be either measured or calculated from the fluorescence decay data. Using iterative fitting procedures, the best fit to the photon numbers in the time channels was obtained. In the context of NAD(P)H and FAD analysis, the n-Exponential Tail Fit multiexponential fitting model was used (Fitting range: 1.503-11.976 ns; exponential components: 2), representing the various decay times and amplitude coefficients associated with these fluorophores. The final FLIM image was generated by assigning brightness based on the total photon number in each pixel and colour based on a selected decay parameter, such as the lifetime or amplitude ratio (1- 3 nm) to visualize the FLIM image.

In order to extrapolate the mean lifetime of each intrinsic fluorophore the following formula was employed:

$$\tau_{m} = a_1\,\tau_1 + a_2\,\tau_2 \qquad a_{amplitude} = \text{proportion (\%)}; t_m = \text{mean lifetime}$$

2.3.8.2.   FLIM time lapse video generation

The subsequent analysis of the time-lapse data was performed using the open-source image processing software Fiji. The fluorescent channel corresponding to NAD(P)H or FAD was processed using the Surface Plot plugin within the software. This processing technique generates a time-lapse video representing the intensity along the y' axis and the sample's dimensions along the x' and z' axes. Representative images derived from this video are presented to depict the results.

The FLIM imaging procedure was supported by the Light Microscopy Facility, a Core Facility of the CMCB Technology Platform at TU Dresden.

2.3.9.   Thioredoxin Reductase Activity assay

The evaluation of thioredoxin reductase activity in cells or freshly isolated kidney tubules was conducted in accordance with the manufacturer's guidelines (Abcam, Cat#ab83463).

In this assay, Thioredoxin Reductase (TrxR) catalyses the reduction of 5,5'-dithiobis(2-nitrobenzoic) acid (DTNB) using NADPH I/NADPH, resulting in the formation of 5-thio-2-nitrobenzoic acid (TNB^{2-}), which generates a distinctive yellow color (λ_{max} = 412 nm). Notably, in crude biological samples, other enzymes like glutathione reductase and glutathione peroxidase can also reduce DTNB. To distinguish TrxR-specific activity, a TrxR-specific inhibitor is utilized.

The assay comprises two stages: the initial measurement determines the total DTNB reduction by the sample, while the second measurement gauges the DTNB reduction by the sample in the presence of the TrxR-specific inhibitor. The difference between these two results represents the DTNB reduction attributable to TrxR.

Briefly, 50 µL of tubules or 2×10^6 cells were homogenized in 100 µL of cold Assay Buffer while keeping the samples on ice. The samples were then centrifuged at 10,000 g for 15 minutes at +4°C, and the resulting supernatant was collected for the assay. The protein concentration was determined by Bradford Reagent (Fisher Scientific, USA).

2 to 50 µL of the samples or 10 µL of TrxR positive control were pipetted in a 96 well plate (Corning™ Costar™, Germany). The volume was adjusted to 50 µL by adding Assay Buffer. Two separate sets of samples were tested: one with 10 µL TrxR Inhibitor (to test background enzyme activity) and the other with 10 µL Assay Buffer (to test total DTNB reduction). To prepare the TNB standard (calibrator) dilutions, manufacturer's recommendations were followed, using concentration range 0, 10, 20, 30, 40, and 50 nmol per well.

For each sample well and positive control, 40 µL of Reaction Mix, containing Assay Buffer, DNTB Solution, and NADPH I / NADPH, were added. Immediately, the optical density (OD_{412nm}) of the samples were measured at 412nm (0 h value, T_1). The two obtained values are A_{1t} and A_{1l}. Subsequently, the OD_{412nm} was measured at time T_2 after incubating the reaction at 25°C for 20 minutes to acquire values A_{2t} and A_{2l}, ensuring protection from light during this process.

The optical density of TNB^{2-} produced by TrxR was calculated as follows:

$$\Delta A_{412nm} = (A_{2t} - A_{2l}) - (A_{1t} - A_{1l}),$$

where A1t and A2t represent the samples mixed with the assay buffer, and A1l and A2l indicate the samples treated with the inhibitor.

The ΔA_{412nm} was then applied to the TNB standard curve to determine ΔB in nanomoles of TNB. TrxR activity was then calculated as follows:

$$\text{TrxR Activity (mU/ml)} = \frac{\Delta B}{(T2 - T1) \times V} \cdot \text{Sample Dilution Factor}$$

Where:

- ΔB represents the TNB quantity obtained from the TNB standard curve in nanomoles.
- T1 is the time of the initial reading (A_{1t} and A_{1l}) in minutes.
- T2 is the time of the subsequent reading (A_{2t} and A_{2l}) in minutes.
- V represents the volume of the preprocessed sample added to the reaction well in milliliters.

A single unit of TrxR is equivalent to the enzyme amount that generates 1.0 micromole of TNB per minute at 25°C. The oxidation of 1 mole of NADPH I/NADPH to NADP yields 2 moles of TNB, so 1 TNB unit is equal to 0.5 NADP units.

2.3.10. Bilateral kidney Ischemia and Reperfusion injury (IRI)

The bilateral kidney ischemia and reperfusion injury (IRI) model was performed according to a previously published surgical protocol (Tonnus, Al-Mekhlafi, et al., 2018; Tonnus, Meyer, et al., 2021). Prior the start of the experimental procedure, mice were administered an injection of Ferrostatin-1 (Merck Millipore) diluted in DMSO at a dosage of 10 mg/kg. In the control group, a 2% DMSO vehicle solution was injected. Male mice were carefully matched based on weight, age, and genetic background. 15 min before the surgery, all mice were administered intraperitoneally 0.1 µg/g body weight of buprenorphine-HCl (Temgesic®, Eumedica) intraperitoneally for analgesia. Anesthesia was induced using 3 l/min of volatile isoflurane mixed with pure oxygen in the induction chamber of a COMPAC5 small animal anesthesia unit (VetEquip, the Netherlands). Once an appropriate level of narcosis was achieved, typically within 2 minutes, mice were positioned supine on a temperature-controlled self-regulated heating system set to 38 °C. Their extremities were secured with stripes. Anesthesia was maintained at a dose of 1.5 l/min of isoflurane. Breathing patterns and analgesia levels were continuously monitored visually.

The abdomen was gradually opened in layers to create a 2 cm wide opening. Blunt retractors (Fine Science Tools, Germany) were placed for easy access. The caecum and gut were gently moved and positioned to the left side, resting on a PBS-soaked sterile gauze. Another piece of PBS-soaked gauze was used to sandwich the gut, lifting the duodenum for better visualization of the aorta abdominalis. The liver was carefully pushed cranially using a cotton bud to fully expose the right renal pedicle. Under the aid of a surgical microscope (Carl Zeiss, Jena, Germany), sharp forceps were used to create retroperitoneal holes in the renal pedicle, both cranially and caudally. Through these access points, a 100 g pressure micro serrefine (FST 18055-03) was placed on the pedicle to induce ischemia, and a timer was started.

The cotton bud was then removed, and the packed gut was shifted to the right side to expose the left renal pedicle. If necessary, the cotton bud was used to gently move the spleen or stomach aside. Retroperitoneal access was established once again

by creating holes with sharp forceps, and another 100 g pressure micro serrefine was applied. The time between the placement of both serrefines was recorded, typically around 40 seconds (ensured to be less than 1 minute in all cases). The gut was returned to the abdominal cavity, and the opening was covered with the two gauze pieces. After 23 minutes from the initial timer start, the retractors were repositioned, and the gut was mobilized again to expose the right kidney. After exactly 24 minutes (with a tolerance of 1 second), the vascular clamp was removed, and the gut was shifted to the right side. Following the recorded time difference, the clamp on the left side was also removed. Visual confirmation of reperfusion was obtained for both sides before the gut was placed back into the abdominal cavity. The parietal peritoneum and the skin were closed separately using continuous sutures with a 6-0 monocryl thread (Ethicon). Isoflurane administration was stopped immediately, and 1 mL of pre-warmed PBS was given intraperitoneally to prevent dehydration and monitor potential suture leakage. The mice were divided into pairs of two and returned to their cages. Analgesia was provided by administering 0.1 µg/g buprenorphine-HCl (Temgesic®, Eumedica) every 8 hours. After a 48-hour observation period, blood was collected via retroorbital puncture, and the mice were euthanized by neck dislocation. The right kidney was extracted and subjected to fixation in 4 % normal buffered formalin (ElectronMicrocopy Science, Cat#15710), for a duration of 24 hours. It was then transferred to 70 % ethanol (Roth, Cat#K.9285) and stored at room temperature. On the other hand, the left kidney was promptly frozen in liquid nitrogen and subsequently transferred to a storage temperature of -80 °C. For survival analysis, mice were closely monitored up to 7 days.

2.3.11. Immunohistology and semi-quantitative scoring

The organs were dissected and placed in 4 % neutral-buffered formaldehyde solution (ElectronMicrocopy Science, Cat#15710). They were fixed for 24 hours and subsequently transferred to 70% ethanol (Roth, Cat#K.9285) for storage.

To prepare the sections for Periodic Acid-Schiff (PAS) staining, the Morphisto 12153 kit was utilized with a modified protocol. First, the samples were dewaxed by immersing them in xylene for two rounds of 10 minutes each. Rehydration followed, involving sequential immersion in ethanol solutions: two times in 100 %, two times in 96 %, once in 70 %, once in 40 % ethanol, and finally in distilled water, with each step lasting 1 minute. Thin sections (3-5 µm) were prepared from the paraffin blocks and stained with

a 1 % periodic acid solution for 3 minutes. After a brief 30-second rinse under tap water, they were rinsed in distilled water for 1 minute. Next, the samples were incubated in Schiff's reagent for 2 minutes and 30 seconds, followed by a 1-minute rinse under tap water and a 1-minute rinse in distilled water. To counterstain, the samples were exposed to acidified Mayer's haematoxylin for 3 minutes, then rinsed under tap water for 3 minutes, and again in distilled water for 1 minute. Dehydration was carried out by sequentially immersing the samples in ethanol solutions: 1 minute each in 40 % and 70 %, three times in 96 %, and twice in 100 %. Finally, the samples were cleared with two rounds of 2-minute immersion in xylene and mounted using Cytoseal or an alternative medium containing xylene.

The stained sections were then examined using an Axio Imager microscope (Zeiss) at magnifications of 100×, 200×, and 400×. Micrographs of the sections were captured using an AxioCam MRm Rev. 3 FireWire camera and AxioVision ver. 4.5 software (Zeiss). To assess organ damage, an experienced pathologist evaluated the stained sections in a double-blind manner, utilizing a scoring system (nodular sclerosis score) that ranged from 0 (no tissue damage) to 5 (severe glomerular damage). The scoring was based on the degree of morphological changes observed in the renal tissue under light microscopy. The morphological damage to the glomeruli following the onset of diabetic kidney disease, was assessed according to the extent of sclerotic lesions. The scale included the following categories: not present (0), mild (1), moderate (2), severe (3 to 4), and very severe (5). The evaluation was performed on a minimum of three different animals.

The PAS staining procedure was supported by the Histology Facility, a Core Facility of the CMCB Technology Platform at TU Dresden.

2.3.12. Measurements of sulfur-containing metabolites by ultra-performance liquid chromatography-mass spectroscopy (LC-MS)

The preparation of freshly isolated kidney tubules for liquid chromatography-mass spectroscopy (LC-MS) was performed according to a modified previously published protocol (Barayeu *et al.*, 2023).

Briefly, the isolated tubules (see **Section 2.2.3.** for isolation protocol) were washed twice with cold NaCl (0.9 %) solution. Subsequently, any excess liquid was carefully removed. To ensure cell lysis, 200 µl of a 25mM MBB (Monobromobimane) solution in 50 % MeOH was added to the tubules. The volume of MBB solution was

adjusted based on the cell quantity, ensuring sufficient coverage to lyse all cells. The samples were then incubated in the dark at room temperature for 20 minutes. Following the incubation period, the tubules were snap frozen in liquid nitrogen, stored at -80 °C, and finally shipped to the designated location on dry ice for further analysis.

The cell suspension was spun down at 14,000g for 10 minutes, and 3 μl of supernatant was applied to an Accucore 150 Amide HILIC HPLC column (100×2.1 mm, 2.6-μm particle size) equipped with a guard cartridge (at 30 °C). Mobile phase 'A' was 5 mM ammonium acetate in 5 % acetonitrile (CH3CN); mobile phase 'B' was 5 mM ammonium acetate in 95 % CH3CN. The liquid chromatography (LC) gradient program was: 98 % B for 1 minute, followed by a linear decrease to 40 % B within 5 minutes, then maintaining 40 % B for 13 minutes, then returning to 98% B in 1 minute and finally 5 min 98 % B for column equilibration. The flow rate was 350 μl min–1. The eluent was directed to the electrospray ionization (ESI) source of the Q Exactive (QE) MS from 0.5 min to 19 min after sample injection. Each sample was run with the parallel reaction monitoring (PRM) method for monobromobimane alkylated metabolites. PRM method: scan type: PRM positive mode; runtime: 0.5-10 minutes. ddMS2 settings: resolution: 17,500; AGC target: 2×105; maximum injection time: 200 ms; loop count: 1; CE: 20, 50 and 80; isolation window: 1.2 m/z. For normalization among the samples, the protein pellets were dried on air and then dissolved in 200 μl 100 mM NaOH. The total protein content was determined by performing a BCA assay. PRM data were processed with Skyline (21.2.0.425) (MacLean *et al.,* 2010) and normalized to total protein.

The LC-MS measurements were supported by the laboratory of Tobias P. Dick at the DKFZ in Heidelberg, Germany.

2.4. Statistical analysis

Statistical analyses were conducted using Prism 8, a software by GraphPad (San Diego, CA, USA). In the survival experiments, we utilized a Kaplan-Meier curve to plot the animals and employed the log-rank test to evaluate the null hypothesis of no difference between groups. For all other experiments, we applied a two-tailed parametric t-test to compare normally distributed datasets, and performed a one-way ANOVA followed by post hoc Tukey's multiple comparisons test to analyse data involving multiple groups. Significance was determined with $*p \leq 0.05$, $**p \leq 0.01$, or $***p \leq 0.001$, unless otherwise specified. Unless indicated otherwise, the bar graphs show the mean value accompanied by the standard deviation (SD).

Results

3. Results

3.1. Characterization of diabetic kidney disease in GIPR[dn] mice

The main experimental platform for this study concerning a diabetic mouse model were GIPR[dn] mice. These mice suffer from early onset of diabetes mellitus, in parallel with premature onset of diabetic kidney disease due to the overexpression of a dominant negative version of the human GIP receptor, under the control of a rat pro-insulin 2 gene promoter on a CD1 mouse background (Herbach *et al.*, 2009). These unique characteristics of GIPR[dn] mice make them a proper tool for investigating the mechanisms and progression of DKD.

To follow the development of diabetic nephropathy in these animals, biochemical analyses on blood serum as well as qualitative morphological analyses of the kidneys of male GIPR[dn] transgenic mice and non-transgenic littermate controls (CD1 mice) were performed at 7, 10, 25, 40, and 50 weeks of age.

3.1.1. Blood glucose

To evaluate the progression of Type 2 Diabetes in GIPR[dn] mice, blood glucose levels of transgenic mice and their wild type littermates were assessed at the specific time intervals. A small incision was made on the mice's tail, and a tiny amount (0.5 µl) of blood was placed directly on GlucoSmart® test strips, which were part of the GlucoseSmart®Swing2 mg/dl blood glucose meter. As early as 7 weeks old, the transgenic mice exhibited significantly elevated glucose levels in comparison to the control group, while blood glucose levels of control mice remained stable over the period sampled (**Figure 8**).
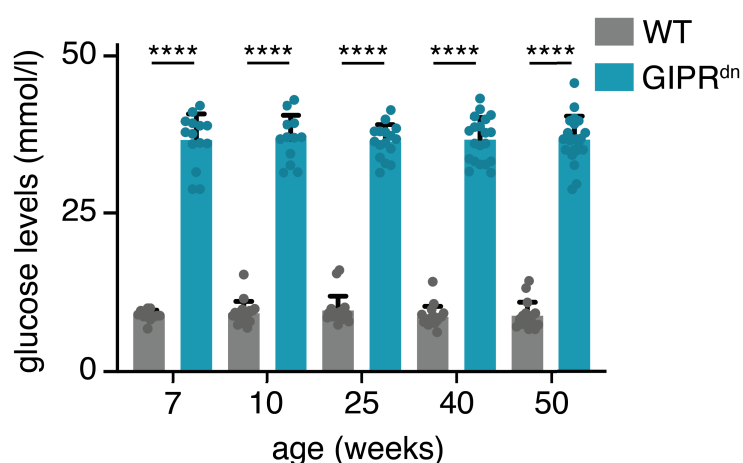
Figure 8. GIPR[dn] mice show higher glucose levels compared to WT littermates.
The glucose level of GIPR[dn] mice is significantly higher than that of sex-matched littermates at any given time point. The following sample sizes were used for each age group: 7-week-old group (N = 13 WT mice, N = 14 GIPR[dn] mice), 10-week-old group (N = 18 WT mice, N = 12 GIPR[dn] mice), 25-week-old group (N = 19 WT mice, N = 16 GIPR[dn] mice), 40-week-old group (N = 19 WT mice,

N = 20 GIPR^{dn} mice), and 50-week-old group (N = 17 WT mice, N = 22 GIPR^{dn} mice). Data are presented as mean ± SD. Statistical analysis was performed using an unpaired t-test with Welch's correction, with the following significance levels: **** $p < 0.0001$.

3.1.2. Body weight

In parallel, periodic measurements of body weights were conducted, and the resulting data were plotted for the chosen time points. Overall, the body weight of the transgenic mice was significantly lower than the wild type littermates irrespective of the age of sampling. The data showed that GIPR^{dn} mice failed to gain weight over time (**Figure 9.**).
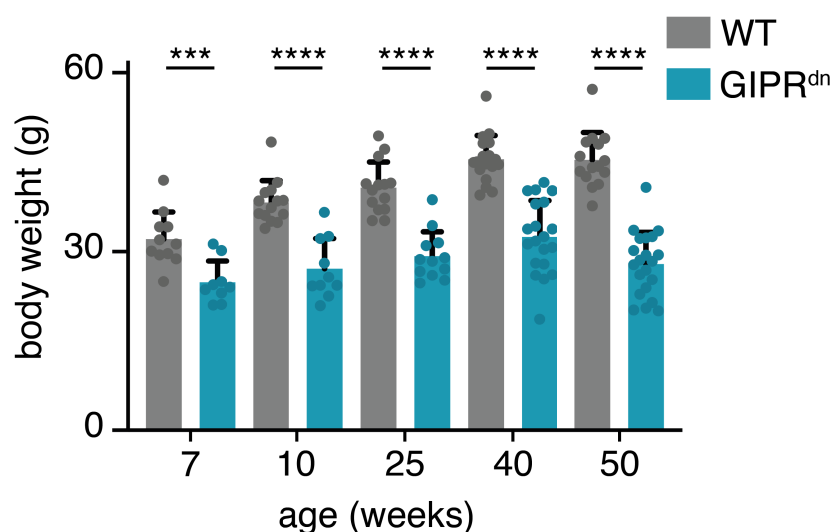
Figure 9. Transgenic (GIPR^{dn}) mice fail to gain weight over time compared to WT littermates. The body weight of GIPR^{dn} mice is significantly lower than that of sex-matched controls irrespective of the age of sampling. The following sample sizes were used for each age group: 7-week-old group (N = 11 WT mice, N = 9 GIPR^{dn} mice), 10-week-old group (N = 14 WT mice, N = 10 GIPR^{dn} mice), 25-week-old group (N = 14 WT mice, N = 12 GIPR^{dn} mice), 40-week-old group (N = 18 WT mice, N = 20 GIPR^{dn} mice), and 50-week-old group (N = 15 WT mice, N = 21 GIPR^{dn} mice). Data are presented as mean ± SD. Statistical analysis was performed using an unpaired t-test with Welch's correction, with the following significance levels: *** $p < 0.001$, **** $p < 0.0001$.

3.1.3. Serum parameters

To monitor the progression of DKD in GIPR^{dn} mice, serum creatinine and serum urea levels were used as markers for the evaluation of kidney function. Blood samples were collected from the retroorbital plexus and sent to the Institut für Klinische Chemie und Laboratoriumsmedizin (IKL, Universitätsklinikum Dresden) for serum extraction and analysis. For each time point analysed, both serum creatinine and serum urea levels were significantly higher in transgenic mice compared to their wild type littermates (**Figure 10**).

Figure 10. GIPR^{dn} mice show elevated levels of serum creatinine and serum urea compared to the wild type controls.

A. Serum creatinine levels of GIPR^{dn} mice are significantly elevated compared to those of sex-matched control mice. The following sample sizes were used for each age group: 7-week-old group (N = 5 WT mice, N = 7 GIPR^{dn} mice), 10-week-old group (N = 6 WT mice, N = 4 GIPR^{dn} mice), 25-week-old group (N = 7 WT mice, N = 10 GIPR^{dn} mice), 40-week-old group (N = 9 WT mice, N = 10 GIPR^{dn} mice), and 50-week-old group (N = 7 WT mice, N = 19 GIPR^{dn} mice). **B.** Serum urea levels of GIPR^{dn} mice are significantly higher than that of WT littermates. The following sample sizes were used for each age group: 7-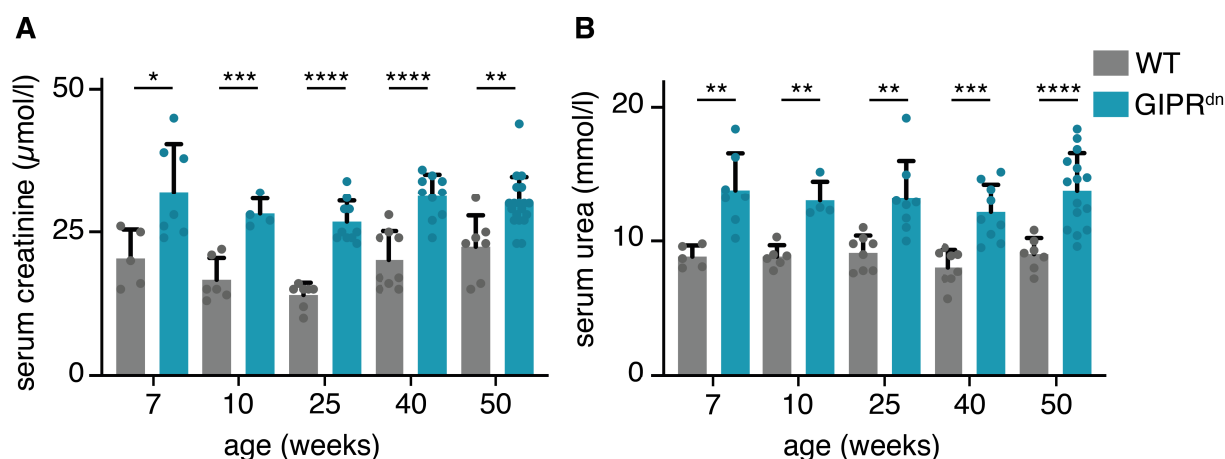week-old group (N = 5 WT mice, N = 7 GIPR^{dn} mice), 10-week-old group (N = 6 WT mice, N = 4 GIPR^{dn} mice), 25-week-old group (N = 8 WT mice, N = 8 GIPR^{dn} mice), 40-week-old group (N = 8 WT mice, N = 9 GIPR^{dn} mice), and 50-week-old group (N = 7 WT mice, N = 15 GIPR^{dn} mice). For all bar graphs data are presented as mean ± SD. Statistical analysis was performed using an unpaired t-test with Welch's correction, with the following significance levels: * $p < 0.05$, ** $p \leq 0.01$, *** $p < 0.001$, **** $p < 0.0001$.

3.1.4. Histological analysis of the kidneys

To further assess the kidney function of the diabetic mice at specific time points, morphological analysis of kidney sections obtained from both GIPR^{dn} and WT littermates were conducted. Kidney sections were stained using standard PAS (Periodic Acid-Schiff stain) protocol, and images were captured at final magnifications of 200×, and 400×.

At 7 weeks of age, there were no detectable differences in morphology between the transgenic and control mice sections. However, starting from 10 weeks of age, glomerular lesions specifically in GIPR^{dn} kidneys were observed, while the WT littermates showed no signs of such damage. The glomerular damage became even more evident when observed at a higher magnification of 400× (**Figure 11**). The glomeruli of the transgenic mice showed various changes, such as mesangial expansion, hyalinosis, and segmental sclerosis. All together these morphologies are known as Kimmelstiel-Wilson lesions (Kimmelstiel & Wilson, 1936), signs of diabetic glomerulosclerosis in human DKD patients. Additionally, adhesions were observed between the glomerular tuft and the Bowman's capsule.
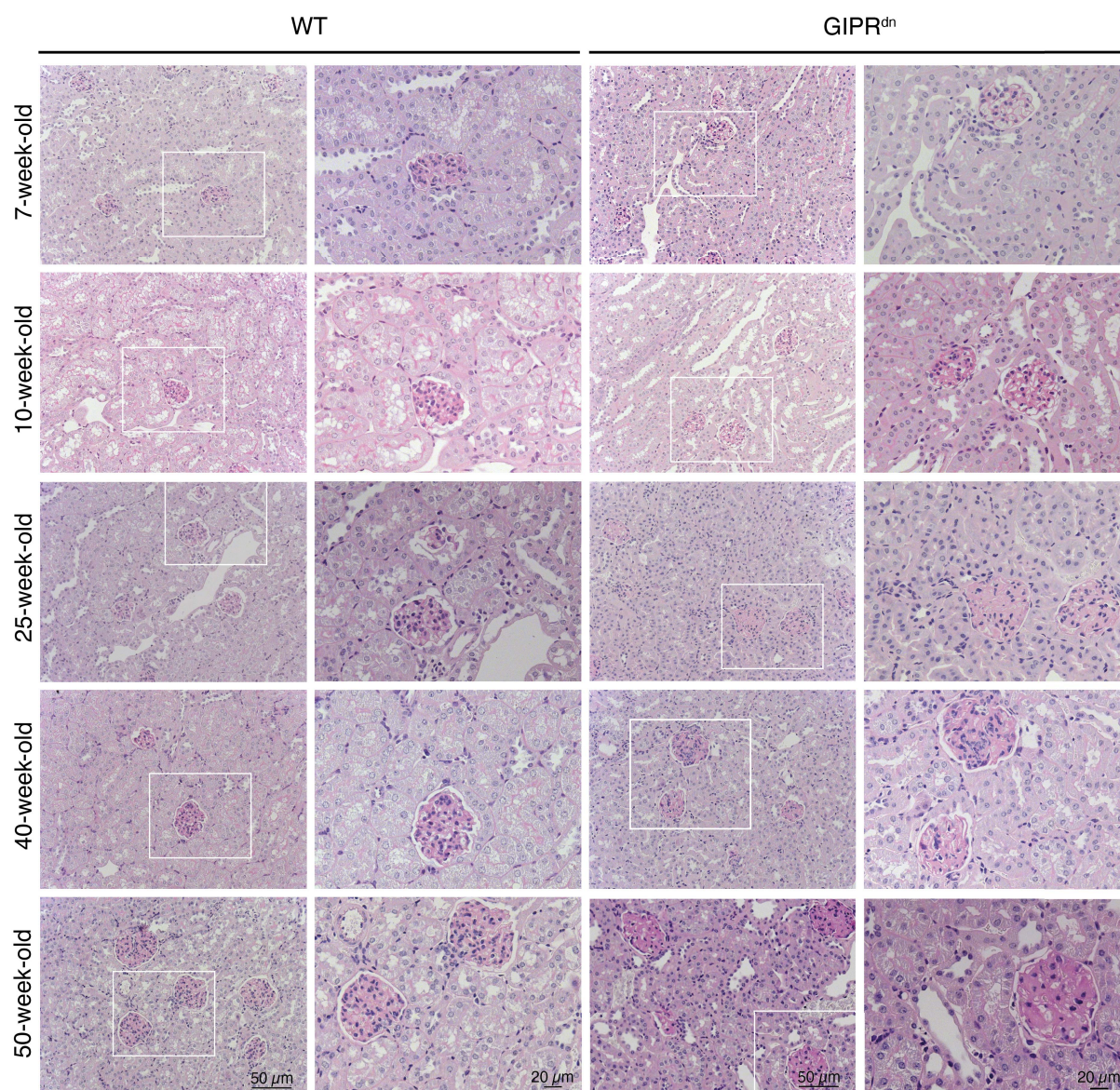
Figure 11. GIPR^{dn} kidney sections show signs of glomerulosclerosis already at 10 weeks of age.

Representative microphotographs of periodic acid-Schiff (PAS)-stained histological sections of male control kidneys and age-matched GIPR^{dn} male at 200× and 400× final magnifications. The white rectangles indicate the corresponding magnified area on the right. At 7 week of age, no discernible differences between wild type and transgenic sections are noticeable. However, starting from the 10th week of age, the transgenic mice exhibit mesangial expansion, hyalinosis, and widespread adhesion between the glomerular tuft and the Bowman's capsule.

The stained sections were then examined by an experienced pathologist in a double-blind manner and the glomerular damage was evaluated utilizing a scoring system that ranged from 0 (no tissue damage) to 5 (severe glomerular damage) (**Figure 12**). The data indicates that at the age of 7 weeks, the onset of diabetic nephropathy is at an initial stage in GIPR^{dn} mice. However, by the time they reach 10 weeks of age, the severity of the damage is already

severe. This damage continues to escalate in intensity with advancing age, reaching its peak at 50 weeks.
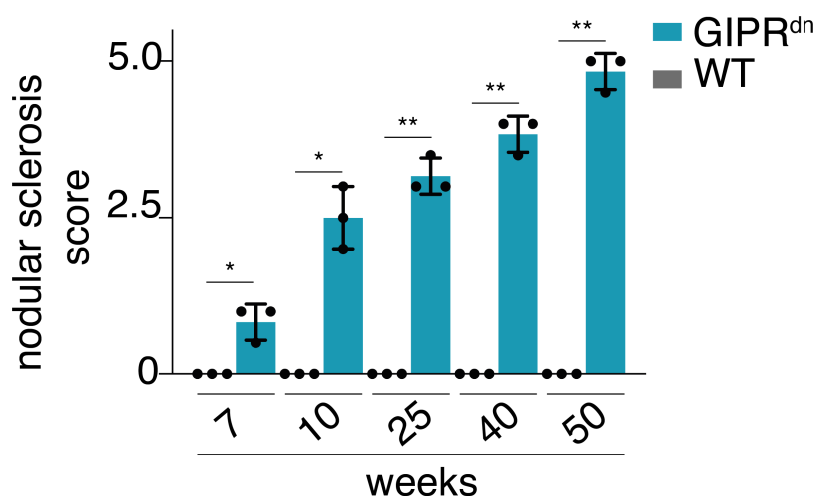
Figure 12. Nodular sclerosis score quantification of PAS-stained WT and GIPR^{dn} kidney sections.

The nodular sclerosis score of GIPR^{dn} mice is significantly elevated compared to those of sex-matched control mice. Data are presented as mean ± SD. Statistical analysis was performed using an unpaired t-test with Welch's correction, with the following significance levels: * $p < 0.05$, ** $p \leq 0.01$.

In summary, the evaluation of kidney function markers such as serum creatinine and serum urea (see **Section 3.1.3.**), together with morphological analysis of the kidneys in GIPR^{dn} mice and littermate controls, consistently pointed towards the establishment of a reliable model for evaluating diabetic nephropathy.

3.2. The spontaneous death of GIPR^{dn} tubules is characterized by a non-random pattern of necrotic cell death

Following the observation of diabetes as well as DKD onset and progression, in GIPR^{dn} mice, the subsequent phase of the project focused on the impact of diabetes on factor such as sensitivity to acute tubular necrosis (ATN), nephron loss, and sensitivity to acute kidney injury (AKI). Specifically, the focus was on comprehending the role of kidney tubules and ferroptosis-induced cell death in contributing to the development of DKD.

Notably, non-random propagation of cell death was observed in wild-type murine kidney tubules treated with ferroptosis inducers, demonstrating a specific pattern (Linkermann *et al.*, 2014). To explore the potential occurrence of a similar phenomenon in spontaneous tubular necrosis a protocol to isolate murine kidney tubules was established. Upon the

isolation of kidney tubules, the quantification of spontaneous necrosis can be achieved through LDH release. The LDH release assay relies on the principle that when cells are damaged or undergo cell death, their cell membrane integrity is compromised, allowing intracellular components, including LDH, to leak into the extracellular space. This release of LDH can serve as a marker of cellular damage and death.

As illustrated in **Figure 13A**, 10-week-old GIPR^{dn} mice exhibited elevated levels of LDH release compared to their wild-type littermates. The percentage of LDH release assay (Y values) was used to calculate the speed of cell death propagation spontaneously happening in kidney tubules (**Figure 13B**), and a significantly accelerated rate of cell death propagation in tubules isolated from GIPR^{dn} mice was observed (**Figure 13C**). To enhance the visualization of this effect, a 3D printed double chamber separated by a central glass slide was used to run microscopy analysis of the tubules (**Figure 13D**). This setup was used to record time-lapse videos of cell death propagation using SYTOX green as a dye for necrotic cells (**Figure 13E-F**). In contrast to tubules isolated from 10-week-old GIPR^{dn} mice, isolation at 7 weeks of age did not result in significantly different cell death propagation, as assessed by this method.

Subsequently, fluorescence lifetime imaging (FLIM) microscopy was employed to detect NAD(P)H autofluorescence and NAD(P)H lifetime during tubular cell death propagation. As demonstrated in **Figure 13G**, the mean NAD(P)H lifetime appeared to be longer in wild-type littermates, although NAD(P)H autofluorescence remained largely unchanged. While we cannot conclusively infer significant diabetic nephropathy-induced differences from this experiment, it clearly demonstrates that cell death propagation in the kidney tubules correlates with a loss of NAD(P)H autofluorescence and NAD(P)H lifetime.

Collectively, these data indicated a non-random spontaneous tubular necrosis occurring in both GIPR^{dn} and WT samples.
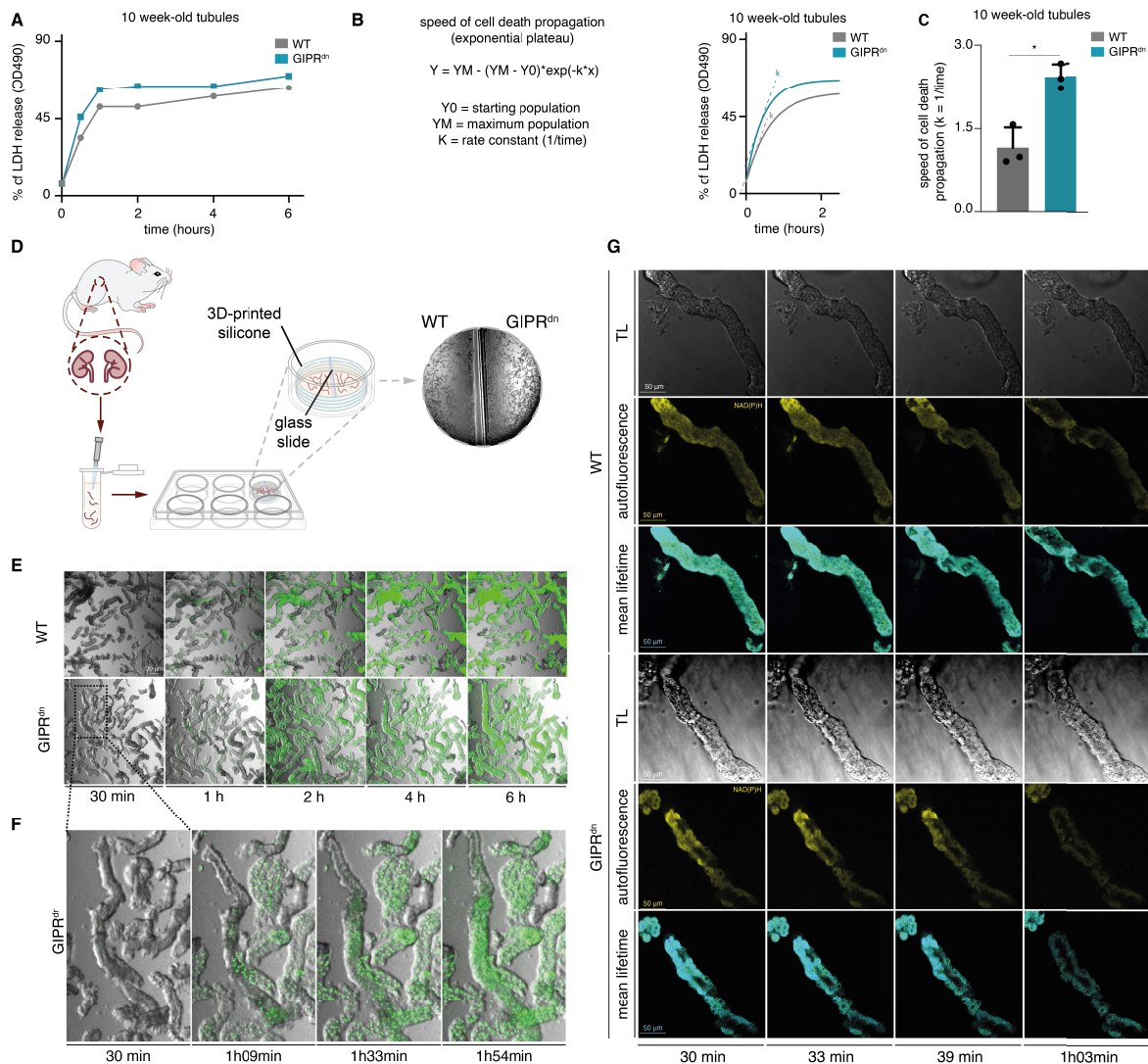
Figure 13. GIPRdn tubules undergo synchronized regulated necrosis (SRN).

A. Representative LDH release experiment of WT and GIPRdn tubules isolated from 10-week-old mice undergoing spontaneous death. **B.** Representative calculation of the speed of cell death propagation using the Y value of A. **C.** Quantification of the speed of cell death propagation of WT and GIPRdn kidney tubules undergoing spontaneous death. Data are presented as mean ± SD. Statistical analysis was performed using an unpaired t-test with Welch's correction, with the following significance levels: * $p < 0.05$ **D.** Schematic representation of the 3D printed chamber used to simultaneously monitor isolated tubules from GIPRdn and WT mice. The glass slide in the middle of the chamber prevents any communication of the samples. **E.** Still images of time lapse imaging of freshly isolated WT and GIPRdn murine kidney tubules stained with SYTOX green (pseudo-coloured in green) at different time points (final magnification of 25x). **F.** Zoomed-in still images of GIPRdn tubules stained with SYTOX green (pseudo-coloured in green) at different time points. **G.** Still images of transmitted light and NADH autofluorescence intensity captured with two-photon confocal microscopy at different time points.

3.3. GIPR^{dn} tubules are more prone to undergo spontaneous death compared to WT tubules

To more precisely investigate the impact of DN development on the sensitization to tubular necrosis, three independent experiments involving tubular isolation to assess LDH release were conducted at each time point. Before the isolation of the kidney tubules, glucose levels were measured in both transgenic mice and wild type control groups (**Table 13**).

Table 13. WT and GIPR^{dn} glucose levels from the mice used in LDH release experiments. Data are presented as means ± SD.

age (weeks)	glucose levels (mmol/l)	
	GIPR^{dn}	WT
7	36.6 ± 4.0	9.1 ± 0.3
10	36.6 ± 4.0	11.6 ± 2.0
25	35.0 ± 2.0	9.8 ± 0.3
40	33.4 ± 2.0	9.0 ± 1.0
50	35.1 ± 2.5	9.4 ± 0.5

The freshly isolated tubules were isolated, cultured in a 24-well plate, and spontaneous tubular death was evaluated over a period of 6 hours with the use of the LDH release assay. The assessment was performed at various time points (0, 0.5, 1, 2, 4, and 6 hours).

In accordance with **Figure 13E-F**, no significant differences in LDH release from isolated tubules were observed at the age of 7 weeks (**Figure 14A-C**). However, across all older age groups examined (10 weeks, 25 weeks, 40 weeks, and 50 weeks), LDH release from GIPR^{dn} mice consistently exceeded that from age-matched littermate controls (**Figure 14D-O**).

Microscopic examinations of the tubules indicated that throughout the duration of the experiment, necrotic tubules underwent morphological changes and exhibited a "whitened" appearance when observed under a microscope (**Figure 14. C, F, I, L, O**).

Collectively, these data indicate that the onset of diabetic nephropathy-induced sensitization to ferroptosis in kidney tubules occurs between 7 and 10 weeks of age.
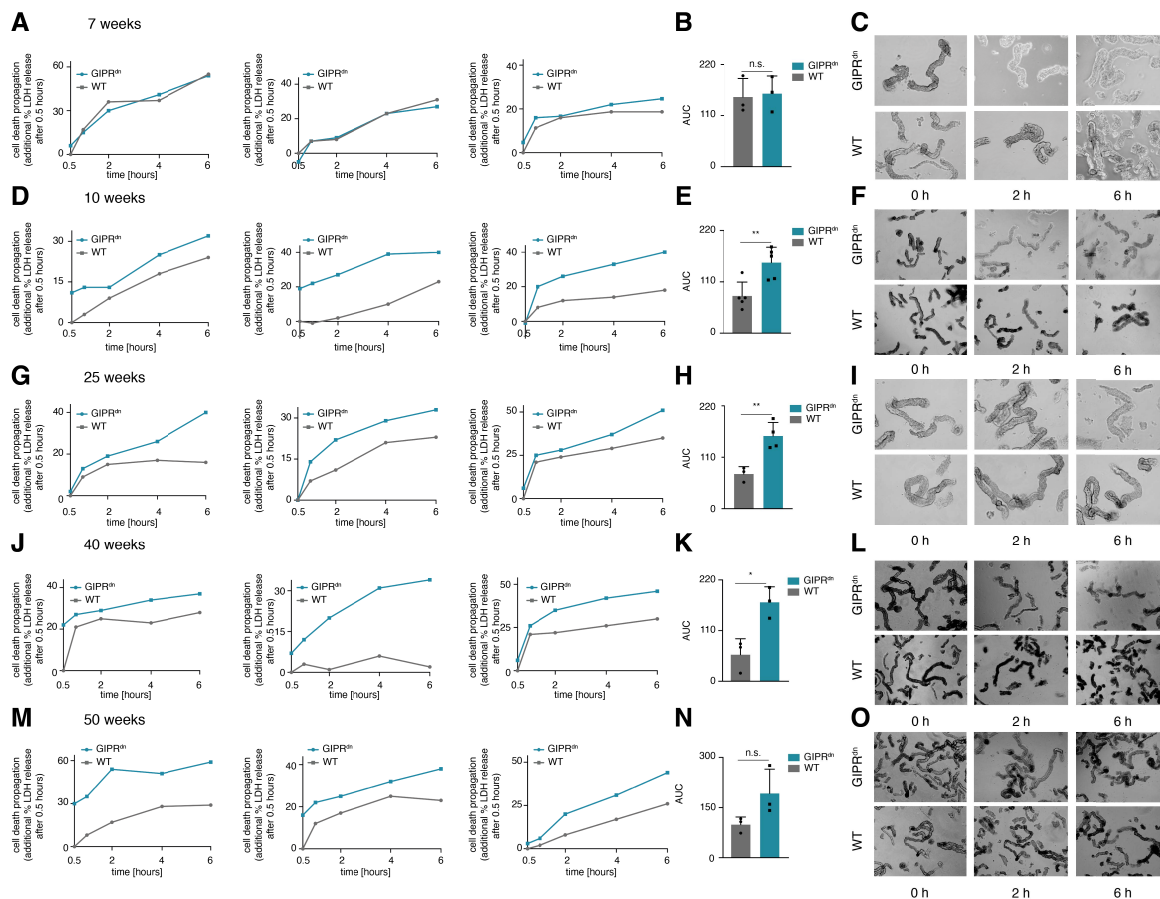
Figure 14. GIPRdn tubules show an increased sensitivity to spontaneous tubular necrosis compared to the WT controls.

A, D, G, J, M. Representative single LDH release experiments of WT and GIPRdn tubules isolated from mice of different ages undergoing spontaneous death (data are shown as additional LDH release after 0.5 h). **B, E, H, K, N.** Corresponding area under the curve (AUC) quantification of the independent LDH release experiments. **C, F, I, L, O.** Representative images of freshly isolated WT and GIPRdn kidney tubules at indicated time points (final magnification 100x). All experiments were independently repeated 3 times (N = 3). Data are presented as means ± SD. Statistical analysis was performed using a Welch´s t-test with the following significance levels: * p < 0.05, ** p ≤ 0.01.

3.4. Spontaneous necrosis of GIPRdn and WT tubules is partially mediated by ferroptosis

To address the hypothesis on the contribution of ferroptosis to spontaneous necrosis of both GIPRdn and WT tubules the ferroptosis inhibitor Fer-1 was added to the medium of freshly isolated tubules.

Before the isolation of the kidney tubules, glucose levels were measured in both transgenic mice and wild type control groups (see **Table 14**).

Table 14. WT and GIPR^{dn} glucose levels from the mice used in LDH release experiments. Data are presented as means ± SD.

age (weeks)	glucose levels (mmol/l)	
	GIPR^{dn}	WT
7	37.0 ± 2.0	8.0 ± 1.0
10	35.0 ± 2.0	8.0 ± 1.0
25	38.0 ± 0.4	9.0 ± 1.0
40	38.0 ± 6.0	10.0 ± 4.0
50	35 ± 5.0	10.0 ± 3.0

The freshly isolated tubules were cultured in the presence of 30 µM Fer-1 and the LDH release was measured over 6 hours. The data obtained from the experiments indicated no difference when the experiments were performed on tubules obtained from 7-week-old mice regardless their genetic background (**Figure 15A, B**). However, starting from 10 weeks of age, the measured LDH levels were lower in both WT and GIPR^{dn} samples treated with the ferroptosis inhibitor compared to those treated with the vehicle control (**Figure 15C, D**). Although the trend remained clear and persisted across the following considered time points, statistical significance was not observed (**Figure 15E, F, G, H, I, J**).
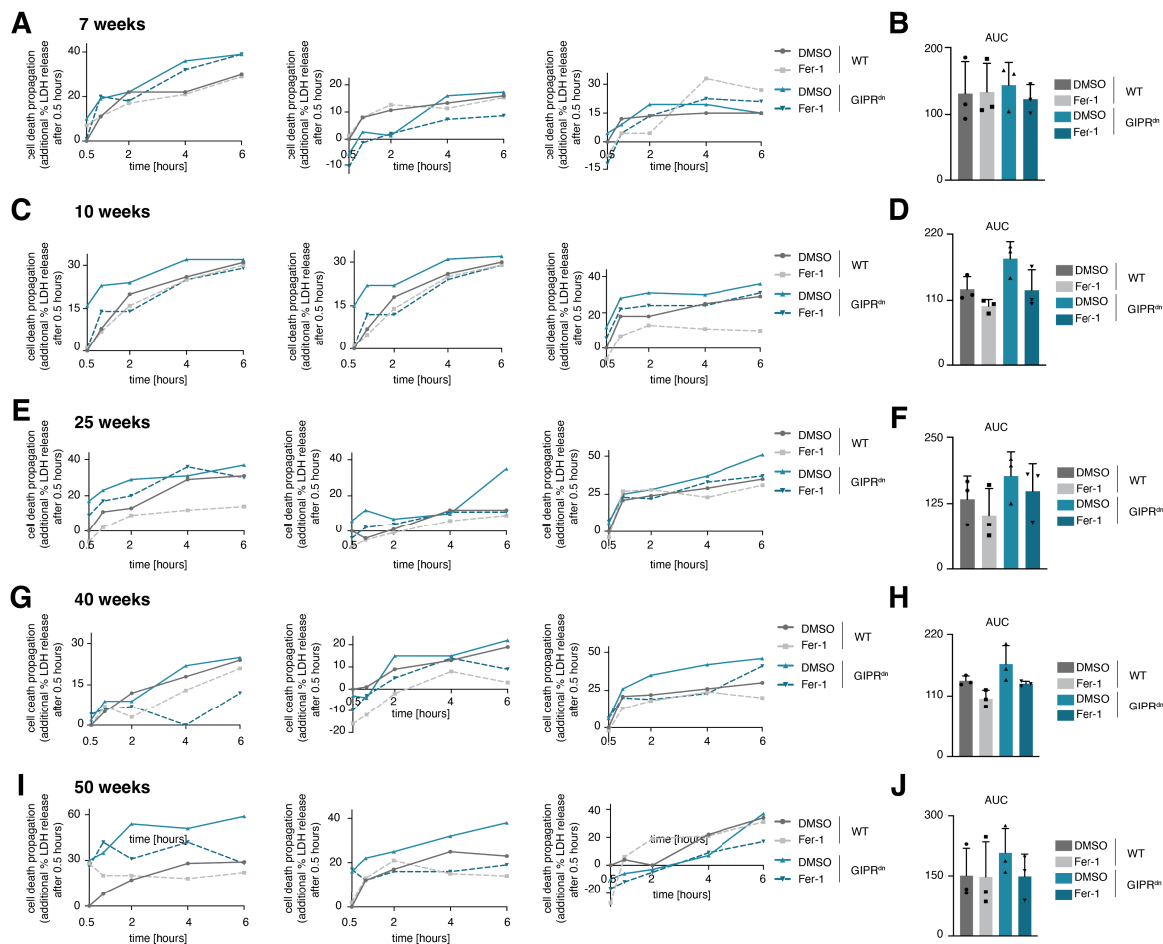
Figure 15. The LDH release of WT and GIPR^{dn} tubules undergoing spontaneous tubular necrosis is reduced in the presence of a ferroptosis inhibitor.

A, C, E, G, I. Representative single LDH release experiments of WT and GIPR^{dn} tubules belonging to mice of different ages undergoing spontaneous death and treated with vehicle (DMSO) or 30 µM Ferrostatin-1 (Fer-1); data are shown as additional LDH release after 0.5 h. **B, D, F, H, J.** Corresponding area under the curve (AUC) quantification of the independent LDH release experiments. All experiments were independently repeated 3 times (N = 3). Data are presented as means ± SD.

In summary, the observed trend, even in the absence of statistical significance, underscores the potential importance of ferroptosis modulation as a mechanism for mitigating tubular necrosis.

3.5. GIPR^{dn} tubules show downregulation of the PRX pathway compared to the non-diabetic tubules

To explore the high susceptibility of GIPR^{dn} tubules to ferroptosis compared to WT tubules, Western Blot analyses targeting proteins recognized for their involvement in ferroptosis were performed on freshly isolated kidney tubules from both GIPR^{dn} and WT littermate mice.

The Western Blot results indicated an equal expression of GPX4 in both WT and GIPRdn tubules, while a slight lower expression of ACSL4 was detected in the GIPRdn tubules compared to the WT samples. Most intriguingly, however, a clear and almost complete vanishing of the ferroptocide-target protein TXNRD1 and a decrease in expression of both peroxiredoxin 1 and thioredoxin 1 (PRX1 and TRX1), were noticed. (**Figure 16A**).

g
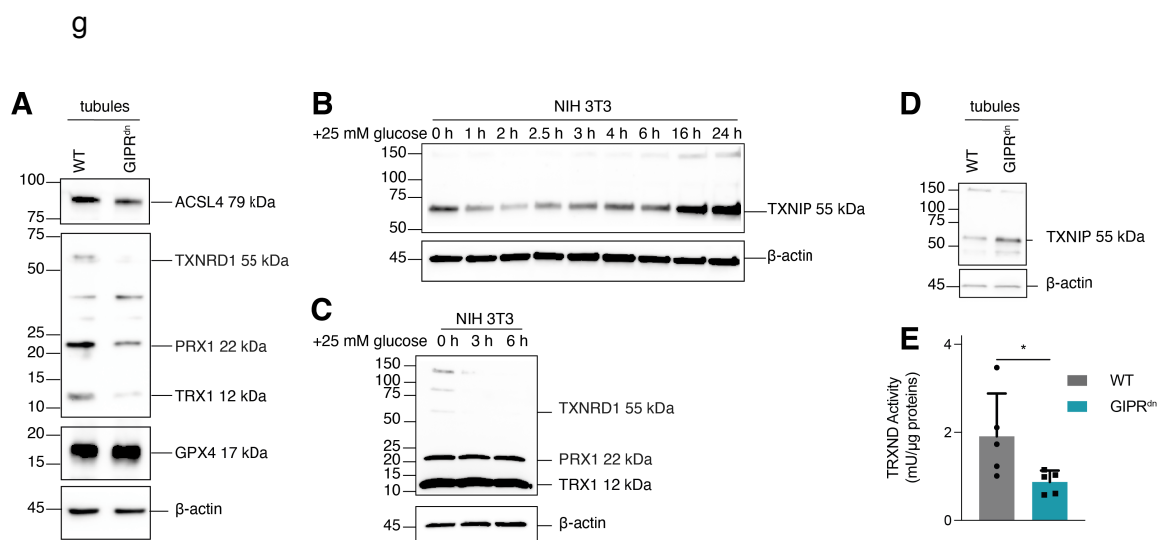
Figure 16. The TRX pathway is altered in GIPRdn kidney tubules compared to WT tubules.
A. Western blot analysis of WT and GIPRdn kidney tubules against ACSL4, TXNRD1, PRX1, TRX, and GPX4. **B.** Western blot analysis of cell lysates of NIH 3T3 against TXNIP after the addition of 25 mM glucose in the cell culture medium for 0, 1, 2, 2.5, 3, 4, 6, 16, and 24 h. **C.** Western blot analysis of cell lysates of NIH 3T3 against TXNRD1, PRX1, and TRX after the addition of 25 mM glucose in the cell culture medium for 0, 3 and 6 h. **D.** Western blot analysis of WT and GIPRdn kidney tubules against TXNIP. For all western blots β-actin was used as the loading control. **E.** Thioredoxin reductase activity in WT (N = 5) and GIPRdn kidney tubules (N = 5). All experiments were independently repeated independently at least 3 times (N = 3). Bar graph data are presented as means ± SD. Statistical analysis was performed using a Welch´s t-test. * $p < 0.05$.

These data prompted us to investigate a known TXNRD1 regulating factor, referred to as thioredoxin interacting protein (TXNIP), which is known to be upregulated upon extracellular hyperglycaemia (N. Wu *et al.*, 2013). Indeed, the Western Blot results showed that TXNIP was upregulated in NIH 3T3 cells upon supplementation of the media with 25 mM of glucose. Likewise, upon glucose supplementation, baseline expression levels of TXNRD1 were reduced to an extent that precluded detection by Western Blot (**Figure 16C**). Importantly, much higher levels of TXNIP were detected in lysates of kidney tubules obtained from GIPRdn mice compared to WT littermates (**Figure 16D**). These data suggest a previously unrecognized interaction between TXNRD1-regualted sensitivity to tubular necrosis controlled by hyperglycemia-induced TXNIP expression.

To examine the functional role of TXNRD in kidney tubules, a Thioredoxin reductase activity assay was conducted on both GIPR[dn] and WT kidney tubules. The results clearly indicated a significant decrease in the activity of TXNRD in the GIPR[dn] tubular samples (**Figure 16E**).

In light of these findings, to further assess the involvement of TXNRD1 in the sensitization of kidney tubules to necrosis, tubules isolated from both WT and GIPR[dn]-littermate mice were treated with ferroptocide (FTC). WT and GIPR[dn] tubules were isolated and treated with DMSO as a vehicle control, 10 µM FTC, and 30 µM Fer-1 serving as a protection control, or the combined co-treatment of FTC and Fer-1. The LDH release assay was utilized as a readout for the experiments. Despite the already heightened levels of LDH release and accelerated cell death propagation observed in tubules from GIPR[dn] mice, the addition of FTC significantly intensified these characteristics. As anticipated, the administration of Fer-1 reversed this phenotype (**Figure 17 A-B**). Statistical analysis performed on the area under the curve resulting from the experiments highlighted the significant difference between the DMSO-treated tubules and those treated with FTC (**Figure 17C**). This experiment unequivocally verified the functional role of TXNRD1 in the sensitization of ferroptosis induced by hyperglycemia.

Collectively these data point towards the pivotal role of ferroptosis in enhancing the susceptibility of diabetic tubules to spontaneous necrotic cell death.
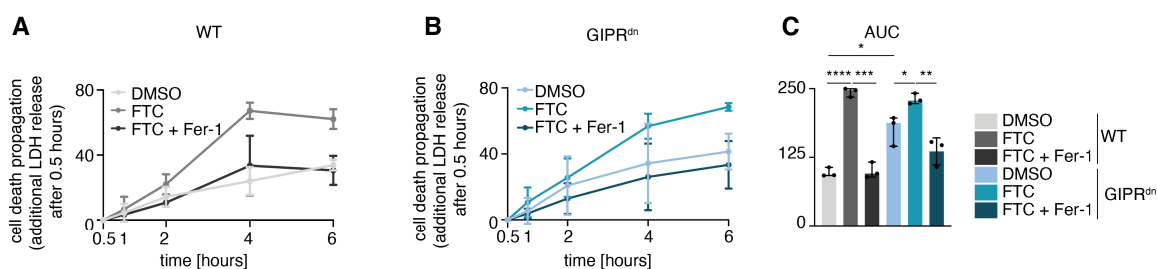
Figure 17. Ferroptocide treatment further sensitize kidney tubules to undergo necrosis.
A. LDH release experiments of WT or **B.** GIPR[dn] tubules treated with vehicle, 30 µM FTC, 30 µM Fer-1 or co-treated with FTC and Fer-1 (data are shown as additional LDH release after 0.5 h). **C.** Corresponding area under the curve (AUC) quantification of the independent LDH release experiments. All experiments were independently repeated 3 times (N = 3). Statistical analysis was performed using an unpaired t-test with Welch's correction, with the following significance levels: * $p < 0.05$, ** $p \leq 0.01$, *** $p < 0.001$, **** $p < 0.0001$.

3.6.   GIPR[dn] tubules show altered hydropersulfides pathway

Recent findings suggest that ferroptosis sensitivity is influenced by the hydropersulfides pathway (Barayeu *et al.*, 2023; Lange & Olzmann, 2022). To investigate this,

Western Blot analyses were performed on GIPR[dn] and WT kidney tubules, focusing on molecules related to this pathway. Lower protein expression levels of CBS were detected, while the expression of CSE, Sulfide:quinone reductase (SQR), and Human Persulfide Dioxygenase (ETHE1) remained unchanged (**Figure 18A, B**).

To explore the potential role of hydropersulfides in diabetes-induced heightened sensitivity to ferroptosis, levels of glutathione (GSH), glutathione hydrotrisulfide (GSSSH), cysteine, cysteine persulfide, and hydrogen disulfide (H_2S_2) were assessed via liquid chromatography–mass spectrometry (LC-MS) in isolated tubules. The obtained relative peak areas indicated a general lower level of hydropersulfides in GIPR[dn] tubules compared to the WT ones (**Figure 18C-G**).

Altogether, these data suggest a potential link between the relative deficiency in hydropersulfides and diabetes-induced hypersensitivity to ferroptosis through diminished CBS function.
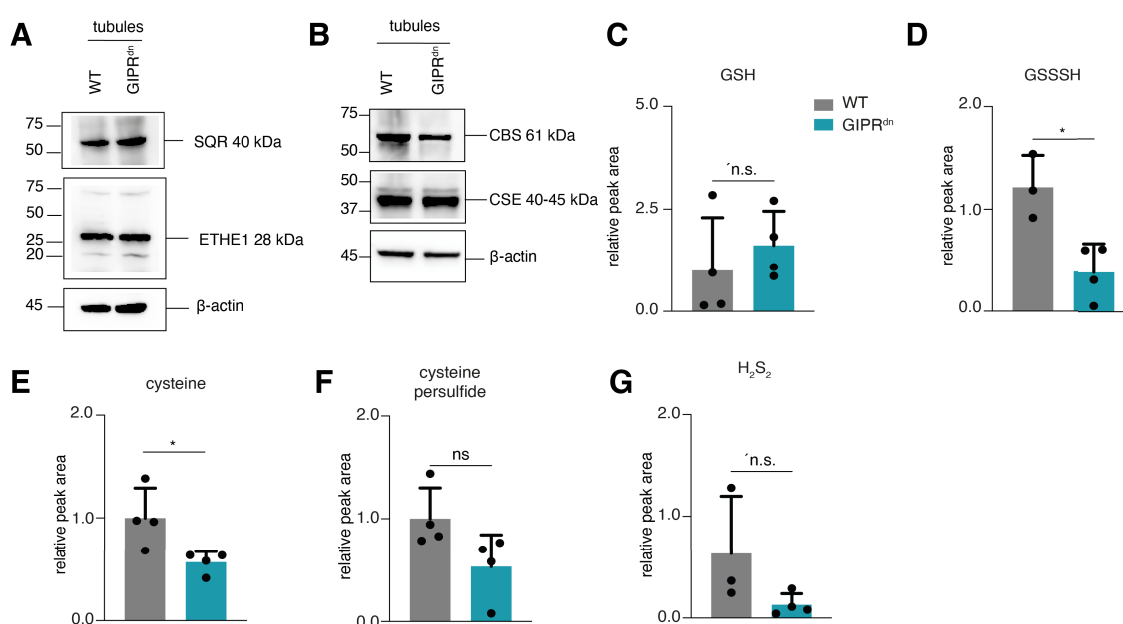
Figure 18. Deficiency in hydropersulfides in GIPR[dn] kidney tubules is due to diminished CBS function.
A. Western blot analysis of WT and GIPR[dn] kidney tubules against SQR and ETHE1. **B.** Western blot analysis of WT and GIPR[dn] kidney tubules against CBS and CSE. For all western blots β-actin was used as the loading control. **C-G**. Relative levels of sulfur metabolites related to hydropersulfide generation as assessed by LC/MS and presented as relative peak area, normalized to the protein content in each sample. GSH; glutathione, GSSH; glutathione hydrotrisulfide; H_2S_2; hydrogen disulfide, CysSSH; cysteine persulfide. *$P<0.05$; n.s. = non-significant.

3.7. GIPR[dn] tubules show altered etherglycerophospholipids (etherPLs) pathway

In addition to the hydropersulfide pathway, another pathway has been recognized for its significance in influencing ferroptosis sensitivity. Two recent studies have underscored the crucial role of etherPLs synthesis in the ferroptosis process. (Perez *et al.*, 2022; Y. Zou, Henry, *et al.*, 2020).

In light of this, alkylglycerone phosphate synthase (AGPS) and fatty acyl-CoA reductase 1 (FAR1), protein levels were investigated via Western Blot analysis in WT and GIPR[dn] kidney tubules (**Figure 19A-B**). GIPR[dn] tubules exhibited elevated protein expression levels of AGPS compared to the WT sample, whereas FAR1 protein levels were reduced.
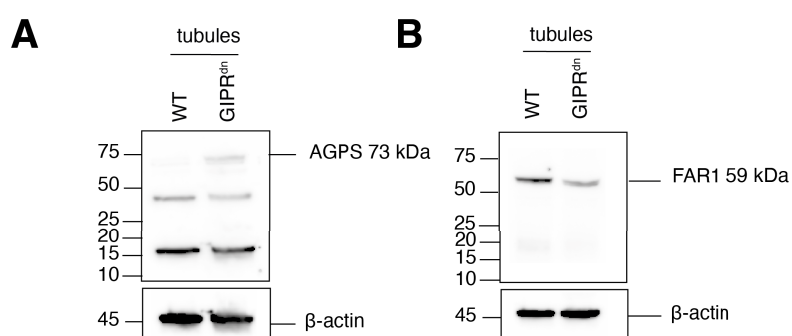
Figure 19. The etherglycerophospholipids (etherPLs) pathway is compromised in GIPR[dn] kidney tubules.
A. Western blot analysis of WT and GIPR[dn] kidney tubules against AGPS. **B.** Western blot analysis of WT and GIPR[dn] kidney tubules against FAR1. For all western blots β-actin was used as the loading control.

3.8. Ferrostatin-1 but not Empagliflozin reverses ferroptosis induction in different cell lines as well as in isolated kidney tubules

Empagliflozin is a drug that belongs to the category of SGLT2 inhibitors. These medications are commonly used to treat diabetes mellitus. While the exact mechanism of action of SGLT2 inhibitors might not be fully understood, their effectiveness is based on their ability to bind to and inhibit the SGLT2 transporter found in the proximal renal tubules (Zinman *et al.*, 2015).

To explore the hypothesis suggesting a potential connection between empagliflozin and the inhibition of spontaneous tubular necrosis, partially mediated by ferroptosis, the drug was initially assessed using two established cell lines commonly employed for the study of ferroptosis: the human fibrosarcoma cell line HT1080 and the human kidney tubular cell line CD10. HT1080 cells were treated with compounds from the four different types of ferroptosis inducers (FINs): 5 µM erastin (**Figure 20A**), 1.13 µM RSL3 (**Figure 20B**), 10 µM FINO2

(**Figure 20C**), 10 µM FIN56 (**Figure 20D**), as well as the necrosis inducer FTC at a concentration of 10 µM (**Figure 20E**). The induced ferroptosis was inhibited by co-treatment with 1 µM Fer-1. Empagliflozin was investigated in combination with each of the FINs and FTC at a final concentration of 1 or 10 µM. Flow cytometry analysis of the cells was performed after indicated time points and showed no effect of annexin V and 7AAD staining in the samples treated with each of the FINs and FTC and the ones co-treated with the two different concentrations of empagliflozin.

Figure 20. Empagliflozin does not affect ferroptosis-induced cell death in HT1080 cells.
A. HT1080 cells were treated for 24 h with erastin (5 μM), **B.** 3 h with RSL3 (1.13 μM), **C.** 12 h with FINO2 (10 μM), **D.** 24 h with FIN56 (10 μM), and **E.** 3 h with Ferroptocide (FTC) (10 μM). In all cases 1 μM Fer-1 was added as a protection control to inhibit the induced cell death. In parallel, empagliflozin was tested at a final concentration of 1 μM or 10 μM. Cells were stained with annexin V and co-stained with 7AAD. All experiments were independently repeated independently 3 times (N = 3) and DMSO was used as vehicle control. Bar graph

data are presented as means ± SD. Statistical analysis was performed using a Welch´s t-test (n.s. = non significant).

Similar experiments were conducted also in human kidney tubular cells named CD10-135. The cells were induced to ferroptosis by treatment with the four different types FINs, as well as the necrosis inducer FTC at the same concentrations, while protection from ferroptosis was achieved by using 1 µM Ferrostatin-1. Empagliflozin was investigated as a co-treatment at a final concentration of 1 or 10 µM (**Figure 21A, B, C, D, E**). Flow cytometry analysis of the cells showed no effect on the annexin V and 7AAD staining in the samples treated with each of the selected compounds and the ones co-treated with empagliflozin, regardless of its concentration.

Collectively, these findings pointed towards a limited impact of empagliflozin on the evaluated markers of cell response to ferroptosis induction, implying that its influence on this particular aspect of cellular behaviour might be subdued or absent.
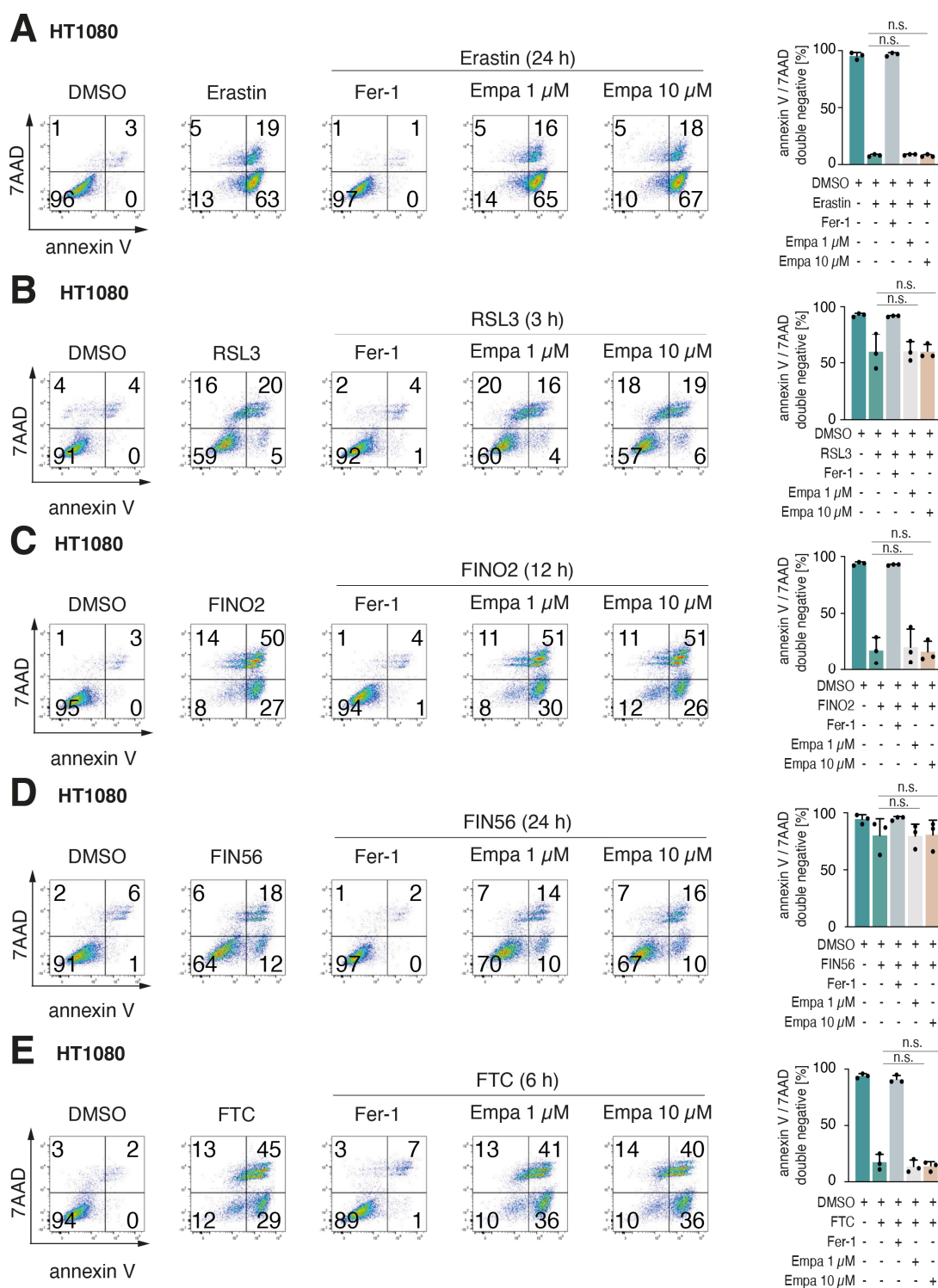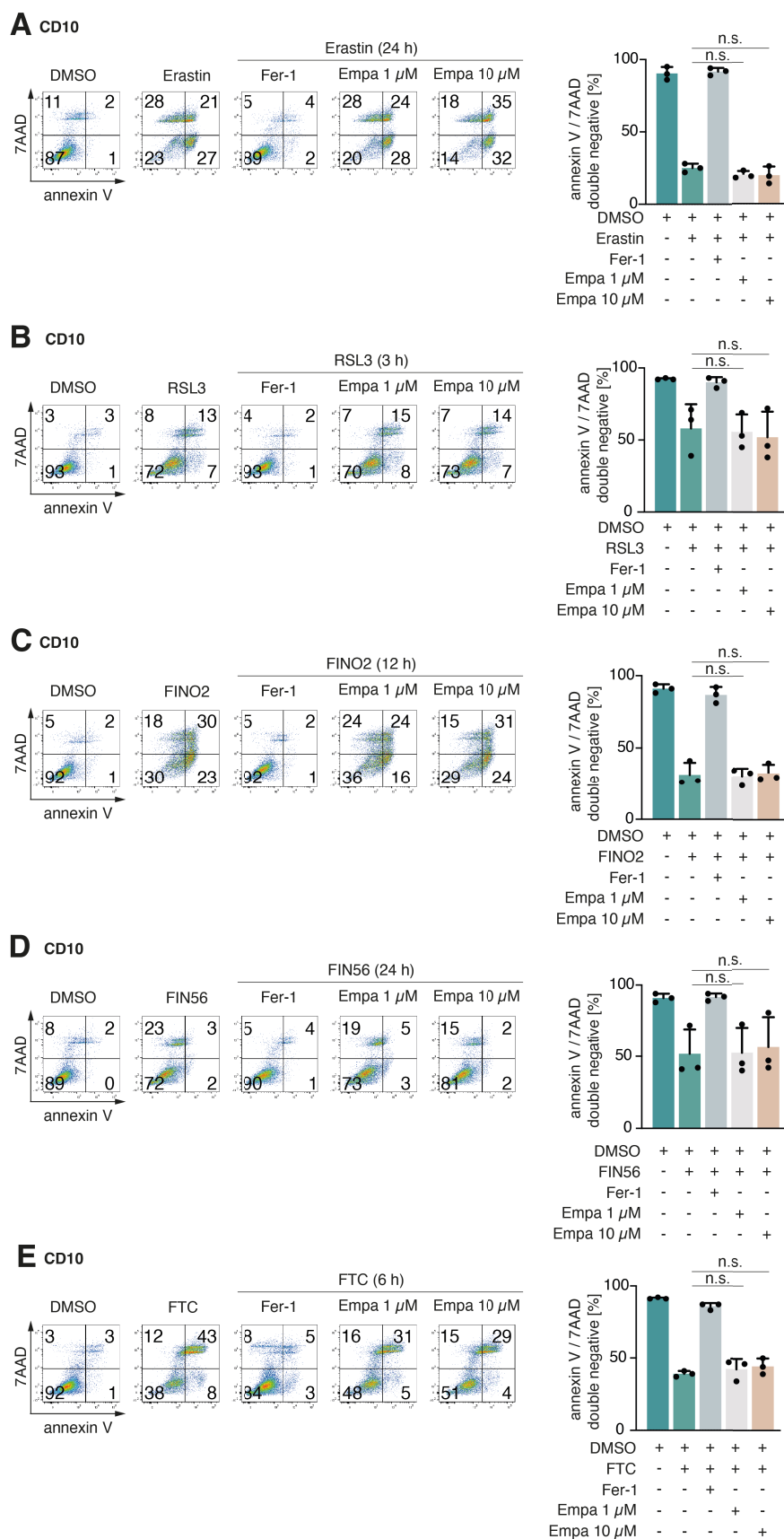
Figure 21. Empagliflozin does not affect ferroptotic-induced cell death in CD10 cells.

A-E. CD10 cells were treated for 24 h with erastin (5 µM), **B.** 3 h with RSL3 (1.13 µM), **C.** 12 h with FINO2 (10 µM), **D.** 24 h with FIN56 (10 µM), and **E.** 3 h with Ferroptocide (FTC) (10

µM). In all cases 1 µM Fer-1 was added as a protection control to inhibit the induced cell death. In parallel, empagliflozin was tested at a final concentration of 1 µM or 10 µM. Cells were stained with annexin V and co-stained with 7AAD. All experiments were independently repeated independently 3 times (N = 3) and DMSO was used as vehicle control. Bar graph data are presented as means ± SD. Statistical analysis was performed using a Welch´s t-test (n.s. = not significant).

To disprove the hypothesis that empagliflozin has a role in the inhibition of spontaneous tubular necrosis, freshly isolated kidney tubules from WT mice were isolated and treated with 30 µM Fer-1, 30 µM empagliflozin and the combination of the two. As a readout for the experiments LDH release assay was used. The quantification of data obtained from the experiments pointed out that there was no significant difference in LDH release between vehicle-treated tubules and those treated with empagliflozin. However, co-treatment with Fer-1 and empagliflozin resulted in significantly lower LDH release compared to treatment with empagliflozin alone (**Figure 22A-B**).
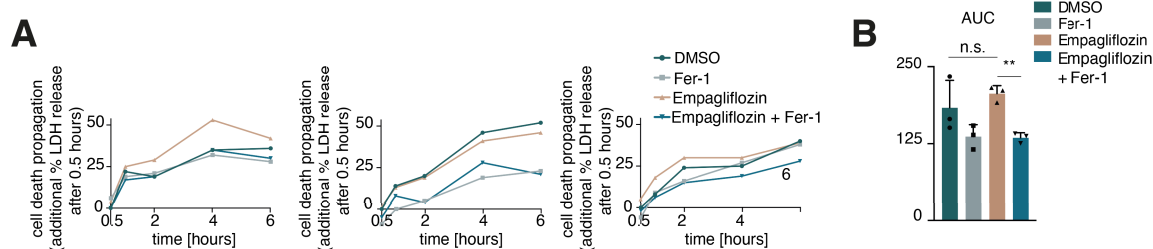
Figure 22. Empagliflozin does not affect spontaneous necrosis in kidney tubules.
A. Representative single LDH release experiments of WT tubules treated with vehicle control (DMSO), 30 µM Ferrostatin-1 (Fer-1) or 30 µM Empagliflozin (data are shown as additional LDH release after 0.5 h). **B.** Corresponding area under the curve (AUC) quantification of the independent LDH release experiments. All experiments were independently repeated 3 times (N = 3). Data are presented as means ± SD. Statistical analysis was performed using a Welch´s t-test with the following significance levels: ** $p ≤ 0.01$; n.s. = not significant.

3.9. GIPR[dn] mice are more sensitive to IRI-induced acute kidney injury compared to their WT littermates

Given the heightened susceptibility of diabetic patients to AKI (Anders *et al.*, 2018; Y. Chen *et al.*, 2020b; Kellum *et al.*, 2021; Monseu *et al.*, 2015; Thakar *et al.*, 2011), and the known contribution of ferroptosis to AKI (Linkermann *et al.*, 2014; Martin-Sanchez, Ruiz-Andres, Poveda, Carrasco, Cannata-Ortiz, Sanchez-Niño, Ortega, *et al.*, 2017), ferroptosis hypersensitivity in a functional in vivo context was evaluated. To achieve this, the well-recognized clamp ischemia model of bilateral kidney ischemia-reperfusion injury (IRI) (Tonnus, Al-Mekhlafi, *et al.*, 2018) was utilized.

Diverse mouse backgrounds show a different sensibility to the IRI surgery. Therefore, IRI experiments in CD1 mice were performed to establish the baseline values of creatinine and urea 48 hours upon the onset of reperfusion. The surgery was performed on four different age groups (8 to 10 weeks old) for 0, 24, 28, 36 and 40 minutes of total ischemia. 48 hours following reperfusion the animals were sacrificed and blood and kidneys were collected for further analysis. Notably, at an ischemia duration of 24 minutes before reperfusion, both serum creatinine and serum urea remained only minimally elevated, indicating 24 minutes as a suitable ischemia time for the subsequent experiments on GIPRdn and WT littermates (**Figure 23A, B**).

To investigate whether the transgenic mice are more sensitive to IRI compared to the WT littermates, 25-weeks-old CD1 male and 25-weeks-old GIPRdn male were utilized for the IRI experiment. Before the start of the surgery blood glucose levels (**Figure 23C**) as well as body weight (**Figure 23D**) were measured for each mouse. The mice were subjected to 24 min ischemia and observed for 168 h following the onset of reperfusion. While all but one out of 15 wild-type littermates survived this experiment, all GIPRdn mice succumbed within 36 hours following the onset of reperfusion (**Figure 23E**). This observation substantiates the hypersensitivity of GIPRdn mice, reminiscent of diabetic patients who are known to be highly sensitive to acute kidney injury.
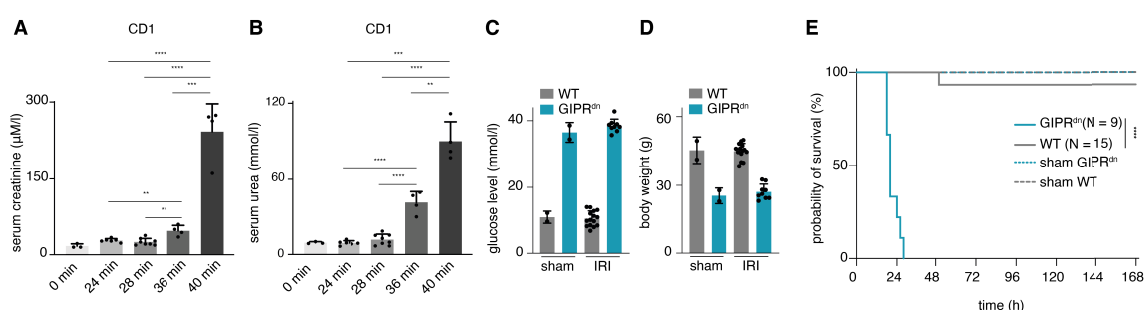
Figure 23. GIPRdn mice are extremely sensitive to acute kidney injury.
A. Serum creatinine levels derived from mice exposed to progressively longer time of renal ischemia. The following sample sizes were used for each age group: 0 min, N = 3; 24 min N = 6; 28 min N = 8; 36 min N = 4; 40 min N = 4. **B.** Serum urea levels derived from mice exposed to progressively longer time of renal ischemia. The following sample sizes were used for each age group: 0 min, N = 3; 24 min N = 6; 28 min N = 8; 36 min N = 4; 40 min N = 4. **C.** Glucose levels of WT and GIPRdn mice utilised for the renal ischemia reperfusion injury experiment. **D.** Body weight of WT and GIPRdn mice used for the renal ischemia reperfusion injury experiment. **E.** Kaplan–Meier survival plot of indicated groups of mice following renal ischemia reperfusion experiment. Bar graph data are presented as means ± SD. Statistical analysis was performed using an unpaired t-test with Welch's correction or log-rank test, with the following significance levels: * $p < 0.05$, ** $p \leq 0.01$, *** $p < 0.001$, **** $p < 0.0001$.

3.10. Ferrostatin-1 ameliorates the sensitivity of GIPR^{dn} to ischemia reperfusion injury-induced acute kidney injury

The contribution of ferroptotic cell death to acute kidney injury induced by IRI (Tonnus, Meyer, *et al.*, 2021), in combination with the data obtained so far in this thesis, lead to test the hypothesis that the inhibition of ferroptosis via ferroptosis inhibitors could ameliorate the high mortality rate of the GIPR^{dn} male mice subjected to IRI-induced AKI. Therefore, the ferroptosis inhibitor Fer-1 was injected in GIPR^{dn} male mice prior to the IRI challenge.

In more detail, before the start of the surgery for each mouse blood glucose levels (**Figure 24A**) as well as the body weight (**Figure 24B**) were measured. The mice were treated either with vehicle solution or 10 mg/kg body weight Fer-1 intraperitoneally 30 min prior the induction of bilateral kidney IRI. The mice were subjected to 24 min ischemia and observed for 168 h following the onset of reperfusion. As shown by the survival curve, the vehicle injected mice were sensitive to the IRI surgery, and died in the first 36 h after the onset of reperfusion, while the percentage of surviving diabetic mice was significantly higher after a single dose of Fer-1 prior the onset of reperfusion (**Figure 24C**).

In summary, the experiment indicates that ferroptosis plays a role in tubular necrosis and contributes to AKI induced by IRI. Moreover, these findings imply that targeting tubular ferroptosis could be a viable therapeutic strategy in the context of diabetes.
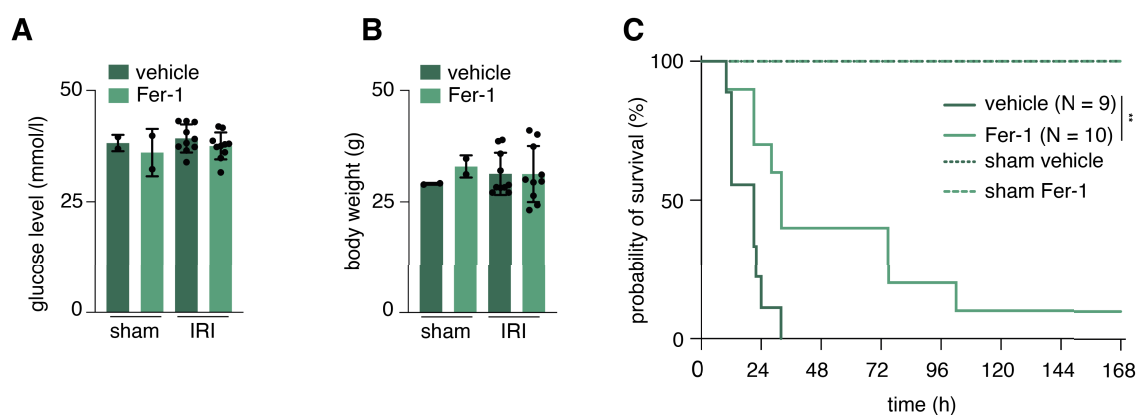
Figure 24. Ferrostatin-1 partially rescues GIPR^{dn} mice from death after renal IRI.

A. Glucose levels of GIPR^{dn} mice utilized for the renal ischemia reperfusion injury experiment. **B.** Body weight of GIPR^{dn} mice utilised for the renal ischemia reperfusion injury experiment. **C.** Kaplan–Meier survival plot of indicated groups of mice following renal ischemia reperfusion experiment. The following sample sizes were used for each group: N = 10 vehicle injected, N = 10 Fer-1 injected, N = 2 sham vehicle, N = 2 sham Fer-1. Statistical analysis was performed using a log-rank test, with the following significance levels: ** $p \leq 0.01$.

Discussion

4. Discussion

4.1. The GIPR^{dn} mouse model

DM is frequently associated with chronic kidney damage, which represents the most common reason for dependence on chronic dialysis therapy (Y. Chen *et al.*, 2020b; Fineberg *et al.*, 2013a). DKD is among the most concerning complications linked to diabetes in humans and represents the primary cause of ESRD. More than 25% of individuals with diabetes are affected by CKD, and estimates suggest that 40% of diabetic patients will experience CKD at some point in their lives (de Boer *et al.*, 2022). To date, there are no therapeutic options available that can reverse or stop the progression of ESRD associated with DKD. Consequently, these patients require renal replacement therapies such as transplantation or dialysis (Daehn *et al.*, 2023). For this reason, understanding the underlying cellular and molecular causes of DKD is imperative to develop more effective therapeutic options to address this unmet clinical need.

Inadequate amount of knowledge concerning the multi-organ complications of diabetes can be attributed to the absence of suitable animal models that recapitulate the features of established human DN (Giralt-López *et al.*, 2020). Mice exhibiting genetic deficiencies in either the leptin receptor (db/db) or leptin itself (ob/ob) have been extensively used as models for T2DM. However, these models show modest albuminuria and mesangial expansion, but lack overt glomerulosclerosis (Azushima *et al.*, 2018; King, 2012). To overcome this issue, several models have undergone crossbreeding with a genetically susceptible background, and the development of knockout and transgenic strains has been created to enhance the robustness of these models (Clee *et al.*, 2005; Kakoki *et al.*, 2004; Leiter & Reifsnyder, 2004; K. J. Williams *et al.*, 2007; Zhao *et al.*, 2006; Zheng *et al.*, 2004*)*. Among them, the GIPR^{dn} mouse model, primarily designed to explore the significance of the GIP/GIP receptor axis *in vivo* for the enteroinsular axis (Herbach *et al.*, 2005; Volz *et al.*, 1995), showed for the first time the most severe kidney alterations, mirroring those observed in human patients. This establishes it as a promising model for investigations of DN.

In the present study, a more comprehensive characterization of GIPR^{dn} mice was conducted to assess the onset and progression of diabetes and the development of diabetic kidney disease. In contrast to previous studies, which assessed their characterization at 17 and 28 weeks of age (Herbach *et al.*, 2008, 2009), this project involved a long-term characterization of the mice with five distinct time points: 7, 10, 25, 40, and 50 weeks of age. This timeline provides insights into the manifestations of the disease at early and late stages, providing a more thorough understanding of the disease.

As DN is a continuous and progressive disease process, markers showing the renal damage were investigated. The data presented on this thesis revealed that serum urea and serum creatinine heightened levels manifested as early as at the age of 7 weeks in GIPR^{dn} mice (**Figure 10**). Additionally, histological analysis (**Figure 11, Figure 12**) displayed the development of glomerulosclerosis, characterized by mesangial expansion, hyalinosis, segmental sclerosis, and adhesions between the glomerular tuft and Bowman's capsule. These features are clinically recognized as Kimmelstiel-Wilson lesions (Kimmelstiel and Wilson, 1936), and are indicative of human diabetic glomerulosclerosis. Overall, GIPR^{dn} mice exhibited severe kidney abnormalities mimicking the initial, middle, and late phases of human DKD depending on the age of the mice. Notably, these mice displayed characteristic thickening of the glomerular basement membrane, followed by renal hypertrophy, glomerulosclerosis, tubular dysfunction, and proteinuria. In contrast to previous, GIPR^{dn} mice capture the extent of kidney pathological changes associated with diabetes mellitus in humans. Even though when GIPR^{dn} mice were initially described, significant proteinuria levels were reported at the age of 17 weeks (Herbach *et al.*, 2009), all assays related to tubular damage in this thesis indicated an onset of increased sensitivity to ferroptosis at the age of 10 weeks (**Figure 13A-C**, **Figure 14D-F**). These data suggest an early onset of glomerular disease than previously assumed followed by subsequent changes in the tubular system.

We propose a model in which high levels of filtered proteins and glucose from the luminal tubular side, together with non-enzymatic glycosylation such as advanced glycosylation end products (AGEs), directly contribute to the diabetic tubulopathy of this mouse via primarily filtered urine and the bloodstream. Furthermore, unlike studies primarily focusing on young mice (less than 22 weeks of age) in ferroptosis pathway exploration in DKD (Feng *et al.*, 2021; Kim *et al.*, 2021; Yao *et al.*, 2022), GIPR^{dn} mice showcase a progressive diabetic nephropathy with age, enabling the examination of older mice and thus end-stage DKD which more accurately represents the demographic typically affected by diabetic kidney complications. As a result, this diabetic mouse model proves exceptionally suitable for investigating structural and functional changes in progressive kidney alterations in diabetes, extending well beyond chronic hyperglycemia. Moreover, this mouse model can offer insights into both the clinical and biological aspects of DKD. For instance, it can be utilized to investigate the presence and impact of comorbidities such as hypertension or dyslipidemia, commonly found in DKD patients (Alegre-Díaz *et al.*, 2016). Finally, it provides an opportunity to study the response to standard diabetic therapies, including SGLT2 inhibitors or GLP1 receptor agonists.

4.2 Ferroptosis in diabetic nephropathy

4.2.1. Ferroptotic cell death is involved in the spontaneous death of diabetic tubules

The connection between diabetes and progressive kidney damage primarily focusing on glomerular damage has been previously described (Tervaert *et al.*, 2010). However, recent insights into the pathophysiology of DKD suggest that tubules significantly contribute to the progression of CKD (Löwen *et al.*, 2021). This progression is notably characterized by the loss of nephrons, the functional units of the kidney, further exacerbated by episodes of AKI with ATN. Epidemiological data indicate that existing diabetes predisposes individuals to these acute injuries, but the underlying mechanisms remain unclear (Girman *et al.*, 2012). In addition to DN, AKI can arise from toxic damage, such as chemotherapy, or redox stress, as seen in events like infarction, sepsis and organ transplantation (Kellum *et al.*, 2021). The best studied RCD mechanism contributing to tubular damage is ferroptosis, but its role in the pathophysiological course of diabetic nephropathy has not been conclusively studied so far.

It has been shown that ferroptosis is the major cause of kidney tubular necrosis in AKI (Linkermann *et al.*, 2014; Martin-Sanchez, Ruiz-Andres, Poveda, Carrasco, Cannata-Ortiz, Sanchez-Niño, Ruiz Ortega, *et al.*, 2017), explaining the loss of nephrons and suggesting this type of regulated cell death as a potential therapeutic target. Considering patients previously diagnosed with diabetes mellitus are particularly sensitive to these episodes of AKI which are associated with severe complications due to advanced DN, exploring the exact connections is of paramount importance. Notably, in renal tubules ferroptosis induction exhibits unique dynamics that have been referred to as a "wave-of-death" or synchronized regulated necrosis (SRN) (Linkermann *et al.*, 2014; Tonnus, Meyer, *et al.*, 2021). This non-random cell death propagation was observed in erastin micro-perfused renal tubules and after direct infusion of erastin. Establishment of live imaging of murine renal tubules undergoing spontaneous tubular necrosis and stained with the general necrosis marker SYTOX green, allowed the observation of the SRN phenomenon both in WT and GIPR^{dn} samples (**Figure 13E, F**). Similar non-random cell death propagation has also been observed in cell culture models and *in vivo* in zebrafish (Katikaneni *et al.*, 2020; S. E. Kim *et al.*, 2016; Riegman *et al.*, 2019, 2020). Together with the previously published literature, these findings highlight the central role of ferroptosis in the cellular demise of tubular cells.

While it has been demonstrated that ferroptosis signals can propagate in a SRN manner (S. E. Kim *et al.*, 2016; Linkermann *et al.*, 2014; Riegman *et al.*, 2020), the underlying factors leading this phenomenon were not extensively investigated. A proposed hypothesis suggested that the signal may propagate via gap junctions, where one cell undergoing

ferroptosis could render the neighbouring cell more prone to a similar fate. Particularly, this could lead to signal propagation in the tightly connected tubular epithelium. The resulting decreased redox capacity of the dying cells would create a NAD(P)H gradient, with higher concentrations observed inside living cells and lower concentrations in dying cells (Belavgeni *et al.*, 2020; Maremonti *et al.*, 2022; Tonnus, Meyer, *et al.*, 2021). Through FLIM analysis of isolated kidney tubules from both WT and GIPR[dn] mice, this thesis demonstrates, for the first time, a correlation between cell death propagation and the loss of NAD(P)H content (and consequently redox capacity) during the occurrence of the "wave-of-death" phenomenon (**Figure 13G.**). While attempts of incorporating FLIM microscopy into studies related to kidney pathophysiology have been made (Bugarski *et al.*, 2018; Hirakawa *et al.*, 2018; Ranjit *et al.*, 2021), this thesis marks the first relevant connection with the ferroptosis field validating this long-term hypothesis.

Until recently, ferroptosis had not been extensively investigated in the context of diabetes, and the available publications related to DKD and ferroptosis on PubMed are limited, with only 80 publications beginning from the year 2020. Although ferroptosis has been investigated in some studies involving mice that are interpreted as diabetic (Feng *et al.*, 2021; S. Kim *et al.*, 2021; Y. Wang *et al.*, 2023; Yao *et al.*, 2022), none of the models used could fully replicate DN as seen in humans (Brosius *et al.*, 2009). Building on the microscopical observation of ferroptosis signal propagation and the resultant NAD(P)H gradient in both WT and GIPR[dn] kidney tubules, LDH release assays were performed to reveal a distinct pattern of spontaneous cell death in GIPR[dn] and WT tubular samples (**Figure 14**). The data underscored a notable increase in LDH release levels in GIPR[dn] tubules compared to age-matched controls, particularly evident from 10 weeks of age and persisting until 50 weeks of age. Furthermore, the quantification of spontaneous necrosis indicates an accelerated rate of cell death propagation in the same GIPR[dn] samples (**Figure 13A, B, C.**). This heightened sensitivity of diabetic kidney tubules to undergo spontaneous cell death was partially mitigated by adding the ferroptosis inhibitor Fer-1 to the tubules in culture media. These results, along with the live imaging and FLIM analysis, clearly highlight a central role of ferroptosis in this phenomenon. Therefore, these data contribute a first strong piece of evidence for the involvement of ferroptosis in DKD. Notably, our results stem from a more reliable model of DKD. Notably, the obtained LDH results stem from a more reliable model of DKD in contrast to previous studies, that involved 12 to 22 week old mice (Feng *et al.*, 2021; Y. Wang *et al.*, 2023), given that the experimental procedure was extended until the 50th week of age in diabetic mice. Connecting all these puzzle pieces together, a more comprehensive correlation between the chronicity observed in the human diabetic disease and the GIPR[dn] mouse model could be made.

4.2.2. Possible mechanisms behind the enhanced sensitivity of the GIPR^{dn} kidney tubules to ferroptosis

The importance of ferroptosis in the kidney was initially identified in the context of renal ischemic-reperfusion injury (Linkermann *et al.*, 2014; Martin-Sanchez, Ruiz-Andres, Poveda, Carrasco, Cannata-Ortiz, Sanchez-Niño, Ortega, *et al.*, 2017), but how about its role in DKD? While the role of ferroptosis and the protective effects of ferrostatins have been characterized in healthy WT mice (Friedmann Angeli *et al.*, 2014a; Martin-Sanchez, Ruiz-Andres, Poveda, Carrasco, Cannata-Ortiz, Sanchez-Niño, Ruiz Ortega, *et al.*, 2017; Mishima *et al.*, 2022; Von Mässenhausen *et al.*, 2022), little is known about the role of ferroptosis in aged and diabetic mice.

The proposed mechanism involves iron-chelating agents offering renal protection by mitigating oxidative stress, inflammation, and tubular interstitial fibrosis (Li *et al.*, 2021; C. Zou *et al.*, 2017). Nevertheless, the precise mechanism through which excessive iron accelerates the progression of DKD remains unclear. Given that the ferroptosis process involves an increase in lipid ROS production leading to oxidative stress, and considering the kidney's rich mitochondrial structure, which is particularly susceptible to oxidative stress damage, it becomes evident that the traditional pathogenesis of DKD, involving oxidative stress, may also intersect with ferroptosis. Several studies have proposed the mitochondrial overproduction of superoxide anions ($O_2^{\cdot-}$) as a source of oxidant stress and a primary event in the pathogenesis of DKD (Chouchani *et al.*, 2016; Coughlan *et al.*, 2009; Forbes *et al.*, 2008; Nishikawa *et al.*, 2000). Therefore, a first hypothesis is that significant increase of $O_2^{\cdot-}$ concentration in diabetic kidney tubules may function as a "starter" to further reactions, such as the Fenton reaction and subsequent lipid peroxidation initiation and the concomitant propagation of the peroxidation cascade (Daehn *et al.*, 2023). More recent studies on the role of ferroptosis in DKD revealed decreased expression of GPX4, increased ACSL4 expression (Feng *et al.*, 2021; Y. Wang *et al.*, 2023), and reduced Nrf2 levels (Li *et al.*, 2021) in cells cultured in high fat/high glucose conditions as well as in *in vivo* models of DN. Reduced mRNA expression levels of SLC7A11 and GPX4 found in human kidney biopsies samples further support the connection of ferroptosis with DKD (S. Kim *et al.*, 2021). Even though the aforementioned publications show differences at the mRNA level, the data presented in this thesis showed no changes at the protein level for GPX4 and ACSL4 in tubular lysates form diabetic mice compared with WT samples (**Figure 16A**).

Notably, GIPR^{dn} tubules exhibited a significant reduction in proteins related to the TRX antioxidant system, the second major antioxidant pathway in mammalian cells after the

cysteine-GSH-GPX4 axis (J. Lu & Holmgren, 2014). A major negative regulator of this system is thioredoxin interacting protein (TXNIP) (Hwang *et al.*, 2014). Notably, hyperglycemia has been demonstrated to induce AMPK-dependent TXNIP degradation to drive GLUT1 and GLUT4 incorporation into the plasma membrane, protecting the cytosol from glucose overload (Waldhart *et al.*, 2017; N. Wu *et al.*, 2013) . In line with previous studies that demonstrated the upregulation of TXNIP in the presence of hyperglycemic conditions (Fang *et al.*, 2011; Schulze *et al.*, 2004; Turturro *et al.*, 2007), our data show elevated TXNIP protein expression in both cells treated with high glucose and in kidney tubules isolated from GIPR[dn] mice (**Figure 16A**). Furthermore, a thioredoxin reductase activity assay showed a significant decrease in TXNRD activity in GIPR[dn] tubules (**Figure 16E**), supporting the inhibitory effects of TXNIP. The following new hypothesis is that the glucose regulatory circuit in the kidney tubules leads to an increase in ferroptosis sensitivity through the TXNIP-dependent downregulation of TXNRD1. Previously, TXNIP has been linked to the activation of the nucleotide-binding oligomerization domain-like receptor protein-3 inflammasome and the stimulation of another form of cell death, pyroptosis (He *et al.*, 2015; Oslowski *et al.*, 2012). In addition to these data, the findings of this thesis may point to a new, previously undiscovered role of TXNIP in ferroptosis. TXNIP has been associated with both CKD and DN in both human patients (Park *et al.*, 2022) and mice (Shah *et al.*, 2015), substantiating the potential role of TXNIP in ferroptosis supported by data of this thesis.

To establish the direct involvement of the thioredoxin system in sensitizing tubules to ferroptosis, experiments with FTC treatment were conducted. The results confirmed that the addition of FTC intensified cell death in GIPR[dn] tubules, highlighting the functional role of TXNRD1 and TRX1 in the hyperglycemia-induced sensitization to spontaneous necrotic cell death (**Figure 17**). The thioredoxin system, an independent redox system distinct from GPX4, introduces a new layer of complexity to our understanding of the ferroptotic mechanism, as well as its involvement in diabetic nephropathy. As to how the TRX pathway is connected with the unaltered levels of GPX4 in the GIPR[dn] tubules remains an open question (**Figure 16A**). While GPX4 counteracts iron-dependent lipid peroxidation directly (Friedmann Angeli *et al.*, 2014b), the thioredoxin system acts by catalysing protein disulphide to thiol changes (J. Lu & Holmgren, 2014). Database observations show consistent expression of TRXND1, TXNIP and TRX, in kidney tubules across all developmental stages (*The Human Nephrogenesis Atlas*, 2023), reflecting the stability observed in GPX4. Furthermore, analogous to GPX4, complete deletion of TRXND1 or TRX1 is embryonically lethal at the early stages of embryogenesis (Jakupoglu *et al.*, 2005), emphasizing the fundamental role of the thioredoxin system in cellular function. Just as GPX4 requires an inducible conditional knockout system to conduct tubular

research (Friedmann Angeli *et al.*, 2014a; Ingold *et al.*, 2018; Seiler *et al.*, 2008), the comprehensive understanding of the thioredoxin system would require similar approaches. Another piece of evidence pointing towards the involvement of ferroptosis in the GIPR[dn] mice, was the inhibitory effect of Fer-1-treated mice undergoing IRI (**Figure 24**). Therefore, until now it is evident that GIPR[dn] mice are susceptible to a ferroptosis-driven challenge, while tubules isolated from these mice show a partially mitigated spontaneous necrosis upon Fer-1 treatment. If we combine these pieces together with the imbalance of the thioredoxin system, the following question arises: does the thioredoxin system also play a role in regulating lipid peroxidation or even protein peroxidation? This prompts a broader inquiry into the definition of ferroptosis beyond its association with lipid peroxidation. It is therefore obvious that more research is required to comprehensively understand the interplay between the thioredoxin system and ferroptosis.

Other potential mechanisms influencing ferroptosis sensitivity include the transulfuration pathway and the synthesis of ether phospholipids (etherPLs). Studies conducted by Barayeu *et al.* and Wu *et al.* unveiled that endogenous hydropersulfides function as hydrogen atom donors, effectively scavenging lipid radicals and suppressing lipid peroxidation as well as ferroptosis, independent of the canonical GPX4 pathway (Barayeu *et al.*, 2023; Z. Wu *et al.*, 2022). Consistent with these previously published findings, Western Blot analyses indicated lower protein levels of CBS in GIPR[dn] tubules, suggesting a potential association between reduced CBS function and heightened sensitivity to ferroptosis (**Figure 18B**). This connection was further supported by LC-MS analysis, which revealed lower levels of hydropersulfides in GIPR[dn] tubules compared to wild-type tubules (**Figure 18C-G**). Notably, this marks the first instance of an imbalance in persulfide synthesis reported in the context of DKD.

Unlike hydropersulfides, the plasticity of ether lipids has recently been demonstrated to sensitize cells to ferroptosis (Y. Zou, Henry, *et al.*, 2020). According to Wander and colleagues, glucose plays a regulatory role in modulating the expression of dihydroxyacetone phosphate (DHAP), a crucial substrate for AGPS, the sole enzyme capable of forming the ether bond, making it a fundamental player in the synthesis of ether lipids (Wanders *et al.*, 2023). GIPR[dn] tubules exhibited elevated AGPS and reduced FAR1 expression (**Figure 19**), further implicating alterations in etherPLs synthesis in the heightened ferroptosis susceptibility observed in diabetic tubules. How glucose levels may stimulate an AGPS-dependent change in the plasticity of the ether lipids remains an open question, that would require a thorough investigation utilizing lipidomics in tubules isolated from WT and GIPR[dn] mice. It is noteworthy that existing literature on other diabetic mouse models (Xu *et al.*, 2023), underscores

variations in lipid metabolic processes. Consequently, the findings presented in this thesis have substantial relevance within the broader context of diabetes-related lipid alterations. Various signaling pathways of regulated necrosis have already been described in relation to nephrological pathologies. It was revealed that ferroptosis contribute to tubular necrosis in the pathophysiology of AKI (Belavgeni *et al.*, 2020; Maremonti *et al.*, 2022; Tonnus, Meyer, *et al.*, 2021), and overview of the essential mechanisms of ferroptosis in kidney disease or in kidney transplantations has already been published (Linkermann, 2016; Linkermann *et al.*, 2014; Martin-Sanchez, Ruiz-Andres, Poveda, Carrasco, Cannata-Ortiz, Sanchez-Niño, Ruiz Ortega, *et al.*, 2017). Furthermore, the efficacy of specific inhibitors of this cell death pathway has been demonstrated multiple times in various mouse models (Devisscher *et al.*, 2018; Skouta *et al.*, 2014; Tonnus, Meyer, *et al.*, 2021). As diabetic patients are more prone to undergo AKI, now, these inhibitors were investigated in the context of diabetes mellitus. The experiments conducted in this thesis not only highlighted the hypersensitivity of GIPR[dn] mice to AKI-induced IRI but also demonstrated a beneficial effect of Fer-1 administration, significantly increasing the survival rate of diabetic mice (**Figure 24**). These findings suggest a potential therapeutic strategy targeting tubular ferroptosis in the context of diabetes-induced AKI, in line with previous published studies, showcasing that Fer-1 effectively alleviates kidney damage in young mice with DKD (S. Kim *et al.*, 2021; X. Zhang & Li, 2022). Notably, these existing preclinical models of IRI in established diabetes mellitus are scarce and often lack representation of diabetic kidney disease features (De Ponte *et al.*, 2021; Grynberg *et al.*, 2022; Ozbilgin *et al.*, 2016; Q. Wang *et al.*, 2022). Furthermore, considering the demographic and epidemiological characteristics of human diabetes, which typically develops at an advanced age (Girman *et al.*, 2012), experiments in aged mice as conducted here become more relevant.

Even though the focus of this thesis is primarily on ferroptosis, there is evidence suggesting the involvement of other cell death pathways such as necroptosis in AKI (Degterev *et al.*, 2005; Degterev & Linkermann, 2016; Linkermann, 2016; Tonnus, Meyer, *et al.*, 2021). Therefore, exploring the potential role of necroptosis in this disease could be an intriguing avenue for future investigation in the context of DKD.

4.3. Therapeutic consequences of the study

4.3.1. SGLT2 inhibitor empagliflozin does not have a protective effect on diabetic tubules undergoing spontaneous death

Sodium–glucose cotransporter 2 inhibitors (SGLT2i), which inhibit the coupled reabsorption of sodium and glucose from the proximal tubule, were proven to have excellent

renoprotective effects in T2DM patients (Neuen *et al.,* 2019; Perkovic *et al.,* 2019*;* Vergara *et al.*, 2022; Wanner *et al.,* 2016). However, further evidence is needed to confirm their renoprotective effects in T1DM (Gillard *et al.*, 2020). Additionally, the underlying mechanisms of the renoprotective role of SGLT2i are not fully understood. Previous studies have shown that SGLT2i mediate their effects via antioxidative stress pathways (Z. Liu *et al.*, 2021; Ravindran & Munusamy, 2022; Shin *et al.*, 2016). Moreover, different published studies claimed a direct effect of SGLT2i on ferroptosis inhibition both *in vitro* and *in vivo* in the context of DKD (Q. Lu *et al.*, 2023; Y. Wang *et al.*, 2023). However, these studies often utilize mouse models that may not fully mimic the characteristics of diabetic kidney disease, and the cell culture experiments lack controls with established ferroptosis-sensitive cell lines. In contrast to these evidences, the data of this thesis show no significant impact of the SGLT2i empagliflozin both in cell culture of established ferroptosis-sensitive cell lines (**Figure 20, Figure 21**), and in tubules isolated from GIPR^{dn} mice and their WT littermates (**Figure 22**). No additional effect was observed after co-treatment of cells or tubules with empagliflozin and Fer-1. Given the benefits of a SGLT2i and the involvement of ferroptosis in diabetic nephropathay, new therapies with the combination of these drugs might point towards future clinical approaches. Currently, teams in Belgium, Munich, and the United States are actively working on translational projects to introduce ferroptosis inhibitors into clinical applications. Considering ferroptosis inhibitors as a therapeutic option requires critical consideration of side effect profiles. Until now, it is rather unclear what the physiological or patho-physiological role of ferroptosis is, but evidence in lower vertebrates, like fish, place ferroptosis as a defence mechanism against viruses (Belavgeni *et al.*, 2023). Notably, at the highest doses applied to vertebrates, no specific adverse effects have been reported by multiple groups developing drugs or tool compounds for ferroptosis inhibition, indicating suitable pharmacokinetic and pharmacodynamic properties and emphasizing their potential safety (Degterev & Linkermann, 2016; Devisscher *et al.*, 2018; Hofmans *et al.*, 2016). Given existing data showing that ferroptosis is a non-immunogenic type of regulated cell death (Wiernicki *et al.*, 2022), could ferroptosis be placed in diabetes as a patho-physiological event occurring aiming to prevent a more systematic evolvement of the disease? Nevertheless, such question is beyond the scope of this thesis. The research at hand indicated that inhibiting ferroptosis could prove beneficial for diabetic patients experiencing AKI in ICU. Immediate treatment with ferroptosis inhibitors for these patients might be possible without substantial side effects, though conclusive evidence would require confirmation through clinical trials. Given the ongoing increase in the number of patients with diabetes mellitus who experience a significantly elevated risk of complications in this context (Y. Chen *et al.*, 2020b; Fineberg *et al.*, 2013b; Thomas *et al.*,

2015), it is of highly importance to evaluate ferrostatins ability to reduce tissue damage in AKI. Achieving an improvement in patient care related to AKI in diabetic patients would make a meaningful difference.

Beyond diabetes-related AKI, the potential of ferroptosis inhibitors entering clinical applications extends to diverse scenarios. For instance, *Mycobacterium tuberculosis* drives macrophages to undergo ferroptosis (Amaral *et al.*, 2023, 2023), facilitating the spread of the bacteria. A ferroptosis inhibitor holds promise in preventing this mechanism, presenting an opportunity unrelated to ischemia-reperfusion and transplantation. Once approved, such inhibitors could be more easily tested for other diseases as safety concerns would progressively decrease upon more common use of the drugs.

4.4. Outlook and limitations of the study

The exploration of regulated cell death mechanisms, particularly ferroptosis, in the context of diabetes mellitus has gained attention only in recent years, notably since 2018. This emerging field has become pivotal in unveiling novel insights into the intricate molecular pathways associated with diabetic complications. The data presented in this thesis further contribute to this evolving landscape, shedding light on a potential new mechanism linking ferroptosis to one of the most challenging complications of diabetes mellitus, DKD (see **Figure 25**). Understanding the regulatory aspects of cell death processes in diabetes not only provides a more exhaustive comprehension of disease progression but also opens avenues for targeted therapeutic interventions. This research emphasizes the urgency and importance of continued investigations into regulated cell death pathways, such as ferroptosis, to address the complex interplay between diabetes mellitus and its associated complications.

The utilization of multicellular complex systems, such as renal tubules, highlights an opportunity to study RCD in the pathophysiologically relevant model of DM.
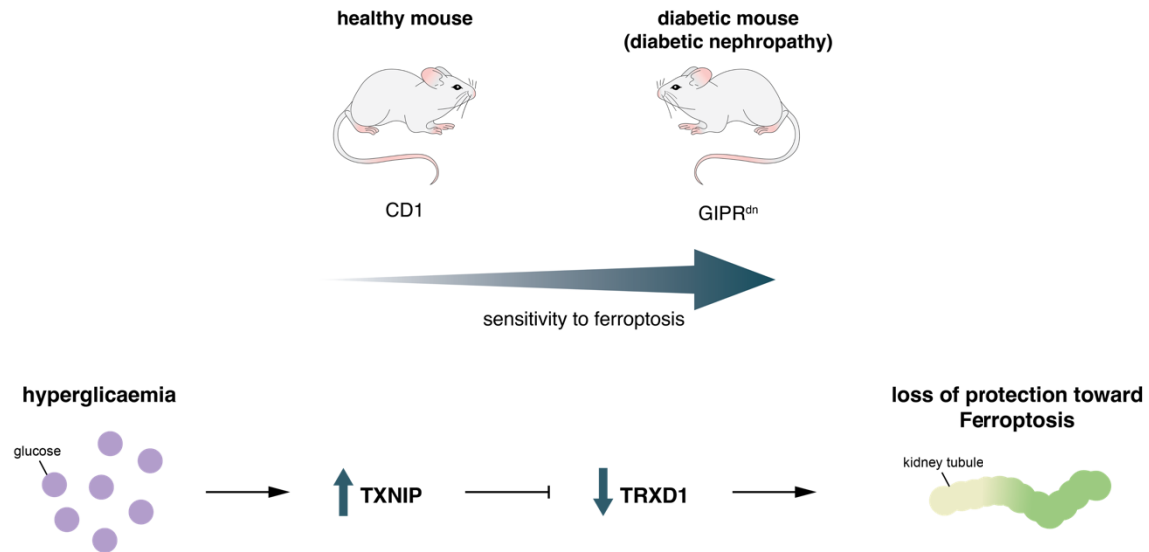
Figure 25. Graphical abstract of the possible mechanism behind DKD and ferroptosis sensitivity.

The data presented in this thesis suggest that in a context of hyperglycemia, there is an upregulation of TXNIP and a consequent downregulation of TRXND1 with a consequent loss of surveillance toward ferroptosis.

The *ex vivo* system of isolated renal tubules offers advantages over traditional cell culture, as it allows for a more comprehensive exploration of cellular responses within a three-dimensional tissue context. However, inherent limitations exist, including the absence of typical hormones or stimuli present in the kidney, preventing direct linkage of observations in the tubules to *in vivo* effects. Indeed, the system operates independently of the immune system, emphasizing the need for careful interpretation and consideration of these limitations when extrapolating findings to the *in vivo* context. Despite this drawback, the system's independence from systemic effects of the body provides its own set of advantages, depending on the specific scientific questions being addressed. In this thesis the isolated tubules were of fundamental importance for uncovering the potential mechanism linking hyperglicemia and DM to a heightened sensitivity to ferroptosis. This mechanism seems to involve a direct interaction between TXNIP and TRXND1. However, experiments for exploring this connection directly, for example immunoprecipitation assays were not performed. Future experiments directed toward elucidating the intricacies of this interaction may provide a more comprehensive understanding of its implications in the context of ferroptosis. Additionally, our data pointed out elevated AGPS and reduced FAR1 protein levels in the GIPR^{dn} tubules, highlighting potential alterations in ether phospholipid synthesis. Further comprehensive lipidomic studies are warranted to delve deeper into the specific alterations in etherPLs and their role in ferroptosis susceptibility. While the GIPR^{dn} mouse model has proven valuable,

limitations exist, particularly in the CD1 background and the inherent suffering of this mouse line due to diabetic complications, restricting the application of additional mutations. To further investigate the interaction of the TRX system to ferroptosis, alternative mouse models such as an inducible TRX knockout mouse attempting to rescue acute kidney injury induced by ischemia-reperfusion injury (IRI) with Fer-1 could provide valuable insights. Lastly, this thesis focused mainly on the use of Fer-1. Other ferroptosis inhibitors, such as the small molecule 3203, with improved pharmacodynamic and kinetic properties, or other inhibitors like Liproxstatin-1, would solidify our understanding of the therapeutic landscape for ferroptosis in the diabetic context. Even though literature and data of this thesis support the involvement of ferroptosis in diabetic nephropathy, other cell death pathways should be investigated, to further strengthen the hypothesis that ferroptosis is the solely involved pathway or disapprove partially the hypothesis. With necroptosis also playing a role in IRI models of the kidney, future perspectives should take this into consideration. There is yet a connection to be made between ferroptosis and the other types of regulated cell death. Ultimately, in addressing scientific inquiries, the optimal strategy involves integrating various technologies and utilizing all available resources—be it cells, organoids, or mice—in the most impartial manner possible.

References

Ahmad, E., Lim, S., Lamptey, R., Webb, D. R., & Davies, M. J. (2022). Type 2 diabetes. *The Lancet*, *400*(10365), 1803–1820. https://doi.org/10.1016/S0140-6736(22)01655-5

Alegre-Díaz, J., Herrington, W., López-Cervantes, M., Gnatiuc, L., Ramirez, R., Hill, M., Baigent, C., McCarthy, M. I., Lewington, S., Collins, R., Whitlock, G., Tapia-Conyer, R., Peto, R., Kuri-Morales, P., & Emberson, J. R. (2016). Diabetes and Cause-Specific Mortality in Mexico City. *New England Journal of Medicine*, *375*(20), 1961–1971. https://doi.org/10.1056/NEJMoa1605368

Amaral, E. P., Costa, D. L., Namasivayam, S., Riteau, N., Kamenyeva, O., Mittereder, L., Mayer-Barber, K. D., Andrade, B. B., & Sher, A. (2019). A major role for ferroptosis in *Mycobacterium tuberculosis* –induced cell death and tissue necrosis. *Journal of Experimental Medicine*, *216*(3), 556–570. https://doi.org/10.1084/jem.20181776

Amaral, E. P., Namasivayam, S., Queiroz, A. T. L., Fukutani, E., Hilligan, K. L., Aberman, K., Fisher, L., Bomfim, C. C. B., Kauffman, K., Buchanan, J., Santuo, L., Gazzinelli-Guimaraes, P. H., Costa, D. L., Teixeira, M. A., Barreto-Duarte, B., Rocha, C. G., Santana, M. F., Cordeiro-Santos, M., Barber, D. L., … Sher, A. (2023). BACH1 promotes tissue necrosis and Mycobacterium tuberculosis susceptibility. *Nature Microbiology*, *9*(1), 120–135. https://doi.org/10.1038/s41564-023-01523-7

American Diabetes Association. (2010). Diagnosis and Classification of Diabetes Mellitus. *Diabetes Care*, *33*(Supplement_1), S62–S69. https://doi.org/10.2337/dc10-S062

Anders, H.-J., Huber, T. B., Isermann, B., & Schiffer, M. (2018). CKD in diabetes: Diabetic kidney disease versus nondiabetic kidney disease. *Nature Reviews Nephrology*, *14*(6), Article 6. https://doi.org/10.1038/s41581-018-0001-y

Andrésdóttir, G., Jensen, M. L., Carstensen, B., Parving, H.-H., Rossing, K., Hansen, T. W., & Rossing, P. (2014). Improved Survival and Renal Prognosis of Patients With Type 2 Diabetes and Nephropathy With Improved Control of Risk Factors. *Diabetes Care*, *37*(6), 1660–1667. https://doi.org/10.2337/dc13-2036

Andy KH Lim. (2014). Diabetic nephropathy – complications and treatment. *International Journal of Nephrology and Renovascular Disease*.

Anker, S. D., Butler, J., Filippatos, G., Ferreira, J. P., Bocchi, E., Böhm, M., Brunner–La Rocca, H.-P., Choi, D.-J., Chopra, V., Chuquiure-Valenzuela, E., Giannetti, N., Gomez-Mesa, J. E., Janssens, S., Januzzi, J. L., Gonzalez-Juanatey, J. R., Merkely, B., Nicholls, S. J., Perrone, S. V., Piña, I. L., … Packer, M. (2021). Empagliflozin in Heart Failure with a Preserved Ejection Fraction. *New England Journal of Medicine*, *385*(16), 1451–1461. https://doi.org/10.1056/NEJMoa2107038

Arnér, E. S. J., & Holmgren, A. (2000). Physiological functions of thioredoxin and thioredoxin reductase. *European Journal of Biochemistry*, *267*(20), 6102–6109. https://doi.org/10.1046/j.1432-1327.2000.01701.x

Azushima, K., Gurley, S. B., & Coffman, T. M. (2018). Modelling diabetic nephropathy in mice. *Nature Reviews Nephrology*, *14*(1), 48–56. https://doi.org/10.1038/nrneph.2017.142

Banjac, A., Perisic, T., Sato, H., Seiler, A., Bannai, S., Weiss, N., Daniel, P., Conrad, M., & Bornkamm, G. (2008). *The cystine/cysteine cycle: A redox cycle regulating susceptibility versus resistance to cell death*.

Bannai, S., & Kitamura, E. (1980). Transport interaction of L-cystine and L-glutamate in human diploid fibroblasts in culture. *Journal of Biological Chemistry*, *255*(6), 2372–2376. https://doi.org/10.1016/S0021-9258(19)85901-X

Barayeu, U., Schilling, D., Eid, M., Xavier Da Silva, T. N., Schlicker, L., Mitreska, N., Zapp, C., Gräter, F., Miller, A. K., Kappl, R., Schulze, A., Friedmann Angeli, J. P., & Dick, T. P. (2023). Hydropersulfides inhibit lipid peroxidation and ferroptosis by scavenging radicals. *Nature Chemical Biology*, *19*(1), 28–37. https://doi.org/10.1038/s41589-022-01145-w

Belavgeni, A., Maremonti, F., Tonnus, W., Stadtmüller, M., Gavali, S., Mallais, M., Flade, K., Brucker, A., Becker, J. N., Beer, K., Tmava, M., Stumpf, J., Gembardt, F., Hugo, C., Giacca, M., Hale, B. G., Perakakis, N., Sha, W., Pratt, D. A., … Linkermann, A. (2023). vPIF-1 is an insulin-like antiferroptotic viral peptide. *Proceedings of the National Academy of Sciences*, *120*(21), e2300320120. https://doi.org/10.1073/pnas.2300320120

Belavgeni, A., Meyer, C., Stumpf, J., Hugo, C., & Linkermann, A. (2020). Ferroptosis and Necroptosis in the Kidney. *Cell Chemical Biology*, *27*(4), 448–462. https://doi.org/10.1016/j.chembiol.2020.03.016

Bersuker, K., Hendricks, J. M., Li, Z., Magtanong, L., Ford, B., Tang, P. H., Roberts, M. A., Tong, B., Maimone, T. J., Zoncu, R., Bassik, M. C., Nomura, D. K., Dixon, S. J., & Olzmann, J. A. (2019). The CoQ oxidoreductase FSP1 acts parallel to GPX4 to inhibit ferroptosis. *Nature*, *575*(7784), 688–692. https://doi.org/10.1038/s41586-019-1705-2

Brosius, F. C., Alpers, C. E., Bottinger, E. P., Breyer, M. D., Coffman, T. M., Gurley, S. B., Harris, R. C., Kakoki, M., Kretzler, M., Leiter, E. H., Levi, M., McIndoe, R. A., Sharma, K., Smithies, O., Susztak, K., Takahashi, N., & Takahashi, T. (2009). Mouse models of diabetic nephropathy. *Journal of the American Society of Nephrology*, *20*(12), 2503–2512. https://doi.org/10.1681/ASN.2009070721

Brown, J. C. (1988). 5 Enteroinsular axis. *Baillière's Clinical Endocrinology and Metabolism*, *2*(2), 359–373. https://doi.org/10.1016/S0950-351X(88)80037-5

Buchan, A. M., Polak, J. M., Capella, C., Solcia, E., & Pearse, A. G. (1978). Electronimmunocytochemical evidence for the K cell localization of gastric inhibitory polypeptide (GIP) in man. *Histochemistry*, *56*(1), 37–44. https://doi.org/10.1007/BF00492251

Bugarski, M., Martins, J. R., Haenni, D., & Hall, A. M. (2018). Multiphoton imaging reveals axial differences in metabolic autofluorescence signals along the kidney proximal tubule. *American Journal of Physiology - Renal Physiology*, *315*(6), F1613–F1625. https://doi.org/10.1152/ajprenal.00165.2018

Chadha, C., Pittas, A. G., Lary, C. W., Knowler, W. C., Chatterjee, R., Phillips, L. S., Aroda, V. R., Lewis, M. R., Pratley, R., Staten, M. A., Nelson, J., Rasouli, N., Brodsky, I., & D2d Research Group. (2020). Reproducibility of a prediabetes classification in a contemporary population. *Metabolism Open*, *6*, 100031. https://doi.org/10.1016/j.metop.2020.100031

Chatterjee, S., Khunti, K., & Davies, M. J. (2017). Type 2 diabetes. *The Lancet*, *389*(10085), 2239–2251. https://doi.org/10.1016/S0140-6736(17)30058-2

Chen, L., Hambright, W. S., Na, R., & Ran, Q. (2015). Ablation of the Ferroptosis Inhibitor Glutathione Peroxidase 4 in Neurons Results in Rapid Motor Neuron Degeneration and Paralysis. *The Journal of Biological Chemistry*, *290*(47), 28097–28106. https://doi.org/10.1074/jbc.M115.680090

Chen, Y., Lee, K., Ni, Z., & He, J. C. (2020a). Diabetic Kidney Disease: Challenges, Advances, and Opportunities. *Kidney Diseases*, *6*(4), 215–225. https://doi.org/10.1159/000506634

Chen, Y., Lee, K., Ni, Z., & He, J. C. (2020b). Diabetic Kidney Disease: Challenges, Advances, and Opportunities. *Kidney Diseases*, *6*(4), 215–225. https://doi.org/10.1159/000506634

Cheng, J. B., & Russell, D. W. (2004). Mammalian Wax Biosynthesis: I. IDENTIFICATION OF TWO FATTY ACYL-COENZYME A REDUCTASES WITH DIFFERENT SUBSTRATE SPECIFICITIES AND TISSUE DISTRIBUTIONS*. *Journal of Biological Chemistry*, *279*(36), 37789–37797. https://doi.org/10.1074/jbc.M406225200

Chouchani, E. T., Kazak, L., Jedrychowski, M. P., Lu, G. Z., Erickson, B. K., Szpyt, J., Pierce, K. A., Laznik-Bogoslavski, D., Vetrivelan, R., Clish, C. B., Robinson, A. J., Gygi, S. P., & Spiegelman, B. M. (2016). Mitochondrial ROS regulate thermogenic energy expenditure and sulfenylation of UCP1. *Nature*, *532*(7597), 112–116. https://doi.org/10.1038/nature17399

Clee, S. M., Nadler, S. T., & Attie, A. D. (2005). Genetic and genomic studies of the BTBR ob/ob mouse model of type 2 diabetes. *American Journal of Therapeutics*, *12*(6), 491–498. https://doi.org/10.1097/01.mjt.0000178781.89789.25

Conrad, M., Angeli, J. P. F., Vandenabeele, P., & Stockwell, B. R. (2016). Regulated necrosis: Disease relevance and therapeutic opportunities. *Nature Reviews Drug Discovery*, *15*(5), 348–366. https://doi.org/10.1038/nrd.2015.6

Conrad, M., & Pratt, D. A. (2019). The chemical basis of ferroptosis. *Nature Chemical Biology*, *15*(12), 1137–1147. https://doi.org/10.1038/s41589-019-0408-1

Coughlan, M. T., Thorburn, D. R., Penfold, S. A., Laskowski, A., Harcourt, B. E., Sourris, K. C., Tan, A. L. Y., Fukami, K., Thallas-Bonke, V., Nawroth, P. P., Brownlee, M., Bierhaus, A., Cooper, M. E., & Forbes, J. M. (2009). RAGE-induced cytosolic ROS promote mitochondrial superoxide generation in diabetes. *Journal of the American Society of Nephrology: JASN*, *20*(4), 742–752. https://doi.org/10.1681/ASN.2008050514

Cui, W., Liu, D., Gu, W., & Chu, B. (2021). Peroxisome-driven ether-linked phospholipids biosynthesis is essential for ferroptosis. *Cell Death & Differentiation*, *28*(8), 2536–2551. https://doi.org/10.1038/s41418-021-00769-0

Daehn, I. S., Ekperikpe, U. S., & Stadler, K. (2023). Redox regulation in diabetic kidney disease. *American Journal of Physiology-Renal Physiology*, *325*(2), F135–F149. https://doi.org/10.1152/ajprenal.00047.2023

de Boer, I. H., Khunti, K., Sadusky, T., Tuttle, K. R., Neumiller, J. J., Rhee, C. M., Rosas, S. E., Rossing, P., & Bakris, G. (2022). Diabetes Management in Chronic Kidney Disease: A Consensus Report by the American Diabetes Association (ADA) and Kidney Disease: Improving Global Outcomes (KDIGO). *Diabetes Care*, *45*(12), 3075–3090. https://doi.org/10.2337/dci22-0027

De Ponte, M. C., Cardoso, V. G., Gonçalves, G. L., Costa-Pessoa, J. M., & Oliveira-Souza, M. (2021). Early type 1 diabetes aggravates renal ischemia/reperfusion-

induced acute kidney injury. *Scientific Reports*, *11*(1), 19028. https://doi.org/10.1038/s41598-021-97839-7

Dean, J. M., & Lodhi, I. J. (2018). Structural and functional roles of ether lipids. *Protein & Cell*, *9*(2), 196–206. https://doi.org/10.1007/s13238-017-0423-5

DeFronzo, R. A. (2009). From the Triumvirate to the Ominous Octet: A New Paradigm for the Treatment of Type 2 Diabetes Mellitus. *Diabetes*, *58*(4), 773–795. https://doi.org/10.2337/db09-9028

DeFronzo, R. A., Ferrannini, E., Groop, L., Henry, R. R., Herman, W. H., Holst, J. J., Hu, F. B., Kahn, C. R., Raz, I., Shulman, G. I., Simonson, D. C., Testa, M. A., & Weiss, R. (2015). Type 2 diabetes mellitus. *Nature Reviews Disease Primers*, *1*(1), Article 1. https://doi.org/10.1038/nrdp.2015.19

DeFronzo, R. A., Reeves, W. B., & Awad, A. S. (2021). Pathophysiology of diabetic kidney disease: Impact of SGLT2 inhibitors. *Nature Reviews Nephrology*, *17*(5), 319–334. https://doi.org/10.1038/s41581-021-00393-8

Degterev, A., Huang, Z., Boyce, M., Li, Y., Jagtap, P., Mizushima, N., Cuny, G. D., Mitchison, T. J., Moskowitz, M. A., & Yuan, J. (2005). Chemical inhibitor of nonapoptotic cell death with therapeutic potential for ischemic brain injury. *Nature Chemical Biology*, *1*(2), 112–119. https://doi.org/10.1038/nchembio711

Degterev, A., & Linkermann, A. (2016). Generation of small molecules to interfere with regulated necrosis. *Cellular and Molecular Life Sciences: CMLS*, *73*(11–12), 2251–2267. https://doi.org/10.1007/s00018-016-2198-x

Devisscher, L., Van Coillie, S., Hofmans, S., Van Rompaey, D., Goossens, K., Meul, E., Maes, L., De Winter, H., Van Der Veken, P., Vandenabeele, P., Berghe, T. V., & Augustyns, K. (2018). Discovery of Novel, Drug-Like Ferroptosis Inhibitors with in Vivo Efficacy. *Journal of Medicinal Chemistry*, *61*(22), 10126–10140. https://doi.org/10.1021/acs.jmedchem.8b01299

Dixon, S. J., Lemberg, K. M., Lamprecht, M. R., Skouta, R., Zaitsev, E. M., Gleason, C. E., Patel, D. N., Bauer, A. J., Cantley, A. M., Yang, W. S., Morrison, B., & Stockwell, B. R. (2012a). Ferroptosis: An Iron-Dependent Form of Nonapoptotic Cell Death. *Cell*, *149*(5), 1060–1072. https://doi.org/10.1016/J.CELL.2012.03.042

Dixon, S. J., Lemberg, K. M., Lamprecht, M. R., Skouta, R., Zaitsev, E. M., Gleason, C. E., Patel, D. N., Bauer, A. J., Cantley, A. M., Yang, W. S., Morrison, B., & Stockwell, B. R. (2012b). Ferroptosis: An Iron-Dependent Form of Nonapoptotic Cell Death. *Cell*, *149*(5), 1060–1072. https://doi.org/10.1016/j.cell.2012.03.042

Dixon, S. J., & Stockwell, B. R. (2014). The role of iron and reactive oxygen species in cell death. *Nature Chemical Biology*, *10*(1), 9–17. https://doi.org/10.1038/nchembio.1416

Dixon, S. J., Winter, G. E., Musavi, L. S., Lee, E. D., Snijder, B., Rebsamen, M., Superti-Furga, G., & Stockwell, B. R. (2015). Human Haploid Cell Genetics Reveals Roles for Lipid Metabolism Genes in Nonapoptotic Cell Death. *ACS Chemical Biology*, *10*(7), 1604–1609. https://doi.org/10.1021/acschembio.5b00245

Doll, S., Freitas, F. P., Shah, R., Aldrovandi, M., Da Silva, M. C., Ingold, I., Goya Grocin, A., Xavier Da Silva, T. N., Panzilius, E., Scheel, C. H., Mourão, A., Buday, K., Sato, M., Wanninger, J., Vignane, T., Mohana, V., Rehberg, M., Flatley, A., Schepers, A., … Conrad, M. (2019). FSP1 is a glutathione-

independent ferroptosis suppressor. *Nature*, *575*(7784), 693–698. https://doi.org/10.1038/s41586-019-1707-0

Doll, S., Proneth, B., Tyurina, Y. Y., Panzilius, E., Kobayashi, S., Ingold, I., Irmler, M., Beckers, J., Aichler, M., Walch, A., Prokisch, H., Trümbach, D., Mao, G., Qu, F., Bayir, H., Füllekrug, J., Scheel, C. H., Wurst, W., Schick, J. A., … Conrad, M. (2017). ACSL4 dictates ferroptosis sensitivity by shaping cellular lipid composition. *Nature Chemical Biology*, *13*(1), 91–98. https://doi.org/10.1038/nchembio.2239

Dolma, S., Lessnick, S. L., Hahn, W. C., & Stockwell, B. R. (2003). Identification of genotype-selective antitumor agents using synthetic lethal chemical screening in engineered human tumor cells. *Cancer Cell*, *3*(3), 285–296. https://doi.org/10.1016/S1535-6108(03)00050-3

Eissele, R., Göke, R., Willemer, S., Harthus, H. P., Vermeer, H., Arnold, R., & Göke, B. (1992). Glucagon-like peptide-1 cells in the gastrointestinal tract and pancreas of rat, pig and man. *European Journal of Clinical Investigation*, *22*(4), 283–291. https://doi.org/10.1111/j.1365-2362.1992.tb01464.x

Elguindy, M. M., & Nakamaru-Ogiso, E. (2015). Apoptosis-inducing Factor (AIF) and Its Family Member Protein, AMID, Are Rotenone-sensitive NADH:Ubiquinone Oxidoreductases (NDH-2). *The Journal of Biological Chemistry*, *290*(34), 20815–20826. https://doi.org/10.1074/jbc.M115.641498

ElSayed, N. A., Aleppo, G., Aroda, V. R., Bannuru, R. R., Brown, F. M., Bruemmer, D., Collins, B. S., Gaglia, J. L., Hilliard, M. E., Isaacs, D., Johnson, E. L., Kahan, S., Khunti, K., Leon, J., Lyons, S. K., Perry, M. L., Prahalad, P., Pratley, R. E., Seley, J. J., … American Diabetes Association. (2023). 2. Classification and Diagnosis of Diabetes: *Standards of Care in Diabetes—2023. Diabetes Care*, *46*(Supplement_1), S19–S40. https://doi.org/10.2337/dc23-S002

Fang, S., Jin, Y., Zheng, H., Yan, J., Cui, Y., Bi, H., Jia, H., Zhang, H., Wang, Y., Na, L., Gao, X., & Zhou, H. (2011). High glucose condition upregulated Txnip expression level in rat mesangial cells through ROS/MEK/MAPK pathway. *Molecular and Cellular Biochemistry*, *347*(1–2), 175–182. https://doi.org/10.1007/s11010-010-0626-z

Feng, X., Wang, S., Sun, Z., Dong, H., Yu, H., Huang, M., & Gao, X. (2021). Ferroptosis Enhanced Diabetic Renal Tubular Injury via HIF-1α/HO-1 Pathway in db/db Mice. *Frontiers in Endocrinology*, *12*. https://www.frontiersin.org/articles/10.3389/fendo.2021.626390

Fineberg, D., Jandeleit-Dahm, K. A. M., & Cooper, M. E. (2013a). Diabetic nephropathy: Diagnosis and treatment. *Nature Reviews Endocrinology*, *9*(12), 713–723. https://doi.org/10.1038/nrendo.2013.184

Fineberg, D., Jandeleit-Dahm, K. A. M., & Cooper, M. E. (2013b). Diabetic nephropathy: Diagnosis and treatment. *Nature Reviews Endocrinology*, *9*(12), Article 12. https://doi.org/10.1038/nrendo.2013.184

Forbes, J. M., Coughlan, M. T., & Cooper, M. E. (2008). Oxidative stress as a major culprit in kidney disease in diabetes. *Diabetes*, *57*(6), 1446–1454. https://doi.org/10.2337/db08-0057

Friedmann Angeli, J. P., Schneider, M., Proneth, B., Tyurina, Y. Y., Tyurin, V. A., Hammond, V. J., Herbach, N., Aichler, M., Walch, A., Eggenhofer, E., Basavarajappa, D., Rådmark, O., Kobayashi, S., Seibt, T., Beck, H., Neff, F., Esposito, I., Wanke, R., Förster, H., … Conrad, M. (2014a). Inactivation of the

ferroptosis regulator Gpx4 triggers acute renal failure in mice. *Nature Cell Biology*, *16*(12), Article 12. https://doi.org/10.1038/ncb3064

Friedmann Angeli, J. P., Schneider, M., Proneth, B., Tyurina, Y. Y., Tyurin, V. A., Hammond, V. J., Herbach, N., Aichler, M., Walch, A., Eggenhofer, E., Basavarajappa, D., Rådmark, O., Kobayashi, S., Seibt, T., Beck, H., Neff, F., Esposito, I., Wanke, R., Förster, H., … Conrad, M. (2014b). Inactivation of the ferroptosis regulator Gpx4 triggers acute renal failure in mice. *Nature Cell Biology*, *16*(12), 1180–1191. https://doi.org/10.1038/ncb3064

Gæde, P., Vedel, P., Larsen, N., Jensen, G. V. H., Parving, H.-H., & Pedersen, O. (2003). Multifactorial Intervention and Cardiovascular Disease in Patients with Type 2 Diabetes. *New England Journal of Medicine*, *348*(5), 383–393. https://doi.org/10.1056/NEJMoa021778

Gallo, L. A., Wright, E. M., & Vallon, V. (2015). Probing SGLT2 as a therapeutic target for diabetes: Basic physiology and consequences. *Diabetes and Vascular Disease Research*, *12*(2), 78–89. https://doi.org/10.1177/1479164114561992

Galluzzi, L., Vitale, I., Aaronson, S. A., Abrams, J. M., Adam, D., Agostinis, P., Alnemri, E. S., Altucci, L., Amelio, I., Andrews, D. W., Annicchiarico-Petruzzelli, M., Antonov, A. V., Arama, E., Baehrecke, E. H., Barlev, N. A., Bazan, N. G., Bernassola, F., Bertrand, M. J. M., Bianchi, K., … Kroemer, G. (2018). Molecular mechanisms of cell death: Recommendations of the Nomenclature Committee on Cell Death 2018. *Cell Death & Differentiation*, *25*(3), Article 3. https://doi.org/10.1038/s41418-017-0012-4

Gao, M., Monian, P., Quadri, N., Ramasamy, R., & Jiang, X. (2015). Glutaminolysis and Transferrin Regulate Ferroptosis. *Molecular Cell*, *59*(2), 298–308. https://doi.org/10.1016/j.molcel.2015.06.011

Gaschler, M. M., Andia, A. A., Liu, H., Csuka, J. M., Hurlocker, B., Vaiana, C. A., Heindel, D. W., Zuckerman, D. S., Bos, P. H., Reznik, E., Ye, L. F., Tyurina, Y. Y., Lin, A. J., Shchepinov, M. S., Chan, A. Y., Peguero-Pereira, E., Fomich, M. A., Daniels, Jacob. D., Bekish, A. V., … Stockwell, B. R. (2018). FINO2 initiates ferroptosis through GPX4 inactivation and iron oxidation. *Nature Chemical Biology*, *14*(5), 507–515. https://doi.org/10.1038/s41589-018-0031-6

Gillard, P., Schnell, O., & Groop, P.-H. (2020). The nephrological perspective on SGLT-2 inhibitors in type 1 diabetes. *Diabetes Research and Clinical Practice*, *170*, 108462. https://doi.org/10.1016/j.diabres.2020.108462

Giralt-López, A., Molina-Van den Bosch, M., Vergara, A., García-Carro, C., Seron, D., Jacobs-Cachá, C., & Soler, M. J. (2020). Revisiting Experimental Models of Diabetic Nephropathy. *International Journal of Molecular Sciences*, *21*(10), Article 10. https://doi.org/10.3390/ijms21103587

Girman, C. J., Kou, T. D., Brodovicz, K., Alexander, C. M., O'Neill, E. A., Engel, S., Williams-Herman, D. E., & Katz, L. (2012). Risk of acute renal failure in patients with Type 2 diabetes mellitus. *Diabetic Medicine*, *29*(5), 614–621. https://doi.org/10.1111/j.1464-5491.2011.03498.x

Gregory, G. A., Robinson, T. I. G., Linklater, S. E., Wang, F., Colagiuri, S., Beaufort, C. de, Donaghue, K. C., Harding, J. L., Wander, P. L., Zhang, X., Li, X., Karuranga, S., Chen, H., Sun, H., Xie, Y., Oram, R., Magliano, D. J., Zhou, Z., Jenkins, A. J., … Ogle, G. D. (2022). Global incidence, prevalence, and mortality of type 1 diabetes in 2021 with projection to 2040: A modelling study.

The Lancet Diabetes & Endocrinology, *10*(10), 741–760. https://doi.org/10.1016/S2213-8587(22)00218-2

Gross, J. L., De Azevedo, M. J., Silveiro, S. P., Canani, L. H., Caramori, M. L., & Zelmanovitz, T. (2005). Diabetic Nephropathy: Diagnosis, Prevention, and Treatment. *Diabetes Care*, *28*(1), 164–176. https://doi.org/10.2337/diacare.28.1.164

Grynberg, K., Tian, L., Tesch, G., Ozols, E., Mulley, W. R., Nikolic-Paterson, D. J., & Ma, F. Y. (2022). Mice with Established Diabetes Show Increased Susceptibility to Renal Ischemia/Reperfusion Injury. *The American Journal of Pathology*, *192*(3), 441–453. https://doi.org/10.1016/j.ajpath.2021.12.003

Hambright, W. S., Fonseca, R. S., Chen, L., Na, R., & Ran, Q. (2017). Ablation of ferroptosis regulator glutathione peroxidase 4 in forebrain neurons promotes cognitive impairment and neurodegeneration. *Redox Biology*, *12*, 8–17. https://doi.org/10.1016/j.redox.2017.01.021

Hanahan, D. (1985). Heritable formation of pancreatic β-cell tumours in transgenic mice expressing recombinant insulin/simian virus 40 oncogenes. *Nature*, *315*(6015), Article 6015. https://doi.org/10.1038/315115a0

Harris, I. S., Treloar, A. E., Inoue, S., Sasaki, M., Gorrini, C., Lee, K. C., Yung, K. Y., Brenner, D., Knobbe-Thomsen, C. B., Cox, M. A., Elia, A., Berger, T., Cescon, D. W., Adeoye, A., Brüstle, A., Molyneux, S. D., Mason, J. M., Li, W. Y., Yamamoto, K., … Mak, T. W. (2015). Glutathione and Thioredoxin Antioxidant Pathways Synergize to Drive Cancer Initiation and Progression. *Cancer Cell*, *27*(2), 211–222. https://doi.org/10.1016/j.ccell.2014.11.019

Haskell, B. D., Flurkey, K., Duffy, T. M., Sargent, E. E., & Leiter, E. H. (2002). The Diabetes-Prone NZO/HILt Strain. I. Immunophenotypic Comparison to the Related NZB/BlNJ and NZW/LacJ Strains. *Laboratory Investigation*, *82*(7), 833–842. https://doi.org/10.1097/01.LAB.0000018915.53257.00

Hassannia, B., Vandenabeele, P., & Vanden Berghe, T. (2019). Targeting Ferroptosis to Iron Out Cancer. *Cancer Cell*, *35*(6), 830–849. https://doi.org/10.1016/j.ccell.2019.04.002

Hayano, M., Yang, W. S., Corn, C. K., Pagano, N. C., & Stockwell, B. R. (2016). Loss of cysteinyl-tRNA synthetase (CARS) induces the transsulfuration pathway and inhibits ferroptosis induced by cystine deprivation. *Cell Death & Differentiation*, *23*(2), 270–278. https://doi.org/10.1038/cdd.2015.93

He, W., Wan, H., Hu, L., Chen, P., Wang, X., Huang, Z., Yang, Z.-H., Zhong, C.-Q., & Han, J. (2015). Gasdermin D is an executor of pyroptosis and required for interleukin-1β secretion. *Cell Research*, *25*(12), Article 12. https://doi.org/10.1038/cr.2015.139

Herbach, N., Goeke, B., Schneider, M., Hermanns, W., Wolf, E., & Wanke, R. (2005). Overexpression of a dominant negative GIP receptor in transgenic mice results in disturbed postnatal pancreatic islet and beta-cell development. *Regulatory Peptides*, *125*(1–3), 103–117. https://doi.org/10.1016/j.regpep.2004.08.021

Herbach, N., Göke, B., Wolf, E., & Wanke, R. (2008). Diets influence the diabetic phenotype of transgenic mice expressing a dominant negative glucose-dependent insulinotropic polypeptide receptor (GIPRdn). *Regulatory Peptides*, *146*(1–3), 260–270. https://doi.org/10.1016/j.regpep.2007.10.005

Herbach, N., Schairer, I., Blutke, A., Kautz, S., Siebert, A., Göke, B., Wolf, E., & Wanke, R. (2009). Diabetic kidney lesions of GIPR [dn] transgenic mice:

Podocyte hypertrophy and thickening of the GBM precede glomerular hypertrophy and glomerulosclerosis. *American Journal of Physiology-Renal Physiology*, *296*(4), F819–F829. https://doi.org/10.1152/ajprenal.90665.2008

Hirakawa, Y., Mizukami, K., Yoshihara, T., Takahashi, I., Khulan, P., Honda, T., Mimura, I., Tanaka, T., Tobita, S., & Nangaku, M. (2018). Intravital phosphorescence lifetime imaging of the renal cortex accurately measures renal hypoxia. *Kidney International*, *93*(6), 1483–1489. https://doi.org/10.1016/j.kint.2018.01.015

Hofmans, S., Berghe, T. V., Devisscher, L., Hassannia, B., Lyssens, S., Joossens, J., Van Der Veken, P., Vandenabeele, P., & Augustyns, K. (2016). Novel Ferroptosis Inhibitors with Improved Potency and ADME Properties. *Journal of Medicinal Chemistry*, *59*(5), 2041–2053. https://doi.org/10.1021/acs.jmedchem.5b01641

Holst, J. J. (2019). The incretin system in healthy humans: The role of GIP and GLP-1. *Metabolism*, *96*, 46–55. https://doi.org/10.1016/j.metabol.2019.04.014

Holst, J. J., Ørskov, C., Vagn Nielsen, O., & Schwartz, T. W. (1987). Truncated glucagon-like peptide I, an insulin-releasing hormone from the distal gut. *FEBS Letters*, *211*(2), 169–174. https://doi.org/10.1016/0014-5793(87)81430-8

Hu, C.-L., Nydes, M., Shanley, K. L., Morales Pantoja, I. E., Howard, T. A., & Bizzozero, O. A. (2019). Reduced expression of the ferroptosis inhibitor glutathione peroxidase-4 in multiple sclerosis and experimental autoimmune encephalomyelitis. *Journal of Neurochemistry*, *148*(3), 426–439. https://doi.org/10.1111/jnc.14604

Huang, D., Shen, P., Wang, C., Gao, J., Ye, C., & Wu, F. (2022). Calycosin plays a protective role in diabetic kidney disease through the regulation of ferroptosis. *Pharmaceutical Biology*, *60*(1), 990–996. https://doi.org/10.1080/13880209.2022.2067572

Hudkins, K. L., Pichaiwong, W., Wietecha, T., Kowalewska, J., Banas, M. C., Spencer, M. W., Mühlfeld, A., Koelling, M., Pippin, J. W., Shankland, S. J., Askari, B., Rabaglia, M. E., Keller, M. P., Attie, A. D., & Alpers, C. E. (2010). BTBR Ob/Ob Mutant Mice Model Progressive Diabetic Nephropathy. *Journal of the American Society of Nephrology*, *21*(9), 1533. https://doi.org/10.1681/ASN.2009121290

Hwang, J., Suh, H.-W., Jeon, Y. H., Hwang, E., Nguyen, L. T., Yeom, J., Lee, S.-G., Lee, C., Kim, K. J., Kang, B. S., Jeong, J.-O., Oh, T.-K., Choi, I., Lee, J.-O., & Kim, M. H. (2014). The structural basis for the negative regulation of thioredoxin by thioredoxin-interacting protein. *Nature Communications*, *5*(1), 2958. https://doi.org/10.1038/ncomms3958

Ingold, I., Berndt, C., Schmitt, S., Doll, S., Poschmann, G., Buday, K., Roveri, A., Peng, X., Porto Freitas, F., Seibt, T., Mehr, L., Aichler, M., Walch, A., Lamp, D., Jastroch, M., Miyamoto, S., Wurst, W., Ursini, F., Arnér, E. S. J., … Conrad, M. (2018). Selenium Utilization by GPX4 Is Required to Prevent Hydroperoxide-Induced Ferroptosis. *Cell*, *172*(3), 409-422.e21. https://doi.org/10.1016/j.cell.2017.11.048

International Diabetes Federation. (n.d.). *International Diabetes Federation*. International Diabetes Federation. Retrieved 16 January 2024, from https://idf.org/

Jakupoglu, C., Przemeck, G. K. H., Schneider, M., Moreno, S. G., Mayr, N., Hatzopoulos, A. K., de Angelis, M. H., Wurst, W., Bornkamm, G. W., Brielmeier,

M., & Conrad, M. (2005). Cytoplasmic Thioredoxin Reductase Is Essential for Embryogenesis but Dispensable for Cardiac Development. *Molecular and Cellular Biology*, *25*(5), 1980–1988. https://doi.org/10.1128/MCB.25.5.1980-1988.2005

James, D. E., Stöckli, J., & Birnbaum, M. J. (2021). The aetiology and molecular landscape of insulin resistance. *Nature Reviews Molecular Cell Biology*, *22*(11), 751–771. https://doi.org/10.1038/s41580-021-00390-6

Jiang, L., Kon, N., Li, T., Wang, S.-J., Su, T., Hibshoosh, H., Baer, R., & Gu, W. (2015). Ferroptosis as a p53-mediated activity during tumour suppression. *Nature*, *520*(7545), Article 7545. https://doi.org/10.1038/nature14344

Jiang, X., Stockwell, B. R., & Conrad, M. (2021). Ferroptosis: Mechanisms, biology and role in disease. *Nature Reviews Molecular Cell Biology*, *22*(4), 266–282. https://doi.org/10.1038/s41580-020-00324-8

Jin, T., & Chen, C. (2022). Umbelliferone delays the progression of diabetic nephropathy by inhibiting ferroptosis through activation of the Nrf-2/HO-1 pathway. *Food and Chemical Toxicology*, *163*, 112892. https://doi.org/10.1016/j.fct.2022.112892

Kagan, V. E., Mao, G., Qu, F., Angeli, J. P. F., Doll, S., Croix, C. S., Dar, H. H., Liu, B., Tyurin, V. A., Ritov, V. B., Kapralov, A. A., Amoscato, A. A., Jiang, J., Anthonymuthu, T., Mohammadyani, D., Yang, Q., Proneth, B., Klein-Seetharaman, J., Watkins, S., … Bayır, H. (2017). Oxidized arachidonic and adrenic PEs navigate cells to ferroptosis. *Nature Chemical Biology*, *13*(1), 81–90. https://doi.org/10.1038/nchembio.2238

Kakoki, M., Takahashi, N., Jennette, J. C., & Smithies, O. (2004). Diabetic nephropathy is markedly enhanced in mice lacking the bradykinin B2 receptor. *Proceedings of the National Academy of Sciences*, *101*(36), 13302–13305. https://doi.org/10.1073/pnas.0405449101

Kanetsuna, Y., Takahashi, K., Nagata, M., Gannon, M. A., Breyer, M. D., Harris, R. C., & Takahashi, T. (2007). Deficiency of endothelial nitric-oxide synthase confers susceptibility to diabetic nephropathy in nephropathy-resistant inbred mice. *The American Journal of Pathology*, *170*(5), 1473–1484. https://doi.org/10.2353/ajpath.2007.060481

Kasper, D. L., & Harrison, T. R. (Eds.). (2005). *Harrison's principles of internal medicine* (16th ed). McGraw-Hill, Medical Pub. Division.

Katikaneni, A., Jelcic, M., Gerlach, G. F., Ma, Y., Overholtzer, M., & Niethammer, P. (2020). Lipid peroxidation regulates long-range wound detection through 5-lipoxygenase in zebrafish. *Nature Cell Biology*, *22*(9), Article 9. https://doi.org/10.1038/s41556-020-0564-2

Kellum, J. A., Romagnani, P., Ashuntantang, G., Ronco, C., Zarbock, A., & Anders, H.-J. (2021). Acute kidney injury. *Nature Reviews Disease Primers*, *7*(1), 52. https://doi.org/10.1038/s41572-021-00284-z

Kieffer, T. J., McIntosh, C. H., & Pederson, R. A. (1995). Degradation of glucose-dependent insulinotropic polypeptide and truncated glucagon-like peptide 1 in vitro and in vivo by dipeptidyl peptidase IV. *Endocrinology*, *136*(8), 3585–3596. https://doi.org/10.1210/endo.136.8.7628397

Kim, S. E., Zhang, L., Ma, K., Riegman, M., Chen, F., Ingold, I., Conrad, M., Turker, M. Z., Gao, M., Jiang, X., Monette, S., Pauliah, M., Gonen, M., Zanzonico, P., Quinn, T., Wiesner, U., Bradbury, M. S., & Overholtzer, M. (2016). Ultrasmall

nanoparticles induce ferroptosis in nutrient-deprived cancer cells and suppress tumour growth. *Nature Nanotechnology*, *11*(11), Article 11. https://doi.org/10.1038/nnano.2016.164

Kim, S., Kang, S.-W., Joo, J., Han, S. H., Shin, H., Nam, B. Y., Park, J., Yoo, T.-H., Kim, G., Lee, P., & Park, J. T. (2021). Characterization of ferroptosis in kidney tubular cell death under diabetic conditions. *Cell Death & Disease*, *12*(2), 160. https://doi.org/10.1038/s41419-021-03452-x

Kimmelstiel, P., & Wilson, C. (1936). Intercapillary Lesions in the Glomeruli of the Kidney. *The American Journal of Pathology*, *12*(1), 83-98.7.

King, A. J. (2012). The use of animal models in diabetes research. *British Journal of Pharmacology*, *166*(3), 877–894. https://doi.org/10.1111/j.1476-5381.2012.01911.x

Klein, S., Gastaldelli, A., Yki-Järvinen, H., & Scherer, P. E. (2022). Why does obesity cause diabetes? *Cell Metabolism*, *34*(1), 11–20. https://doi.org/10.1016/j.cmet.2021.12.012

Knop, F. K., Aaboe, K., Vilsbøll, T., Vølund, A., Holst, J. J., Krarup, T., & Madsbad, S. (2012). Impaired incretin effect and fasting hyperglucagonaemia characterizing type 2 diabetic subjects are early signs of dysmetabolism in obesity. *Diabetes, Obesity & Metabolism*, *14*(6), 500–510. https://doi.org/10.1111/j.1463-1326.2011.01549.x

Kong, L.-L., Wu, H., Cui, W.-P., Zhou, W.-H., Luo, P., Sun, J., Yuan, H., & Miao, L.-N. (2013). Advances in murine models of diabetic nephropathy. *Journal of Diabetes Research*, *2013*. Scopus. https://doi.org/10.1155/2013/797548

Kosugi, T., Heinig, M., Nakayama, T., Connor, T., Yuzawa, Y., Li, Q., Hauswirth, W. W., Grant, M. B., Croker, B. P., Campbell-Thompson, M., Zhang, L., Atkinson, M. A., Segal, M. S., & Nakagawa, T. (2009). Lowering blood pressure blocks mesangiolysis and mesangial nodules, but not tubulointerstitial injury, in diabetic eNOS knockout mice. *The American Journal of Pathology*, *174*(4), 1221–1229. https://doi.org/10.2353/ajpath.2009.080605

Ksiazek, P., Wojewoda, P., Muc, K., & Buraczynska, M. (2003). Endothelial nitric oxide synthase gene intron 4 polymorphism in type 2 diabetes mellitus. *Molecular Diagnosis: A Journal Devoted to the Understanding of Human Disease Through the Clinical Application of Molecular Biology*, *7*(2), 119–123. https://doi.org/10.1007/BF03260027

Lange, M., & Olzmann, J. A. (2022). Hydropersulfides are endogenous antioxidants that inhibit ferroptosis. *Cell Chemical Biology*, *29*(12), 1661–1663. https://doi.org/10.1016/j.chembiol.2022.11.011

Lau, A., & Tymianski, M. (2010). Glutamate receptors, neurotoxicity and neurodegeneration. *Pflugers Archiv: European Journal of Physiology*, *460*(2), 525–542. https://doi.org/10.1007/s00424-010-0809-1

Leiter, E. H., & Reifsnyder, P. C. (2004). Differential Levels of Diabetogenic Stress in Two New Mouse Models of Obesity and Type 2 Diabetes. *Diabetes*, *53*(suppl_1), S4–S11. https://doi.org/10.2337/diabetes.53.2007.S4

Li, S., Zheng, L., Zhang, J., Liu, X., & Wu, Z. (2021). Inhibition of ferroptosis by up-regulating Nrf2 delayed the progression of diabetic nephropathy. *Free Radical Biology and Medicine*, *162*, 435–449. https://doi.org/10.1016/j.freeradbiomed.2020.10.323

Linkermann, A. (2016). Nonapoptotic cell death in acute kidney injury and transplantation. *Kidney International, 89*(1), 46–57. https://doi.org/10.1016/j.kint.2015.10.008

Linkermann, A., & Green, D. R. (2014). Necroptosis. *New England Journal of Medicine, 370*(5), 455–465. https://doi.org/10.1056/NEJMra1310050

Linkermann, A., Skouta, R., Himmerkus, N., Mulay, S. R., Dewitz, C., De Zen, F., Prokai, A., Zuchtriegel, G., Krombach, F., Welz, P.-S., Weinlich, R., Vanden Berghe, T., Vandenabeele, P., Pasparakis, M., Bleich, M., Weinberg, J. M., Reichel, C. A., Bräsen, J. H., Kunzendorf, U., … Krautwald, S. (2014). Synchronized renal tubular cell death involves ferroptosis. *Proceedings of the National Academy of Sciences, 111*(47), 16836–16841. https://doi.org/10.1073/pnas.1415518111

Liu, D., Zhou, W., Mao, L., Cui, Z., & Jin, S. (2022). Identification of ferroptosis-related genes and pathways in diabetic kidney disease using bioinformatics analysis. *Scientific Reports, 12*(1), 22613. https://doi.org/10.1038/s41598-022-26495-2

Liu, N., Lin, X., & Huang, C. (2020). Activation of the reverse transsulfuration pathway through NRF2/CBS confers erastin-induced ferroptosis resistance. *British Journal of Cancer, 122*(2), 279–292. https://doi.org/10.1038/s41416-019-0660-x

Liu, Z., Ma, X., Ilyas, I., Zheng, X., Luo, S., Little, P. J., Kamato, D., Sahebkar, A., Wu, W., Weng, J., & Xu, S. (2021). Impact of sodium glucose cotransporter 2 (SGLT2) inhibitors on atherosclerosis: From pharmacology to pre-clinical and clinical therapeutics. *Theranostics, 11*(9), 4502–4515. https://doi.org/10.7150/thno.54498

Llabani, E., Hicklin, R. W., Lee, H. Y., Motika, S. E., Crawford, L. A., Weerapana, E., & Hergenrother, P. J. (2019). Diverse compounds from pleuromutilin lead to a thioredoxin inhibitor and inducer of ferroptosis. *Nature Chemistry, 11*(6), Article 6. https://doi.org/10.1038/s41557-019-0261-6

Lorent, J. H., Levental, K. R., Ganesan, L., Rivera-Longsworth, G., Sezgin, E., Doktorova, M., Lyman, E., & Levental, I. (2020). Plasma membranes are asymmetric in lipid unsaturation, packing and protein shape. *Nature Chemical Biology, 16*(6), 644–652. https://doi.org/10.1038/s41589-020-0529-6

Löwen, J., Gröne, E. F., Groß-Weißmann, M.-L., Bestvater, F., Gröne, H.-J., & Kriz, W. (2021). Pathomorphological sequence of nephron loss in diabetic nephropathy. *American Journal of Physiology-Renal Physiology, 321*(5), F600–F616. https://doi.org/10.1152/ajprenal.00669.2020

Lu, J., & Holmgren, A. (2014). The thioredoxin antioxidant system. *Free Radical Biology & Medicine, 66*, 75–87. https://doi.org/10.1016/j.freeradbiomed.2013.07.036

Lu, Q., Yang, L., Xiao, J.-J., Liu, Q., Ni, L., Hu, J.-W., Yu, H., Wu, X., & Zhang, B.-F. (2023). Empagliflozin attenuates the renal tubular ferroptosis in diabetic kidney disease through AMPK/NRF2 pathway. *Free Radical Biology and Medicine, 195*, 89–102. https://doi.org/10.1016/j.freeradbiomed.2022.12.088

MacLean, B., Tomazela, D. M., Shulman, N., Chambers, M., Finney, G. L., Frewen, B., Kern, R., Tabb, D. L., Liebler, D. C., & MacCoss, M. J. (2010). Skyline: An open source document editor for creating and analyzing targeted proteomics experiments. *Bioinformatics (Oxford, England), 26*(7), 966–968. https://doi.org/10.1093/bioinformatics/btq054

Mann, J. F. E., Ørsted, D. D., Brown-Frandsen, K., Marso, S. P., Poulter, N. R., Rasmussen, S., Tornøe, K., Zinman, B., & Buse, J. B. (2017). Liraglutide and Renal Outcomes in Type 2 Diabetes. *New England Journal of Medicine*, *377*(9), 839–848. https://doi.org/10.1056/NEJMoa1616011

Maremonti, F., Meyer, C., & Linkermann, A. (2022). Mechanisms and Models of Kidney Tubular Necrosis and Nephron Loss. *Journal of the American Society of Nephrology*, *33*(3), 472. https://doi.org/10.1681/ASN.2021101293

Marso, S. P., Bain, S. C., Consoli, A., Eliaschewitz, F. G., Jódar, E., Leiter, L. A., Lingvay, I., Rosenstock, J., Seufert, J., Warren, M. L., Woo, V., Hansen, O., Holst, A. G., Pettersson, J., Vilsbøll, T., & SUSTAIN-6 Investigators. (2016). Semaglutide and Cardiovascular Outcomes in Patients with Type 2 Diabetes. *The New England Journal of Medicine*, *375*(19), 1834–1844. https://doi.org/10.1056/NEJMoa1607141

Martin-Sanchez, D., Ruiz-Andres, O., Poveda, J., Carrasco, S., Cannata-Ortiz, P., Sanchez-Niño, M. D., Ortega, M. R., Egido, J., Linkermann, A., Ortiz, A., & Sanz, A. B. (2017). Ferroptosis, but Not Necroptosis, Is Important in Nephrotoxic Folic Acid–Induced AKI. *Journal of the American Society of Nephrology*, *28*(1), 218–229. https://doi.org/10.1681/ASN.2015121376

Martin-Sanchez, D., Ruiz-Andres, O., Poveda, J., Carrasco, S., Cannata-Ortiz, P., Sanchez-Niño, M. D., Ruiz Ortega, M., Egido, J., Linkermann, A., Ortiz, A., & Sanz, A. B. (2017). Ferroptosis, but Not Necroptosis, Is Important in Nephrotoxic Folic Acid–Induced AKI. *Journal of the American Society of Nephrology*, *28*(1), 218. https://doi.org/10.1681/ASN.2015121376

Mentlein, R., Gallwitz, B., & Schmidt, W. E. (1993). Dipeptidyl-peptidase IV hydrolyses gastric inhibitory polypeptide, glucagon-like peptide-1(7-36)amide, peptide histidine methionine and is responsible for their degradation in human serum. *European Journal of Biochemistry*, *214*(3), 829–835. https://doi.org/10.1111/j.1432-1033.1993.tb17986.x

Mishima, E., Ito, J., Wu, Z., Nakamura, T., Wahida, A., Doll, S., Tonnus, W., Nepachalovich, P., Eggenhofer, E., Aldrovandi, M., Henkelmann, B., Yamada, K., Wanninger, J., Zilka, O., Sato, E., Feederle, R., Hass, D., Maida, A., Mourão, A. S. D., … Conrad, M. (2022). A non-canonical vitamin K cycle is a potent ferroptosis suppressor. *Nature*, *608*(7924), 778–783. https://doi.org/10.1038/s41586-022-05022-3

Mogensen, C. E., Christensen, C. K., & Vittinghus, E. (1983). The Stages in Diabetic Renal Disease: With Emphasis on the Stage of Incipient Diabetic Nephropathy. *Diabetes*, *32*(Supplement_2), 64–78. https://doi.org/10.2337/diab.32.2.S64

Mohan, S., Reddick, R. L., Musi, N., Horn, D. A., Yan, B., Prihoda, T. J., Natarajan, M., & Abboud-Werner, S. L. (2008). Diabetic eNOS knockout mice develop distinct macro- and microvascular complications. *Laboratory Investigation; a Journal of Technical Methods and Pathology*, *88*(5), 515–528. https://doi.org/10.1038/labinvest.2008.23

Mojsov, S., Weir, G. C., & Habener, J. F. (1987). Insulinotropin: Glucagon-like peptide I (7-37) co-encoded in the glucagon gene is a potent stimulator of insulin release in the perfused rat pancreas. *Journal of Clinical Investigation*, *79*(2), 616–619. https://doi.org/10.1172/JCI112855

Monseu, M., Gand, E., Saulnier, P.-J., Ragot, S., Piguel, X., Zaoui, P., Rigalleau, V., Marechaud, R., Roussel, R., Hadjadj, S., & Halimi, J.-M. (2015). Acute Kidney

Injury Predicts Major Adverse Outcomes in Diabetes: Synergic Impact With Low Glomerular Filtration Rate and Albuminuria. *Diabetes Care, 38*(12), 2333–2340. https://doi.org/10.2337/dc15-1222

Muscelli, E., Mari, A., Casolaro, A., Camastra, S., Seghieri, G., Gastaldelli, A., Holst, J. J., & Ferrannini, E. (2008). Separate impact of obesity and glucose tolerance on the incretin effect in normal subjects and type 2 diabetic patients. *Diabetes, 57*(5), 1340–1348. https://doi.org/10.2337/db07-1315

Nakagawa, T., Sato, W., Glushakova, O., Heinig, M., Clarke, T., Campbell-Thompson, M., Yuzawa, Y., Atkinson, M. A., Johnson, R. J., & Croker, B. (2007). Diabetic endothelial nitric oxide synthase knockout mice develop advanced diabetic nephropathy. *Journal of the American Society of Nephrology: JASN, 18*(2), 539–550. https://doi.org/10.1681/ASN.2006050459

Nauck, M. A., Heimesaat, M. M., Orskov, C., Holst, J. J., Ebert, R., & Creutzfeldt, W. (1993). Preserved incretin activity of glucagon-like peptide 1 [7-36 amide] but not of synthetic human gastric inhibitory polypeptide in patients with type-2 diabetes mellitus. *The Journal of Clinical Investigation, 91*(1), 301–307. https://doi.org/10.1172/JCI116186

Nauck, M. A., & Meier, J. J. (2016). The incretin effect in healthy individuals and those with type 2 diabetes: Physiology, pathophysiology, and response to therapeutic interventions. *The Lancet Diabetes & Endocrinology, 4*(6), 525–536. https://doi.org/10.1016/S2213-8587(15)00482-9

Nauck, M. A., & Meier, J. J. (2018). Incretin hormones: Their role in health and disease. *Diabetes, Obesity and Metabolism, 20*(S1), 5–21. https://doi.org/10.1111/dom.13129

Nauck, M. A., Weber, I., Bach, I., Richter, S., Orskov, C., Holst, J. J., & Schmiegel, W. (1998). Normalization of fasting glycaemia by intravenous GLP-1 ([7-36 amide] or [7-37]) in type 2 diabetic patients. *Diabetic Medicine: A Journal of the British Diabetic Association, 15*(11), 937–945. https://doi.org/10.1002/(SICI)1096-9136(1998110)15:11<937::AID-DIA701>3.0.CO;2-0

Neuen, B. L., Young, T., Heerspink, H. J. L., Neal, B., Perkovic, V., Billot, L., Mahaffey, K. W., Charytan, D. M., Wheeler, D. C., Arnott, C., Bompoint, S., Levin, A., & Jardine, M. J. (2019). SGLT2 inhibitors for the prevention of kidney failure in patients with type 2 diabetes: A systematic review and meta-analysis. *The Lancet Diabetes & Endocrinology, 7*(11), 845–854. https://doi.org/10.1016/S2213-8587(19)30256-6

Nishikawa, T., Edelstein, D., Du, X. L., Yamagishi, S., Matsumura, T., Kaneda, Y., Yorek, M. A., Beebe, D., Oates, P. J., Hammes, H. P., Giardino, I., & Brownlee, M. (2000). Normalizing mitochondrial superoxide production blocks three pathways of hyperglycaemic damage. *Nature, 404*(6779), 787–790. https://doi.org/10.1038/35008121

Nishiyama, A., Matsui, M., Iwata, S., Hirota, K., Masutani, H., Nakamura, H., Takagi, Y., Sono, H., Gon, Y., & Yodoi, J. (1999). Identification of thioredoxin-binding protein-2/vitamin D(3) up-regulated protein 1 as a negative regulator of thioredoxin function and expression. *The Journal of Biological Chemistry, 274*(31), 21645–21650. https://doi.org/10.1074/jbc.274.31.21645

Oberst, A., Dillon, C. P., Weinlich, R., McCormick, L. L., Fitzgerald, P., Pop, C., Hakem, R., Salvesen, G. S., & Green, D. R. (2011). Catalytic activity of the

caspase-8-FLIP(L) complex inhibits RIPK3-dependent necrosis. *Nature*, *471*(7338), 363–368. https://doi.org/10.1038/NATURE09852

Oslowski, C. M., Hara, T., O'Sullivan-Murphy, B., Kanekura, K., Lu, S., Hara, M., Ishigaki, S., Zhu, L. J., Hayashi, E., Hui, S. T., Greiner, D., Kaufman, R. J., Bortell, R., & Urano, F. (2012). Thioredoxin-interacting protein mediates ER stress-induced β cell death through initiation of the inflammasome. *Cell Metabolism*, *16*(2), 265–273. https://doi.org/10.1016/j.cmet.2012.07.005

Ozbilgin, S., Ozkardesler, S., Akan, M., Boztas, N., Ozbilgin, M., Ergur, B. U., Derici, S., Guneli, M. E., & Meseri, R. (2016). Renal Ischemia/Reperfusion Injury in Diabetic Rats: The Role of Local Ischemic Preconditioning. *BioMed Research International*, *2016*, 1–9. https://doi.org/10.1155/2016/8580475

Park, S.-J., Kim, Y., Li, C., Suh, J., Sivapackiam, J., Goncalves, T. M., Jarad, G., Zhao, G., Urano, F., Sharma, V., & Chen, Y. M. (2022). Blocking CHOP-dependent TXNIP shuttling to mitochondria attenuates albuminuria and mitigates kidney injury in nephrotic syndrome. *Proceedings of the National Academy of Sciences*, *119*(35), e2116505119. https://doi.org/10.1073/pnas.2116505119

Perez, M. A., Clostio, A. J., Houston, I. R., Ruiz, J., Magtanong, L., Dixon, S. J., & Watts, J. L. (2022). Ether lipid deficiency disrupts lipid homeostasis leading to ferroptosis sensitivity. *PLoS Genetics*, *18*(9), e1010436. https://doi.org/10.1371/journal.pgen.1010436

Perkovic, V., Jardine, M. J., Neal, B., Bompoint, S., Heerspink, H. J. L., Charytan, D. M., Edwards, R., Agarwal, R., Bakris, G., Bull, S., Cannon, C. P., Capuano, G., Chu, P.-L., de Zeeuw, D., Greene, T., Levin, A., Pollock, C., Wheeler, D. C., Yavin, Y., … Mahaffey, K. W. (2019). Canagliflozin and Renal Outcomes in Type 2 Diabetes and Nephropathy. *New England Journal of Medicine*, *380*(24), 2295–2306. https://doi.org/10.1056/NEJMoa1811744

Petersen, M. C., & Shulman, G. I. (2018). Mechanisms of Insulin Action and Insulin Resistance. *Physiological Reviews*, *98*(4), 2133–2223. https://doi.org/10.1152/physrev.00063.2017

Ranjit, S., Lanzanò, L., Libby, A. E., Gratton, E., & Levi, M. (2021). Advances in fluorescence microscopy techniques to study kidney function. *Nature Reviews. Nephrology*, *17*(2), 128–144. https://doi.org/10.1038/s41581-020-00337-8

Ravindran, S., & Munusamy, S. (2022). Renoprotective mechanisms of sodium-glucose co-transporter 2 (SGLT2) inhibitors against the progression of diabetic kidney disease. *Journal of Cellular Physiology*, *237*(2), 1182–1205. https://doi.org/10.1002/jcp.30621

Reifsnyder, P. C., & Leiter, E. H. (2002). Deconstructing and Reconstructing Obesity-Induced Diabetes (Diabesity) in Mice. *Diabetes*, *51*(3), 825–832. https://doi.org/10.2337/diabetes.51.3.825

Reiniger, N., Lau, K., McCalla, D., Eby, B., Cheng, B., Lu, Y., Qu, W., Quadri, N., Ananthakrishnan, R., Furmansky, M., Rosario, R., Song, F., Rai, V., Weinberg, A., Friedman, R., Ramasamy, R., D'Agati, V., & Schmidt, A. M. (2010). Deletion of the receptor for advanced glycation end products reduces glomerulosclerosis and preserves renal function in the diabetic OVE26 mouse. *Diabetes*, *59*(8), 2043–2054. https://doi.org/10.2337/db09-1766

Riegman, M., Bradbury, M. S., & Overholtzer, M. (2019). Population Dynamics in Cell Death: Mechanisms of Propagation. *Trends in Cancer*, *5*(9), 558–568. https://doi.org/10.1016/j.trecan.2019.07.008

Riegman, M., Sagie, L., Galed, C., Levin, T., Steinberg, N., Dixon, S. J., Wiesner, U., Bradbury, M. S., Niethammer, P., Zaritsky, A., & Overholtzer, M. (2020). Ferroptosis occurs through an osmotic mechanism and propagates independently of cell rupture. *Nature Cell Biology*, *22*(9), 1042–1048. https://doi.org/10.1038/s41556-020-0565-1

Roden, M., & Shulman, G. I. (2019). The integrative biology of type 2 diabetes. *Nature*, *576*(7785), 51–60. https://doi.org/10.1038/s41586-019-1797-8

Sarhan, M., Land, W. G., Tonnus, W., Hugo, C. P., & Linkermann, A. (2018). Origin and Consequences of Necroinflammation. *Physiological Reviews*, *98*(2), 727–780. https://doi.org/10.1152/physrev.00041.2016

Scarpellini, C., Klejborowska, G., Lanthier, C., Hassannia, B., Vanden Berghe, T., & Augustyns, K. (2023). Beyond ferrostatin-1: A comprehensive review of ferroptosis inhibitors. *Trends in Pharmacological Sciences*, *44*(12), 902–916. https://doi.org/10.1016/j.tips.2023.08.012

Schönherr, E., Sunderkötter, C., Iozzo, R. V., & Schaefer, L. (2005). Decorin, a novel player in the insulin-like growth factor system. *The Journal of Biological Chemistry*, *280*(16), 15767–15772. https://doi.org/10.1074/jbc.M500451200

Schönherr, E., Sunderkötter, C., Schaefer, L., Thanos, S., Grässel, S., Oldberg, Å., Iozzo, R. V., Young, M. F., & Kresse, H. (2004). Decorin Deficiency Leads to Impaired Angiogenesis in Injured Mouse Cornea. *Journal of Vascular Research*, *41*(6), 499–508. https://doi.org/10.1159/000081806

Schulze, P. C., Yoshioka, J., Takahashi, T., He, Z., King, G. L., & Lee, R. T. (2004). Hyperglycemia Promotes Oxidative Stress through Inhibition of Thioredoxin Function by Thioredoxin-interacting Protein. *Journal of Biological Chemistry*, *279*(29), 30369–30374. https://doi.org/10.1074/jbc.M400549200

Schwartz, S. S., Epstein, S., Corkey, B. E., Grant, S. F. A., Gavin, J. R., & Aguilar, R. B. (2016). The Time Is Right for a New Classification System for Diabetes: Rationale and Implications of the β-Cell–Centric Classification Schema. *Diabetes Care*, *39*(2), 179–186. https://doi.org/10.2337/dc15-1585

Seibt, T. M., Proneth, B., & Conrad, M. (2019). Role of GPX4 in ferroptosis and its pharmacological implication. *Free Radical Biology and Medicine*, *133*, 144–152. https://doi.org/10.1016/j.freeradbiomed.2018.09.014

Seiler, A., Schneider, M., Förster, H., Roth, S., Wirth, E. K., Culmsee, C., Plesnila, N., Kremmer, E., Rådmark, O., Wurst, W., Bornkamm, G. W., Schweizer, U., & Conrad, M. (2008). Glutathione Peroxidase 4 Senses and Translates Oxidative Stress into 12/15-Lipoxygenase Dependent- and AIF-Mediated Cell Death. *Cell Metabolism*, *8*(3), 237–248. https://doi.org/10.1016/j.cmet.2008.07.005

Shah, A., Xia, L., Masson, E. A. Y., Gui, C., Momen, A., Shikatani, E. A., Husain, M., Quaggin, S., John, R., & Fantus, I. G. (2015). Thioredoxin-Interacting Protein Deficiency Protects against Diabetic Nephropathy. *Journal of the American Society of Nephrology*, *26*(12), 2963–2977. https://doi.org/10.1681/ASN.2014050528

Shi, J., Gao, W., & Shao, F. (2017). Pyroptosis: Gasdermin-Mediated Programmed Necrotic Cell Death. *Trends in Biochemical Sciences*, *42*(4), 245–254. https://doi.org/10.1016/j.tibs.2016.10.004

Shimada, K., Skouta, R., Kaplan, A., Yang, W. S., Hayano, M., Dixon, S. J., Brown, L. M., Valenzuela, C. A., Wolpaw, A. J., & Stockwell, B. R. (2016a). Global survey of cell death mechanisms reveals metabolic regulation of ferroptosis. *Nature*

Chemical Biology 2016 12:7, *12*(7), 497–503. https://doi.org/10.1038/nchembio.2079

Shimada, K., Skouta, R., Kaplan, A., Yang, W. S., Hayano, M., Dixon, S. J., Brown, L. M., Valenzuela, C. A., Wolpaw, A. J., & Stockwell, B. R. (2016b). Global survey of cell death mechanisms reveals metabolic regulation of ferroptosis. *Nature Chemical Biology*, *12*(7), 497–503. https://doi.org/10.1038/nchembio.2079

Shin, S. J., Chung, S., Kim, S. J., Lee, E.-M., Yoo, Y.-H., Kim, J.-W., Ahn, Y.-B., Kim, E.-S., Moon, S.-D., Kim, M.-J., & Ko, S.-H. (2016). Effect of Sodium-Glucose Co-Transporter 2 Inhibitor, Dapagliflozin, on Renal Renin-Angiotensin System in an Animal Model of Type 2 Diabetes. *PLOS ONE, 11*(11), e0165703. https://doi.org/10.1371/journal.pone.0165703

Skouta, R., Dixon, S. J., Wang, J., Dunn, D. E., Orman, M., Shimada, K., Rosenberg, P. A., Lo, D. C., Weinberg, J. M., Linkermann, A., & Stockwell, B. R. (2014). Ferrostatins Inhibit Oxidative Lipid Damage and Cell Death in Diverse Disease Models. *Journal of the American Chemical Society*, *136*(12), 4551–4556. https://doi.org/10.1021/ja411006a

Stafford, W. C., Peng, X., Olofsson, M. H., Zhang, X., Luci, D. K., Lu, L., Cheng, Q., Trésaugues, L., Dexheimer, T. S., Coussens, N. P., Augsten, M., Ahlzén, H.-S. M., Orwar, O., Östman, A., Stone-Elander, S., Maloney, D. J., Jadhav, A., Simeonov, A., Linder, S., & Arnér, E. S. J. (2018). Irreversible inhibition of cytosolic thioredoxin reductase 1 as a mechanistic basis for anticancer therapy. *Science Translational Medicine*, *10*(428), eaaf7444. https://doi.org/10.1126/scitranslmed.aaf7444

Stockwell, B. R. (2022). Ferroptosis turns 10: Emerging mechanisms, physiological functions, and therapeutic applications. *Cell*, *185*(14), 2401–2421. https://doi.org/10.1016/j.cell.2022.06.003

Stockwell, B. R., Angeli, J. P. F., Bayir, H., Bush, A. I., Conrad, M., Dixon, S. J., Fulda, S., Gascón, S., Hatzios, S. K., Kagan, V. E., Noel, K., Jiang, X., Linkermann, A., Murphy, M. E., Overholtzer, M., Oyagi, A., Pagnussat, G. C., Park, J., Ran, Q., … Zhang, D. D. (2017). Ferroptosis: A Regulated Cell Death Nexus Linking Metabolism, Redox Biology, and Disease. *Cell*, *171*(2), 273–285. https://doi.org/10.1016/j.cell.2017.09.021

Stockwell, B. R., Friedmann Angeli, J. P., Bayir, H., Bush, A. I., Conrad, M., Dixon, S. J., Fulda, S., Gascón, S., Hatzios, S. K., Kagan, V. E., Noel, K., Jiang, X., Linkermann, A., Murphy, M. E., Overholtzer, M., Oyagi, A., Pagnussat, G. C., Park, J., Ran, Q., … Zhang, D. D. (2017). Ferroptosis: A Regulated Cell Death Nexus Linking Metabolism, Redox Biology, and Disease. *Cell*, *171*(2), 273–285. https://doi.org/10.1016/J.CELL.2017.09.021

Sun, H., Saeedi, P., Karuranga, S., Pinkepank, M., Ogurtsova, K., Duncan, B. B., Stein, C., Basit, A., Chan, J. C. N., Mbanya, J. C., Pavkov, M. E., Ramachandaran, A., Wild, S. H., James, S., Herman, W. H., Zhang, P., Bommer, C., Kuo, S., Boyko, E. J., & Magliano, D. J. (2022). IDF Diabetes Atlas: Global, regional and country-level diabetes prevalence estimates for 2021 and projections for 2045. *Diabetes Research and Clinical Practice, 183*, 109119. https://doi.org/10.1016/j.diabres.2021.109119

Teiken, J. M., Audettey, J. L., Laturnus, D. I., Zheng, S., Epstein, P. N., & Carlson, E. C. (2008). Podocyte loss in aging OVE26 diabetic mice. *Anatomical Record (Hoboken, N.J.: 2007)*, *291*(1), 114–121. https://doi.org/10.1002/ar.20625

Tervaert, T. W. C., Mooyaart, A. L., Amann, K., Cohen, A. H., Cook, H. T., Drachenberg, C. B., Ferrario, F., Fogo, A. B., Haas, M., de Heer, E., Joh, K., Noël, L. H., Radhakrishnan, J., Seshan, S. V., Bajema, I. M., Bruijn, J. A., & Society, on behalf of the R. P. (2010). Pathologic Classification of Diabetic Nephropathy. *Journal of the American Society of Nephrology*, *21*(4), 556. https://doi.org/10.1681/ASN.2010010010

Thakar, C. V., Christianson, A., Himmelfarb, J., & Leonard, A. C. (2011). Acute kidney injury episodes and chronic kidney disease risk in diabetes mellitus. *Clinical Journal of the American Society of Nephrology: CJASN*, *6*(11), 2567–2572. https://doi.org/10.2215/CJN.01120211

The EMPA-KIDNEY Collaborative Group. (2023). Empagliflozin in Patients with Chronic Kidney Disease. *New England Journal of Medicine*, *388*(2), 117–127. https://doi.org/10.1056/NEJMoa2204233

The Expert Committee on the Diagnosis and Classification of Diabetes Mellitus. (2003). Report of the Expert Committee on the Diagnosis and Classification of Diabetes Mellitus. *Diabetes Care*, *26*(suppl_1), s5–s20. https://doi.org/10.2337/diacare.26.2007.S5

The Human Nephrogenesis Atlas. (n.d.). Retrieved 30 January 2024, from https://sckidney.flatironinstitute.org/

The Lancet. (2023). Diabetes: A defining disease of the 21st century. *The Lancet*, *401*(10394), 2087. https://doi.org/10.1016/S0140-6736(23)01296-5

Thomas, M. C., Brownlee, M., Susztak, K., Sharma, K., Jandeleit-Dahm, K. A. M., Zoungas, S., Rossing, P., Groop, P.-H., & Cooper, M. E. (2015). Diabetic kidney disease. *Nature Reviews Disease Primers*, *1*(1), Article 1. https://doi.org/10.1038/nrdp.2015.18

Tonnus, W., Al-Mekhlafi, M., Hugo, C., & Linkermann, A. (2018). Assessment of In Vivo Kidney Cell Death: Acute Kidney Injury. In A. T. Ting (Ed.), *Programmed Necrosis* (Vol. 1857, pp. 135–144). Springer New York. https://doi.org/10.1007/978-1-4939-8754-2_13

Tonnus, W., Belavgeni, A., Beuschlein, F., Eisenhofer, G., Fassnacht, M., Kroiss, M., Krone, N. P., Reincke, M., Bornstein, S. R., & Linkermann, A. (2021a). The role of regulated necrosis in endocrine diseases. *Nature Reviews Endocrinology*, *17*(8), Article 8. https://doi.org/10.1038/s41574-021-00499-w

Tonnus, W., Belavgeni, A., Beuschlein, F., Eisenhofer, G., Fassnacht, M., Kroiss, M., Krone, N., Reincke, M., Bornstein, S., & Linkermann, A. (2021b). The role of regulated necrosis in endocrine diseases. *Nature Reviews. Endocrinology*, *17*(8), 497–510. https://doi.org/10.1038/S41574-021-00499-W

Tonnus, W., Gembardt, F., Latk, M., Parmentier, S., Hugo, C., Bornstein, S. R., & Linkermann, A. (2018). The clinical relevance of necroinflammation—Highlighting the importance of acute kidney injury and the adrenal glands. *Cell Death and Differentiation*, *26*, 68–82. https://doi.org/10.1038/s41418-018-0193-5

Tonnus, W., Meyer, C., Paliege, A., Belavgeni, A., von Mässenhausen, A., Bornstein, S. R., Hugo, C., Becker, J. U., & Linkermann, A. (2019). The pathological features of regulated necrosis. *The Journal of Pathology*, *247*(5), 697–707. https://doi.org/10.1002/path.5248

Tonnus, W., Meyer, C., Steinebach, C., Belavgeni, A., Von Mässenhausen, A., Gonzalez, N. Z., Maremonti, F., Gembardt, F., Himmerkus, N., Latk, M., Locke,

S., Marschner, J., Li, W., Short, S., Doll, S., Ingold, I., Proneth, B., Daniel, C., Kabgani, N., … Linkermann, A. (2021). Dysfunction of the key ferroptosis-surveilling systems hypersensitizes mice to tubular necrosis during acute kidney injury. *Nature Communications*, *12*(1), 4402. https://doi.org/10.1038/s41467-021-24712-6

Turturro, F., Friday, E., & Welbourne, T. (2007). Hyperglycemia regulates thioredoxin-ROS activity through induction of thioredoxin-interacting protein (TXNIP) in metastatic breast cancer-derived cells MDA-MB-231. *BMC Cancer*, *7*(1), 96. https://doi.org/10.1186/1471-2407-7-96

Vallon, V. (2011). The proximal tubule in the pathophysiology of the diabetic kidney. *American Journal of Physiology-Regulatory, Integrative and Comparative Physiology*, *300*(5), R1009–R1022. https://doi.org/10.1152/ajpregu.00809.2010

Van Bommel, E. J. M., Muskiet, M. H. A., Tonneijck, L., Kramer, M. H. H., Nieuwdorp, M., & Van Raalte, D. H. (2017). SGLT2 Inhibition in the Diabetic Kidney—From Mechanisms to Clinical Outcome. *Clinical Journal of the American Society of Nephrology*, *12*(4), 700–710. https://doi.org/10.2215/CJN.06080616

Vardarli, I., Arndt, E., Deacon, C. F., Holst, J. J., & Nauck, M. A. (2014). Effects of Sitagliptin and Metformin Treatment on Incretin Hormone and Insulin Secretory Responses to Oral and "Isoglycemic" Intravenous Glucose. *Diabetes*, *63*(2), 663–674. https://doi.org/10.2337/db13-0805

Vardarli, I., Nauck, M. A., Köthe, L. D., Deacon, C. F., Holst, J. J., Schweizer, A., & Foley, J. E. (2011). Inhibition of DPP-4 with Vildagliptin Improved Insulin Secretion in Response to Oral as well as "Isoglycemic" Intravenous Glucose without Numerically Changing the Incretin Effect in Patients with Type 2 Diabetes. *The Journal of Clinical Endocrinology & Metabolism*, *96*(4), 945–954. https://doi.org/10.1210/jc.2010-2178

Vergara, A., Jacobs-Cacha, C., Llorens-Cebria, C., Ortiz, A., Martinez-Diaz, I., Martos, N., Dominguez-Báez, P., Van den Bosch, M. M., Bermejo, S., Pieper, M. P., Benito, B., & Soler, M. J. (2022). Enhanced Cardiorenal Protective Effects of Combining SGLT2 Inhibition, Endothelin Receptor Antagonism and RAS Blockade in Type 2 Diabetic Mice. *International Journal of Molecular Sciences*, *23*(21), 12823. https://doi.org/10.3390/ijms232112823

Volz, A., Göke, R., Lankat-Buttgereit, B., Fehmann, H.-C., Bode, H. P., & Göke, B. (1995). Molecular cloning, functional expression, and signal transduction of the GIP-receptor cloned from a human insulinoma. *FEBS Letters*, *373*(1), 23–29. https://doi.org/10.1016/0014-5793(95)01006-Z

Von Mässenhausen, A., Zamora Gonzalez, N., Maremonti, F., Belavgeni, A., Tonnus, W., Meyer, C., Beer, K., Hannani, M. T., Lau, A., Peitzsch, M., Hoppenz, P., Locke, S., Chavakis, T., Kramann, R., Muruve, D. A., Hugo, C., Bornstein, S. R., & Linkermann, A. (2022). Dexamethasone sensitizes to ferroptosis by glucocorticoid receptor–induced dipeptidase-1 expression and glutathione depletion. *Science Advances*, *8*(5), eabl8920. https://doi.org/10.1126/sciadv.abl8920

Waldhart, A. N., Dykstra, H., Peck, A. S., Boguslawski, E. A., Madaj, Z. B., Wen, J., Veldkamp, K., Hollowell, M., Zheng, B., Cantley, L. C., McGraw, T. E., & Wu, N. (2017). Phosphorylation of TXNIP by AKT Mediates Acute Influx of Glucose

in Response to Insulin. *Cell Reports*, *19*(10), 2005–2013. https://doi.org/10.1016/j.celrep.2017.05.041

Wanders, R. J. A., Baes, M., Ribeiro, D., Ferdinandusse, S., & Waterham, H. R. (2023). The physiological functions of human peroxisomes. *Physiological Reviews*, *103*(1), 957–1024. https://doi.org/10.1152/physrev.00051.2021

Wang, L., Cai, H., Hu, Y., Liu, F., Huang, S., Zhou, Y., Yu, J., Xu, J., & Wu, F. (2018). A pharmacological probe identifies cystathionine β-synthase as a new negative regulator for ferroptosis. *Cell Death & Disease*, *9*(10), 1005. https://doi.org/10.1038/s41419-018-1063-2

Wang, Q., Ju, F., Li, J., Liu, T., Zuo, Y., Abbott, G. W., & Hu, Z. (2022). Empagliflozin protects against renal ischemia/reperfusion injury in mice. *Scientific Reports*, *12*(1), 19323. https://doi.org/10.1038/s41598-022-24103-x

Wang, S.-J., Li, D., Ou, Y., Jiang, L., Chen, Y., Zhao, Y., & Gu, W. (2016). Acetylation Is Crucial for p53-Mediated Ferroptosis and Tumor Suppression. *Cell Reports*, *17*(2), 366–373. https://doi.org/10.1016/j.celrep.2016.09.022

Wang, Y., Chang, D., Zhao, M., & Chen, M. (2023). Dapagliflozin Alleviates Diabetic Kidney Disease *via* Hypoxia Inducible Factor 1α/Heme Oxygenase 1-Mediated Ferroptosis. *Antioxidants & Redox Signaling*, ars.2022.0169. https://doi.org/10.1089/ars.2022.0169

Wanner, C., Inzucchi, S. E., Lachin, J. M., Fitchett, D., Von Eynatten, M., Mattheus, M., Johansen, O. E., Woerle, H. J., Broedl, U. C., & Zinman, B. (2016). Empagliflozin and Progression of Kidney Disease in Type 2 Diabetes. *New England Journal of Medicine*, *375*(4), 323–334. https://doi.org/10.1056/NEJMoa1515920

Wiernicki, B., Maschalidi, S., Pinney, J., Adjemian, S., Vanden Berghe, T., Ravichandran, K. S., & Vandenabeele, P. (2022). Cancer cells dying from ferroptosis impede dendritic cell-mediated anti-tumor immunity. *Nature Communications*, *13*(1), 3676. https://doi.org/10.1038/s41467-022-31218-2

Williams, K. J., Qiu, G., Usui, H. K., Dunn, S. R., McCue, P., Bottinger, E., Iozzo, R. V., & Sharma, K. (2007). Decorin Deficiency Enhances Progressive Nephropathy in Diabetic Mice. *The American Journal of Pathology*, *171*(5), 1441–1450. https://doi.org/10.2353/ajpath.2007.070079

Williams, R., Karuranga, S., Malanda, B., Saeedi, P., Basit, A., Besançon, S., Bommer, C., Esteghamati, A., Ogurtsova, K., Zhang, P., & Colagiuri, S. (2020). Global and regional estimates and projections of diabetes-related health expenditure: Results from the International Diabetes Federation Diabetes Atlas, 9th edition. *Diabetes Research and Clinical Practice*, *162*, 108072. https://doi.org/10.1016/j.diabres.2020.108072

Wright, E. M., Loo, D. D. F., & Hirayama, B. A. (2011). Biology of Human Sodium Glucose Transporters. *Physiological Reviews*, *91*(2), 733–794. https://doi.org/10.1152/physrev.00055.2009

Wu, N., Zheng, B., Shaywitz, A., Dagon, Y., Tower, C., Bellinger, G., Shen, C.-H., Wen, J., Asara, J., McGraw, T. E., Kahn, B. B., & Cantley, L. C. (2013). AMPK-Dependent Degradation of TXNIP upon Energy Stress Leads to Enhanced Glucose Uptake via GLUT1. *Molecular Cell*, *49*(6), 1167–1175. https://doi.org/10.1016/j.molcel.2013.01.035

Wu, Z., Khodade, V. S., Chauvin, J.-P. R., Rodriguez, D., Toscano, J. P., & Pratt, D. A. (2022). Hydropersulfides Inhibit Lipid Peroxidation and Protect Cells from

Ferroptosis. *Journal of the American Chemical Society*, *144*(34), 15825–15837. https://doi.org/10.1021/jacs.2c06804

Xu, Y., Li, L., Tang, P., Zhang, J., Zhong, R., Luo, J., Lin, J., & Zhang, L. (2023). Identifying key genes for diabetic kidney disease by bioinformatics analysis. *BMC Nephrology*, *24*(1), 305. https://doi.org/10.1186/s12882-023-03362-4

Yagoda, N., Von Rechenberg, M., Zaganjor, E., Bauer, A. J., Yang, W. S., Fridman, D. J., Wolpaw, A. J., Smukste, I., Peltier, J. M., Boniface, J. J., Smith, R., Lessnick, S. L., Sahasrabudhe, S., & Stockwell, B. R. (2007). RAS-RAF-MEK-dependent oxidative cell death involving voltage-dependent anion channels. *Nature*, *447*(7146), 864–868. Scopus. https://doi.org/10.1038/nature05859

Yang, W. S., SriRamaratnam, R., Welsch, M. E., Shimada, K., Skouta, R., Viswanathan, V. S., Cheah, J. H., Clemons, P. A., Shamji, A. F., Clish, C. B., Brown, L. M., Girotti, A. W., Cornish, V. W., Schreiber, S. L., & Stockwell, B. R. (2014). Regulation of Ferroptotic Cancer Cell Death by GPX4. *Cell*, *156*(1–2), 317–331. https://doi.org/10.1016/j.cell.2013.12.010

Yang, W. S., & Stockwell, B. R. (2008). Synthetic Lethal Screening Identifies Compounds Activating Iron-Dependent, Nonapoptotic Cell Death in Oncogenic-RAS-Harboring Cancer Cells. *Chemistry & Biology*, *15*(3), 234–245. https://doi.org/10.1016/j.chembiol.2008.02.010

Yang, W. S., & Stockwell, B. R. (2016). Ferroptosis: Death by Lipid Peroxidation. *Trends in Cell Biology*, *26*(3), 165–176. https://doi.org/10.1016/j.tcb.2015.10.014

Yao, W., Liao, H., Pang, M., Pan, L., Guan, Y., Huang, X., Hei, Z., Luo, C., & Ge, M. (2022). Inhibition of the NADPH Oxidase Pathway Reduces Ferroptosis during Septic Renal Injury in Diabetic Mice. *Oxidative Medicine and Cellular Longevity*, *2022*, 1193734. https://doi.org/10.1155/2022/1193734

Yin, H., Xu, L., & Porter, N. A. (2011). Free Radical Lipid Peroxidation: Mechanisms and Analysis. *Chemical Reviews*, *111*(10), 5944–5972. https://doi.org/10.1021/cr200084z

Zanchi, A., Moczulski, D. K., Hanna, L. S., Wantman, M., Warram, J. H., & Krolewski, A. S. (2000). Risk of advanced diabetic nephropathy in type 1 diabetes is associated with endothelial nitric oxide synthase gene polymorphism. *Kidney International*, *57*(2), 405–413. https://doi.org/10.1046/j.1523-1755.2000.00860.x

Zhang, X., & Li, X. (2022). Abnormal Iron and Lipid Metabolism Mediated Ferroptosis in Kidney Diseases and Its Therapeutic Potential. *Metabolites*, *12*(1), 58. https://doi.org/10.3390/metabo12010058

Zhang, Z., Sun, L., Wang, Y., Ning, G., Minto, A. W., Kong, J., Quigg, R. J., & Li, Y. C. (2008). Renoprotective role of the vitamin D receptor in diabetic nephropathy. *Kidney International*, *73*(2), 163–171. https://doi.org/10.1038/sj.ki.5002572

Zhao, H. J., Wang, S., Cheng, H., Zhang, M., Takahashi, T., Fogo, A. B., Breyer, M. D., & Harris, R. C. (2006). Endothelial nitric oxide synthase deficiency produces accelerated nephropathy in diabetic mice. *Journal of the American Society of Nephrology: JASN*, *17*(10), 2664–2669. https://doi.org/10.1681/ASN.2006070798

Zheng, S., Noonan, W. T., Metreveli, N. S., Coventry, S., Kralik, P. M., Carlson, E. C., & Epstein, P. N. (2004). Development of Late-Stage Diabetic Nephropathy in

OVE26 Diabetic Mice. *Diabetes*, *53*(12), 3248–3257. https://doi.org/10.2337/diabetes.53.12.3248

Zhou, C., Yool, A. J., Nolan, J., & Byard, R. W. (2013). Armanni-Ebstein lesions: A need for clarification. *Journal of Forensic Sciences*, *58 Suppl 1*, S94-98. https://doi.org/10.1111/j.1556-4029.2012.02274.x

Zhu, H., Cen, J., Hong, C., Wang, H., Wen, Y., He, Q., Yu, Y., Cao, J., & Chen, W. (2023). Targeting Labile Iron-Mediated Ferroptosis Provides a Potential Therapeutic Strategy for Rhabdomyolysis-Induced Acute Kidney Injury. *ACS Chemical Biology*, *18*(6), 1294–1304. https://doi.org/10.1021/acschembio.2c00914

Zilka, O., Poon, J.-F., & Pratt, D. A. (2021). Radical-Trapping Antioxidant Activity of Copper and Nickel Bis(Thiosemicarbazone) Complexes Underlies Their Potency as Inhibitors of Ferroptotic Cell Death. *Journal of the American Chemical Society*, *143*(45), 19043–19057. https://doi.org/10.1021/jacs.1c08254

Zinman, B., Wanner, C., Lachin, J. M., Fitchett, D., Bluhmki, E., Hantel, S., Mattheus, M., Devins, T., Johansen, O. E., Woerle, H. J., Broedl, U. C., & Inzucchi, S. E. (2015). Empagliflozin, Cardiovascular Outcomes, and Mortality in Type 2 Diabetes. *New England Journal of Medicine*, *373*(22), 2117–2128. https://doi.org/10.1056/NEJMoa1504720

Ziyadeh, F. N., & Wolf, G. (2008). Pathogenesis of the Podocytopathy and Proteinuria in Diabetic Glomerulopathy. *Current Diabetes Reviews*, *4*(1), 39–45.

Zou, C., Liu, X., Liu, R., Wang, M., Sui, M., Mu, S., Li, L., Ji, L., & Xie, R. (2017). Effect of the oral iron chelator deferiprone in diabetic nephropathy rats. *Journal of Diabetes*, *9*(4), 332–340. https://doi.org/10.1111/1753-0407.12420

Zou, Y., Henry, W. S., Ricq, E. L., Graham, E. T., Phadnis, V. V., Maretich, P., Paradkar, S., Boehnke, N., Deik, A. A., Reinhardt, F., Eaton, J. K., Ferguson, B., Wang, W., Fairman, J., Keys, H. R., Dančík, V., Clish, C. B., Clemons, P. A., Hammond, P. T., … Schreiber, S. L. (2020). Plasticity of ether lipids promotes ferroptosis susceptibility and evasion. *Nature*, *585*(7826), 603–608. https://doi.org/10.1038/s41586-020-2732-8

Zou, Y., Li, H., Graham, E. T., Deik, A. A., Eaton, J. K., Wang, W., Sandoval-Gomez, G., Clish, C. B., Doench, J. G., & Schreiber, S. L. (2020). Cytochrome P450 oxidoreductase contributes to phospholipid peroxidation in ferroptosis. *Nature Chemical Biology*, *16*(3), Article 3. https://doi.org/10.1038/s41589-020-0472-6

Anlage 1

Erklärungen zur Eröffnung des Promotionsverfahrens

1. Hiermit versichere ich, dass ich die vorliegende Arbeit ohne unzulässige Hilfe Dritter und ohne Benutzung anderer als der angegebenen Hilfsmittel angefertigt habe; die aus fremden Quellen direkt oder indirekt übernommenen Gedanken sind als solche kenntlich gemacht.
2. Bei der Auswahl und Auswertung des Materials sowie bei der Herstellung des Manuskripts habe ich Unterstützungsleistungen von folgenden Personen erhalten:
3. Weitere Personen waren an der geistigen Herstellung der vorliegenden Arbeit nicht beteiligt. Insbesondere habe ich nicht die Hilfe eines kommerziellen Promotionsberaters in Anspruch genommen. Dritte haben von mir weder unmittelbar noch mittelbar geldwerte Leistungen für Arbeiten erhalten, die im Zusammenhang mit dem Inhalt der vorgelegten Dissertation stehen.
4. Die Arbeit wurde bisher weder im Inland noch im Ausland in gleicher oder ähnlicher Form einer anderen Prüfungsbehörde vorgelegt.
5. Die Inhalte dieser Dissertation wurden in folgender Form veröffentlicht:
6. Ich bestätige, dass es keine zurückliegenden erfolglosen Promotionsverfahren gab.
7. Ich bestätige, dass ich die Promotionsordnung der Medizinischen Fakultät der Technischen Universität Dresden anerkenne.
8. Ich habe die Zitierrichtlinien für Dissertationen an der Medizinischen Fakultät der Technischen Universität Dresden zur Kenntnis genommen und befolgt.
9. Ich bin mit den "Richtlinien zur Sicherung guter wissenschaftlicher Praxis, zur Vermeidung wissenschaftlichen Fehlverhaltens und für den Umgang mit Verstößen" der Technischen Universität Dresden einverstanden.

Dresden, den 11/03/2024

Unterschrift des Doktoranden

Anlage 2

Erklärung über die Einhaltung gesetzlicher Bestimmungen

Hiermit bestätige ich die Einhaltung der folgenden aktuellen gesetzlichen Vorgaben im Rahmen meiner Dissertation

☐   das zustimmende Votum der Ethikkommission bei Klinischen Studien, epidemiologischen Untersuchungen mit Personenbezug oder Sachverhalten, die das Medizinproduktegesetz betreffen

………………………………………………………………………..

Hier ist die Unterschrift des Klinik- bzw. Institutsdirektors einzuholen

Aktenzeichen der zuständigen Ethikkommission:

☐   die Einhaltung der Bestimmungen des Tierschutzgesetzes Aktenzeichen der Genehmigungsbehörde zum Vorhaben/zur Mitwirkung: TVV49/2023

………………………………………………………….…………………

Hier ist die Unterschrift des Klinik- bzw. Institutsdirektors einzuholen

☐   die Einhaltung des Gentechnikgesetzes/Projektnummer: 45-8452/138

………………………………………………………….…………………

Hier ist die Unterschrift des Klinik- bzw. Institutsdirektors einzuholen

☐   die Einhaltung von Datenschutzbestimmungen der Medizinischen Fakultät und des Universitätsklinikums Carl Gustav Carus.

Dresden, den 11/03/2024

Unterschrift des Doktoranden